INSTITUTE
FOR
AEROSPACE STUDIES

UNIVERSITY OF TORONTO

BUCKLING OF CIRCULAR CYLINDRICAL SHELLS UNDER DYNAMICALLY APPLIED AXIAL LOADS

BY

J. D. TULK

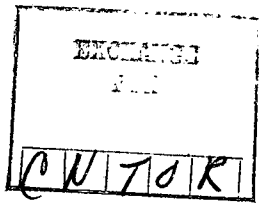

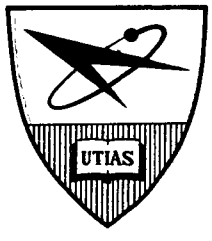

June 1972

UTIAS Report 160

BUCKLING OF CIRCULAR CYLINDRICAL SHELLS UNDER DYNAMICALLY APPLIED AXIAL LOADS

by

J. D. Tulk

Submitted June, 1972.

June, 1972.

UTIAS Report No. 160

ACKNOWLEDGEMENT

Throughout this study I have been fortunate to have received willing and generous assistance from a large number of individuals.

I wish to thank the staff of the University of Toronto Institute for Aerospace Studies and especially Dr. G. N. Patterson, the Director of the Institute who made my studies and research work possible. Also deserving of particular thanks is Dr. R. C. Tennyson whose guidance, assistance and encouragement contributed greatly to my progress.

I am also deeply indebted to Mr. G. Sachade and Mr. J. Bradbury of the Institute's technical staff who assisted in the manufacture of testing apparatus and shell specimens.

During preparation of this thesis I was ably assisted by Mrs. B. Waddell who typed the manuscript and Miss R. Dunn who helped to prepare the figures.

I also wish to thank my wife for her help, encouragement and tolerance.

Throughout this work I received personal support in the form of fellowships from the National Research Council of Canada. The study was funded by the National Research Council of Canada (NRC Grant No. A-2783) and the National Aeronautics and Space Administration (NASA Grant No. NGR 52-026-011, Supplement No. 2).

SUMMARY

A theoretical and experimental study was made of the buckling characteristics of perfect and imperfect circular cylindrical shells subjected to dynamic axial loading.

The experimental tests were performed on a specially designed dynamic testing machine which was capable of producing controlled ramp-type loads at rates ranging from the quasi-static up to higher than 200,000 pounds/second. Ten shell specimens were tested including two near-perfect shells, seven shells with axisymmetric sinusoidal imperfections of a variety of amplitudes and wave-lengths and one shell with quasi-random axisymmetric imperfections. The shells were produced from a photo-elastic epoxy plastic using a spin-casting technique. The imperfection profiles were machined into the shell walls using a high precision hydraulic tracing apparatus. For three of the shells with sinusoidal imperfections, imperfection profiles were cut on the inner surface alone while for the remaining four shells with sinusoidal imperfections and for the shell with quasi-random imperfections, a special manufacturing procedure was adopted which produced shells with matching inner and outer profiles, thus providing effectively constant thickness walls.

Experimental data included dynamic buckling loads (124 data points), high speed photographs of the buckling mode shapes and observations of the dynamic stability of shells subjected to rapidly applied sub-critical loads.

A mathematical model was developed to describe the dynamic behaviour of perfect and imperfect shells. This model was based on the Donnell-Von Kármán compatibility and equilibrium equations and had a wall deflection function incorporating five separate modes of deflection. Close agreement between theory and experiment was found for both dynamic buckling strength and buckling mode shapes.

TABLE OF CONTENTS

NOTATION*

A,B	deflection mode amplitudes
c	$\left[\frac{E}{\rho}\right]^{1/2}$: one-dimensional acoustic wave speed ($= 6.77 \times 10^4$ inch/sec for epoxy)
E	modulus of elasticity
$E\ (w(x,y,t)\ f(x,y,t))$	equilibrium equation
$f\ (x,y,t)$	AIRY stress function
$F_o, F_1, \cdots F_{13}$	coefficients of AIRY stress function
h	shell wall thickness
h	average shell wall thickness
k	constant related to gas flows in loading cylinder of testing machine
K,M,N	axial and circumferential wave-numbers
k_{cr}	$\left[\frac{12(1-\nu^2)}{h^2R^2}\right]^{\frac{1}{4}}$ critical axial wave-number
ℓ	length of sample employed in split Hopkinson bar experiment
L	length of shell
N_x, N_y, N_{xy}	membrane stress resultants
P	axial load on shell
P	air pressure in loading cylinder of testing machine
P_o	initial air pressure in loading cylinder
P_{cl}	$\frac{2\pi Eh^2}{[3(1-\nu^2)]^{\frac{1}{2}}}$ classical buckling load
R	shell radius
t	time
u,v,w	displacements measured in axial, circumferential and radial direction respectively
V	closing velocity of shell end plates

* Symbols not appearing in this table are defined locally in the text.

V_o	$\frac{V}{c}$
$W_o, \ldots W_{02}$	radial displacement function amplitude coefficients
$\underline{w}$	initial radial imperfection
$\underline{W}_1, \ldots \underline{W}_{02}$	imperfection amplitude coefficients
x,y,z	axial, circumferential and radial coordinates, respectively

Greek Symbols

α,β	radial deflection mode wave-numbers
γ	non-linear loading rate parameter
δ_x	axial compression of shell
Δ	Laplace operator
ε	strain
λ	wave-length
τ	shear stress
μ	$\frac{\underline{w}}{\bar{h}}$ imperfection amplitude parameter
ν	Poisson's ratio
ρ	material density
σ_x,σ_y	axial and circumferential stress respectively (tensile = positive)
Σ_x,Σ_y	axial and circumferential uniform compressive stress (compressive = positive)

Superscripts

Dot notation ($\dot{w}$, etc.) represents differentiation with respect to time.

Subscripts

A,B	material type symbols (wave transmission)
cr	critical
cℓ	classical
I	material interface

When a subscript follows a comma, this indicates partial differentiation of the principle variable with respect to the subscript.

1. INTRODUCTION

Thin-walled cylindrical shells are common structural elements in many areas of engineering, especially in the aerospace field. For the designer attempting to build efficient and reliable structures, the stability of these shells under static and dynamic loads is of extreme importance.

It has been recognized for some time that the buckling loads predicted by the classical small-deflection theory are considerably higher than those which may be attained with all but the most meticulously prepared experimental specimens. In a study published in 1934, Donnell[1] attampted to resolve this discrepancy through the use of a large-deflection analysis which considered the effects of initial imperfections and plastic material deformations. However, this theory contained some serious oversimplifications, and the results were far too unreliable to be of any use to the practicing engineer. In 1941 Von Kármán and Tsien[2] used a similar large-deflection theory to show that a stable post-buckled equilibrium state could exist under axial loads substantially lower than the classical buckling load. It was felt that the minimum post-buckling load would provide a useful conservative estimate of the buckling strength of cylindrical shells and a number of workers applied themselves to the task of refining the basic Von Kármán-Tsien approach in pursuit of a true lower bound. This search effectively came to an end in 1966 when Hoff, Madsen and Mayers[3] demonstrated that for shells with very high radius to thickness ratios, the minimum post-buckled equilibrium state could exist with essentially zero axial load.

An alternative approach was followed by Koiter, who in 1945 published a general non-linear theory of elastic stability[4] based on consideration of the effect of initial imperfections on the pre-buckling deformations and, ultimately, on buckling loads. Koiter also prepared a special version of the theory[5] which gave a quantitative relationship between buckling loads and imperfection geometry for the case of axially loaded cylindrical shells with finite axisymmetric imperfections. This very important work was originally published in Dutch and it was not until 1963 when English translations appeared that the theories became well-known outside of the Netherlands. Since that time, however, Koiter's work has become widely accepted, both as a general theory for the stability of imperfection-sensitive structures and as a useful model in the study of the buckling of cylindrical shells. Several contemporary workers have generalized and expanded this basic approach (References 6 to 10) and experimental evidence has been produced which largely confirms the theoretical predications (References 10 to 13). Recently a safe design criterion was proposed[14] which took into account the actual imperfections of realistic shell structures. Good reviews of current theory are found in References 15, 16 and 17.

In addition to the previously cited work on static buckling, efforts have been made to predict the effect of dynamically applied loads on the stability of shells. Budiansky and Hutchinson[18,19] and Danielson[20] presented general theories for the dynamic buckling of imperfection-sensitive structures. Studies more specifically related to cylindrical shells have been made by Agamirov and Vol'mir[21], Coppa and Nash[22], Roth and Klosner[23], Bieniek, Fan and Lackman[24], Dym[25] and Dietz[26]. These investigations have generally been based on some form of the Donnell-Von Kármán large-deflection theory modified to include radial inertia. Roth and Klosner considered a configuration similar to that investigated by Budiansky and Hutchinson, that is, a cylindrical shell

subjected to an axial load applied either stepwise or as a pulse of limited duration. Both Agamirov and Vol'mir and Bieniek, Fan and Lackman studied the case of a dynamically applied external pressure load. Agamirov and Vol'mir also considered the problem of a shell loaded axially at a constant rate (ramp loading). However, while their paper contains an equation governing the motions of the shell wall, no solutions or results were provided.

Nash, Dym and Dietz have each investigated the buckling of shells under a constant rate of axial compression or end shortening. Dym presented a fairly simple analysis involving a single asymmetric deflection mode. No final solution was given; rather, the equation of motion was compared to an earlier equation derived by Hoff to describe the behaviour of an imperfect column loaded in a similar fashion. Nash, in the papers co-authored by himself and A. P. Coppa, followed a similar approach but based his analysis on a two degree of freedom deflection mode of the form:

$$W(x,y,t) = A(t)\sin\alpha x\sin\beta y + B(t)\sin^2\alpha x\sin^2\beta y.$$

The equations of motion of the shell wall derived in this paper were integrated using a Runge-Kutta type numerical procedure. By this technique, Coppa was able to predict theoretical dynamic buckling loads. Unfortunately, due to oversimplification of the mathematical model, especially with respect to the assumed deflection modes, the published results are unreliable. A more sophisticated and generalized form of this theory was given by Dietz who considered the case of dynamic buckling of shells with closely spaced eccentric stiffening. Here, the constant-thickness shell was considered only as a limiting case of the more general configuration and the published results were restricted to the reinforced cases. A three degree of freedom deflection mode was used in this analysis, this being composed of a time dependent term representing uniform radial expansion plus two trigonometric terms similar to those employed by Coppa.

Relatively little experimental work has been done on the dynamic buckling of cylindrical shells. Agamirov and Vol'mir have mentioned some experiments which they claim confirmed the basic trends predicted by their theoretical work but no specific results or descriptions of these experiments are available in the open literature. Coppa[22] and Schwieger[31] have reported experiments in which shell models were buckled under the force of a falling weight. In both cases, however, the shells were simply rolled from sheet and adhesively joined at the seam, a method which provides very irregular and unreliable specimens. Further, in both experiments, the impact loads were applied directly to the free ends of the shells. Static theories and tests have shown that weak or non-existent end constraints of this nature can seriously degrade the load carrying capabilities of the shell structures.

In summary, then, although the buckling of circular cylindrical shells under static loads is fairly well understood at present, the study of the response of these structures to dynamically applied loads is considerably less well advanced. Several major deficiencies are apparent. First, the theoretical analyses attempted so far have generally made use of rather limited imperfection and deflection mode functions and the published results have been restricted to a few specific cases so that it is impossible to make general conclusions. Further, due to the lack of reliable quantitative experimental results, it has not been possible to confirm the theoretical predictions or to check the validity of the assumptions implied in the theoretical studies.

This report contains the results of an experimental study in which a number of carefully manufactured near-perfect and imperfect shell specimens were buckled under dynamic axial loads in a specially designed testing machine. It also outlines the development of a general mathematical model for dynamic shell response and contains a direct comparison between the experimental results and the theoretical predictions. Both regular and quasi-random axisymmetric imperfections are considered and experimentally observed buckling modes are compared to the optimum deflection functions suggested by the theoretical analysis. The mathematical model is based on a modified version of the Donnell-von Karman compatibility and equilibrium equations. A set of non-linear equations governing the shell wall displacements are developed from these using a Galerkin procedure and a solution is found by numerical integration. A five-mode deflection function which includes terms representing uniform radial expansion of the shell wall, axisymmetric and asymmetric sinusoidal deflections is used. This deflection function permits a high degree of flexibility when modelling the behaviour of specific shell geometries.

2. THEORETICAL ANALYSIS

This section describes the development of a mathematical model for prediction of the force-displacement relation and ultimate buckling load of an imperfect cylindrical shell subjected to a dynamically applied axial load.

The development is based on a modified version of the Donnell-von Karman compatibility and equilibrium equations. These are essentially a pair of fourth-order, non-linear differential equations with time and geometric co-ordinates as independent variables. Substitution of a deflection mode function and application of a Galerkin procedure transformed these equations into a series of coupled, time-dependent differential equations governing the radial motions of the shell wall. These equations were then integrated numerically to provide a time history of the behaviour of the shell under application of a dynamic load. This procedure is similar in concept to several of those described in the preceding section. However, the displacement mode function applied here was designed to permit a high degree of flexibility in the analysis of the effect of specific imperfection geometries.

2.1 Compatibility and Equilibrium Equations

The Donnell-von Karman compatibility and equilibrium equations used in this analysis were modified to include terms that accounted for the effect of radial inertia and the existence of initial imperfections. In this formulation, the shell displacements are defined with respect to a Cartesian co-ordinate system with its origin on the shell wall mid-surface, the x and y co-ordinates oriented in the axial and circumferential directions respectively and the z co-ordinate directed radially outward (see Fig.1a). Thus the axial, circumferential and radial deflections at any point on the shell are written as $u(x,y,t)$, $v(x,y,t)$ and $w(x,y,t)$, while the stress field is expressed as an AIRY stress function $f(x,y,t)$ such that

$$\frac{\partial^2 f}{\partial x^2} = N_y = h\sigma_y \qquad 2.1$$

$$\frac{\partial^2 f}{\partial y^2} = N_x = h\sigma_x \qquad 2.2$$

$$\frac{\partial^2 f}{\partial x \partial y} = -N_{xy} = -h\tau_{xy} \qquad 2.3$$

(h is the wall thickness)

The use of the AIRY stress function here serves to satisfy the two-dimensional equilibrium conditions,

$$\frac{\partial N_x}{\partial x} + \frac{\partial N_{xy}}{\partial y} = 0 \qquad 2.4$$

$$\frac{\partial N_y}{\partial y} + \frac{\partial N_{xy}}{\partial x} = 0$$

For the case of a thin-walled shell with shallow imperfections, that is, a shell satisfying the conditions:

$$h \ll R$$

$$| \underline{w}(x,y) | \ll R$$

$$\left| \frac{\partial \underline{w}}{\partial x} \right| \ll 1 \quad \left| \frac{\partial \underline{w}}{\partial y} \right| \ll 1 \qquad 2.5$$

$$R \left| \frac{\partial^2 \underline{w}}{\partial x^2} \text{ or } \frac{\partial^2 \underline{w}}{\partial y^2} \right| \leq O(1)$$

then the following equations hold;

Compatibility Equation:

$$\frac{1}{Eh} \nabla^4 f - \frac{1}{R} (w_{,xx} - \underline{w}_{,xx}) - w^2_{,xy} + \underline{w}^2_{,xy} + w_{,xx} w_{,yy} - \underline{w}_{,xx} - \underline{w}_{,yy} = 0 \qquad 2.6$$

Equilibrium Equation:

$$\frac{Eh^3}{12(1-\nu^2)} \nabla^4 (w-\underline{w}) + \frac{1}{R} f_{,xx} - w_{,xx} f_{,yy} - w_{,yy} f_{,xx} + 2w_{,xy} f_{,xy} + \rho h w_{,tt} = 0 \qquad 2.7$$

where $_{,xx} = \frac{\partial^2}{\partial x^2}$ etc.

$$\nabla^4 = \frac{\partial^4}{\partial x^4} + \frac{2\partial^4}{\partial x^2 \partial y^2} + \frac{\partial^4}{\partial y^4}$$

2.2 Deflection Modes

The radial deflection function assumed in this analysis is of the form:

$$w(x,y,t) = W_o(t) + W_1(t)\cos Kx + W_{20}(t)\cos 2Mx + W_{11}(t)\cos Mx\cos Ny + W_{02}\cos 2Ny \qquad 2.8$$

while the imperfection function has a similar form:

$$\underline{w}(x,y) = \underline{W}_1\cos Kx + \underline{W}_{20}\cos 2Mx + \underline{W}_{11}\cos Mx\cos Ny + \underline{W}_{02}\cos 2Ny \qquad 2.9$$

The first two trigonometric terms of these functions both represent axisymmetric radial wall displacements. While these terms are identical in form, the provision of two independent wavelength parameters is important in that, when investigating the behaviour of shells with sinusoidal axisymmetric imperfections, it is possible to consider either the case where the axial wavelength of the $w_{11}\cos Mx\cos Ny$ deflection mode is directly related to the wavelength of the imperfection (that is, where the imperfection is expressed as $\underline{W}_{20}\cos 2Mx$) or, where the wavelength is independent (where the imperfection is described by $\underline{W}_1\cos Kx$). The advantage of this flexibility will become more apparent later when the case of shells with imperfections whose wavelengths differ greatly from the critical wavelengths is considered.

Through the choice of appropriate values for the circumferential wave number "N" it is possible to provide geometric continuity with respect to radial deflections at $y = 0, 2\pi R$. However, the deflection function used here will not satisfy experimentally realistic end boundary conditions at $x = 0, L$. Nevertheless, it has been shown both experimentally[12] and theoretically[28] that the effects of clamped end constraints are generally localized to the regions adjacent to the ends and that for shells with reasonable length to radius ratios (greater than about 2) the effect on ultimate buckling loads is relatively small. Accordingly, for the present theoretical study, the effects of end constraints are ignored and an "infinitely long" model is considered.

2.3 Stress Function

If the assumed displacement function is substituted into the compatibility equation, the equation is identically satisfied by an AIRY stress function of the form

$$\begin{aligned} f(x,y,t) = {} & F_o(t) + F_1(t)\cos Kx + F_2(t)\cos Kx\cos 2Ny + F_3(t)\cos(K+M)x\cos NY \\ & + F_4(t)\cos(K-M)x\cos Ny + F_{20}(t)\cos 2Mx + F_{11}(t)\cos Mx\cos Ny \\ & + F_{02}(t)\cos 2Ny + F_{22}(t)\cos 2Mx\cos 2Ny + F_{31}(t)\cos 3Mx\cos Ny \\ & + F_{13}(t)\cos Mx\cos 3Ny \end{aligned} \qquad 2.10$$

where

$$F_o = -\tfrac{1}{2}\Sigma_x hy^2 - \tfrac{1}{2}\Sigma_y hx^2$$

$$F_1 = -\frac{Eh}{R}\ \frac{(W_1 - \underline{W}_1)}{K^2}$$

$$F_2 = -Eh\ \frac{4K^2N^2}{(K^2+4N^2)^2}\ (W_1 W_{02} - \underline{W}_1\ \underline{W}_{02})$$

$$F_3 = -Eh\ \frac{K^2N^2}{2((K+M)^2+N^2)^2}\ (W_1 W_{11} - \underline{W}_1\ \underline{W}_{11})$$

$$F_4 = -Eh\ \frac{K^2N^2}{2((K-M)^2+N^2)^2}\ (W_1 W_{11} - \underline{W}_1\ \underline{W}_{11})$$

$$F_{20} = -\frac{Eh}{16M^4}\ -\left[\frac{4M^2}{R}\ (W_{20} - \underline{W}_{20}) + \frac{M^2N^2}{2}\ (W^2_{11} - \underline{W}^2_{11})\right]$$

$$F_{11} = -\frac{Eh}{(M^2+N^2)}\left[\frac{M^2}{R}\ (W_{11} - \underline{W}_{11}) + 2M^2N^2(W_{20}W_{11} - \underline{W}_{20}W_{11} + W_{11}W_{02} - \underline{W}_{11}W_{02})\right]$$

$$F_{02} = -\frac{Eh}{16N^2}\left[\frac{M^2}{2}\ (W^2_{11} - \underline{W}^2_{11})\right] \qquad 2.11$$

$$F_{22} = -\frac{EhM^2N^2(W_{20}W_{02} - \underline{W}_{20}\underline{W}_{02})}{(M^2+N^2)^2}$$

$$F_{31} = -\frac{Eh2M^2N^2\ (W_{20}W_{11} - \underline{W}_{20}\underline{W}_{11})}{(9M^2+N^2)^2}$$

$$F_{13} = -\frac{Eh2M^2N^2\ (W_{11}W_{02} - \underline{W}_{11}\underline{W}_{02})}{(M^2+9N^2)^2}$$

Here Σ_x and Σ_y refer to uniform compressive stresses. A full description of the derivation of these terms is contained in Appendix A.

2.4 Mode Equilibrium Equations

The five-mode displacement and its associated stress function may now be substituted into the equilibrium equation. The displacement function chosen

here represents only an approximate solution to the equilibrium and compatibility equation set so that the equilibrium equation will not be completely satisfied. The error involved may be minimized, however, by satisfying the set of equations produced by applying a Galerkin procedure to the left side of the equilibrium equation.

Thus, if $E[w(x,y,t), f(x,y,t)] = 0$ is the equilibrium equation, then $E(W_o\ldots,F_o\ldots)$ is unequal to zero by some error. This error is minimized by satisfying the equations:

$$\int_o^{2\pi R}\int_o^{L} E(W_o,\ldots F_o,\ldots)\,dxdy = 0 \qquad 2.12$$

$$\int_o^{2\pi R}\int_o^{L} E(W_o,\ldots F_o,\ldots)\,\cos Kx\,dxdy = 0 \qquad 2.13$$

$$\int_o^{2\pi R}\int_o^{L} E(W_o,\ldots F_o,\ldots)\,\cos 2Mx\,dxdy = 0 \qquad 2.14$$

$$\int_o^{2\pi R}\int_o^{L} E(W_o,\ldots F_o,\ldots)\,\cos Mx\cos Ny\,dxdy = 0 \qquad 2.15$$

$$\int_o^{2\pi R}\int_o^{L} E(W_o,\ldots F_o,\ldots)\,\cos 2Ny\,dxdy = 0 \qquad 2.16$$

These equations become, when the integrals are evaluated (see Appendix A):

$$\rho h W_o = \frac{\Sigma_y h}{R} \qquad 2.17$$

$$\rho h W_1 = -\frac{Eh^3}{12(1-\nu^2)} K^4(W_1-\underline{W}_1) + \frac{K^2F_1}{R} + \frac{K^2N^2}{4}\left[W_{11}(F_3+F_4)+8W_{02}F_2\right] + K^2W_1\Sigma_x h \qquad 2.18$$

$$\rho h W_{20} = -\frac{4Eh^3}{3(1-\nu^2)} M^4(W_{20}-\underline{W}_{20}) + \frac{4M^2}{R}F_{20} + M^2N^2\left[W_{11}(F_{11}+F_{31}) + 8W_{02}F_{22}\right] + 4M^2W_{02}\Sigma_x h \qquad 2.19$$

$$\rho h \ddot{W}_{11} = - \frac{Eh^3}{12(1-\nu^2)} (M^2+ N^2)^2 (W_{11}-\underline{W}_{11}) + \frac{M^2}{R} F_{11}$$
$$+ 2M^2N^2\left[W_{20}(F_{11}+ F_{31})+ W_{11}(F_{20}+ F_{02}) + W_{02}(F_{11}+ F_{13})\right]$$
$$+ \frac{K^2N^2}{2} W_1 (F_3+ F_4) + M^2W_{11}\Sigma_x h + N^2W_{11}\Sigma_y h \qquad 2.20$$

$$\rho h \ddot{W}_{02} = - \frac{4Eh^3N^4}{3(1+\nu^2)} (W_{02}-\underline{W}_{02})+ M^2N^2\left[W_{11}(F_{11}+ F_{13})+ 8W_{20}F_{22}\right]$$
$$+ 2K^2N^2W_1F_2 + 4N^2W_{02}\Sigma_y h \qquad 2.21$$

The 'dot' notation on the left side of these equations refers to differentiation with respect to time.

The set of equations 2.17, 2.18, 2.19, 2.20 and 2.21 govern the radial deflection of a cylindrical shell wall subjected to time-dependent stresses. The static buckling equations are essentially identical to equations 2.17 to 2.21 except, of course, that the time differentials would be equal to zero. The static equations are simply a set of non-linear simultaneous algebraic equations instead of a group of coupled, time-dependent differential equations. Various methods have been devised to handle the general static equations. These generally involve either numerical solution schemes or simplifying assumptions. Although a full solution of the static equations is beyond the scope of this discussion, it is quite instructive to consider the very simple case of the buckling of a perfect shell in a single mode. Thus, if it is assumed that all time derivatives, all imperfections and each of $W_1(t)$, $W_{20}(t)$, $W_{02}(t)$ and Σ_y are set to zero, then Equation 2.20 may be re-written as:

$$\frac{Eh^3}{12(1-\nu^2)} (M^2+ N^2)^2 W_{11} + \frac{M^4}{(M^2+N^2)^2} \frac{Eh}{R^2} W_{11} + \frac{(M^4+ N^4)}{16} EhW^3_{11} = M^2W_{11}\Sigma_x h \qquad 2.22$$

If we further restrict our attention to the case of small, finite deflections (that is, if we consider the situation at the point of buckling), the equation becomes

$$\Sigma_x = E\left[\frac{h^2}{12(1-\nu^2)} \frac{(M^2+ N^2)^2}{M^2} + \frac{M^2}{(M^2+N^2)^2R^2}\right] \qquad 2.23$$

This is an expression for the theoretical buckling stress of a perfect shell loaded axially. It is quite simple to show that the minimum value for this stress occurs when the wavelength parameters obey the relationship

$$\frac{(M^2+ N^2)^2}{M^2} = \frac{[12(1-\nu^2)]^{1/2}}{hR} \qquad 2.24$$

This minimum stress, written as,

$$\Sigma_x = \frac{Eh}{R\,[\,3(1-\nu^2)]^{1/2}} \qquad 2.25$$

is termed the classical buckling stress.

Although Equation 2.24 does not imply any specific values for either M or N, it is worthwhile considering two special cases, namely the case where M = N so that:

$$M = N = \left[\frac{3(1-\nu^2)}{4H^2R^2}\right]^{1/4} \qquad 2.26$$

and the case where N = 0 so that:

$$M = 2\left[\frac{3}{4}\cdot\frac{(1-\nu^2)}{h^2R^2}\right]^{1/4} \qquad 2.27$$

It may be seen from Equations 2.26 and 2.27 that the wave number of the optimum axisymmetric mode is just twice the axial wave number of the optimum "checkerboard" type asymmetric mode. The two optimum modes may thus be written as $W_{20}\cos 2Mx$ and $W_{11}\cos Mx\cos Ny$ with M taking the value defined in Equation 2.26. This value is referred to as the critical axial wave number.

2.5 The Closure Condition

In addition to providing continuity in w, u and v at y = 0, $2\pi R$, it is necessary to satisfy the closure condition, that is, to assure that the circumferential distance around the shell at any point on the axis is just sufficient to close the shell without any overlapping or gaps. This condition may be expressed mathematically as

$$\int_0^{2\pi R} v_{,y}\,dy = 0 \qquad 2.28$$

where

$$v_{,y} = \frac{\sigma_y}{E} - \frac{\nu\sigma_x}{E} - \tfrac{1}{2}\left[\left(\frac{\partial w}{\partial y}\right)^2 - \left(\frac{\partial \underline{w}}{\partial y}\right)^2\right] - \frac{w-\underline{w}}{R} \qquad 2.29$$

The first two terms in this expression represent elastic strains due to local stresses in the material, the third term accounts for local slopes or folding effects and the last term takes into account the change in circumference arising from changes in the radius of the cylinder.

Recalling Equations 2.1 and 2.2:

$$\sigma_x(x,y) = \frac{1}{h}\,\frac{\partial^2 f(x,y)}{\partial y^2}$$

$$\sigma_y(x,y) = \frac{1}{h} \frac{\partial^2 f(x,y)}{\partial x^2}$$

and

$$w(x,y) = W_o + W_1 \cos Kx + W_{20} \cos 2Mx + W_{11} \cos Mx \cos Ny + W_{02} \cos Ny$$

$$\underline{w}(x,y) = \underline{W}_1 \cos Kx + \underline{W}_{20} \cos 2Mx + \underline{W}_{11} \cos Mx \cos Ny + \underline{W}_{02} \cos 2Ny$$

the closure condition may be expanded and eventually reduced to the expression

$$\Sigma_y - \nu\Sigma_x + E\left[\frac{N^2}{8}(W^2_{11} - \underline{W}^2_{11}) + N^2(W^2_{02} - \underline{W}^2_{02}) + \frac{W_o}{R}\right] = 0 \qquad 2.30$$

In the absence of any external forces such as external or internal pressure, the uniform circumferential stress Σ_y is directly related to the uniform radial inertia by Equation 2.17 so that it is possible to write:

$$\rho h W_o = \frac{\nu\Sigma_x h}{R} - \frac{Eh}{R}\left[\frac{N^2}{8}(W^2_{11} - \underline{W}^2_{11}) + N^2(W^2_{02} - \underline{W}^2_{02}) + \frac{W_o}{R}\right] \qquad 2.31$$

2.6 Axial Compression

The axial compressive deflection of the shell ends may be written as

$$\delta_x(y) = -\int_o^L u_{,x}(x,y)\, dx \qquad 2.32$$

or, on the average,

$$\delta_x = -\frac{1}{2\pi R}\int_o^{2\pi R}\int_o^L u_{,x}(x,y)\, dxdy \qquad 2.33$$

Here, as in the case of circumferential extension, the axial strain term $u_{,x}(x,y)$ is a function of both elastic stresses and radial displacements, that is;

$$u_{,x}(x,y) = \frac{\sigma_x}{E}(x,y) - \frac{\nu\sigma_y}{E}(x,y) - \frac{1}{2}\left[\left(\frac{\partial w}{\partial x}\right)^2 - \left(\frac{\partial \underline{w}}{\partial x}\right)^2\right] \qquad 2.34$$

With some algebraic manipulation then:

$$\frac{\delta_x}{L} = \frac{\Sigma_x}{E} - \frac{\nu\Sigma_y}{E} + \frac{K^2}{4}(W^2_1 - \underline{W}^2_1) + M^2(W^2_{20} - \underline{W}^2_{20}) + \frac{M^2}{8}(W^2_{11} - \underline{W}^2_{11}) \qquad 2.35$$

Equations 2.18 to 2.21 and 2.31 comprise a coupled system of differential equations with time-dependent solutions $W_o(t)$, $W_1(t)$, $W_{20}(t)$, $W_{11}(t)$ and $W_{02}(t)$

while Equation 2.35 relates the load parameters $\Sigma_x(t)$ and $\Sigma_y(t)$ to the axial compression. Together, these represent the governing equations of a cylindrical shell with regular sinusoidal imperfections subjected to a time-dependent axial compressive load.

2.7 The Four Mode Solution: A Special Case

As mentioned in Section 2.2 above, the five-mode deflection function used in this analysis provides an important degree of flexibility in that it allows for complete independence between the wavelengths of the axisymmetric imperfection mode $\underline{W}_1 \cos Kx$ and the other deflection modes. Nevertheless, a careful examination of Equations 2.18 to 2.21 (with special attention to the stress function coefficients) will reveal that the greatest degree of coupling between the various modes occurs when K = 2M. This is equivalent to saying that the two axisymmetric modes $W_1 \cos Kx$ and $W_{20} \cos 2Mx$ have merged and that the deflection function has been reduced to the form

$$w(x,y,t) = W_o(t) + W_{20}(t)\cos 2Mx + W_{11}(t)\cos Mx \cos Ny + W_{02}(t)\cos 2Ny \qquad 2.36$$

The governing equations for this particular case are identical to those derived in this chapter except that $W_1(t)$ and $\underline{W}_1$ are set to zero throughout.

2.8 Solution

The solutions for the deflection mode equations were obtained by numerically integrating Equations 2.18 to 2.21 and 2.31 on an IBM 1130 digital computer using a fourth-order Runge-Kutta algorithm. The computer program used here was written to describe the behaviour of a shell compressed axially at a pre-determined rate. Values of the radial deflection coefficients ($W_o(t)$, $W_1(t)$, $W_{20}(t)$, etc.), the axial load and non-dimensional axial load* were computed and printed for successive increments of "time" as the shell was compressed. A listing of the computer programs and several sample print-outs are contained in Appendix B.

The computer runs present what is essentially a time history of shell behaviour under axial compression. The buckling points were normally identified by a sharp drop in axial load accompanied by a rapid increase in magnitude of the radial wall deflection coefficients. Figure 2 shows the results of a typical run in graphic form.

When this mathematical model was used to simulate the buckling behaviour of a real shell specimen, the parameters h, R and L were assigned values corresponding to the thickness, radius and length of the shell, respectively. Likewise, the axisymmetric imperfection amplitude and wave-number parameters $\underline{W}_1$ and K (or $\underline{W}_{20}$ and M) were matched to the geometric characteristics of the real shell imperfections. For the theoretical representation of both "perfect" and imperfect shells, a very small initial imperfection in the $W_{11} \cdot \cos Mx \cos Ny$ mode was specified. This term was not meant as

* The non-dimensional load was obtained by dividing the actual load by the classical static buckling load of the perfect shell with equivalent dimensions.

a direct representation of a specific physical feature of the shell but rather as an initial perturbation which would trigger the growth of the radial deflection modes. In the absence of such a perturbation, the theoretical model, being mathematically perfect and immune to any disturbances, would be unable to respond to instabilities.

In contrast with the parameters such as h, R, L and K, which are fixed by the geometry of the shell configuration, the buckling mode wave numbers M and N are not based directly on shell geometry but rather chosen in such a way as to minimize the buckling loads. For perfect shells and shells with imperfections with wavelengths close to the critical value, it was generally found that the optimum wave numbers could be estimated quite closely by assuming that $M = K/2$ and calculating the value of N from Equation 2.24 or 2.26. The exact value of the optimum wave numbers was found by varying these estimates slightly and recomputing the buckling loads until a true lower bound was established.

It should be noted that all solutions were obtained for an infinite shell model, neglecting the effects of boundary conditions. Based on available work for static buckling, the load reductions associated with a clamped end constraint (which was the case for the test models) are of the order of 10%. Furthermore, the equilibrium equations did not include in-plane inertia effects. However, up to the buckling load, the prebuckling deformation is axisymmetric and thus the circumferential inertia term is zero. On the other hand, the axial inertia component is composed of contributions from the rate of the change of the closing velocity (V) and prebuckling radial acceleration terms. After an initial loading phase, the closing velocity is approximately constant and thus the axial inertia can be considered small relative to the radial inertia.

3. EXPERIMENTAL TECHNIQUE

As mentioned in the introductory chapter, a basic objective of this study has been to produce reliable experimental data on the behaviour of near-perfect and imperfect cylindrical shells subjected to dynamic loading. This implies three important steps, namely, a method of manufacturing shell specimens to very precise tolerances, a means of accurately measuring the shells and characterizing their imperfections (including both the imperfections machined into the shells for experimental purposes and those arising inadvertently from the manufacturing technique) and a method of testing the shells under controlled and reproducible conditions. In this study, several modifications of the spin-casting technique were used to produce shells with a variety of pre-determined imperfection geometries. Each shell was carefully measured and then tested on a special dynamic loading machine designed by the author specifically for these experiments (see Figure 6).

3.1 Manufacture of Shell Specimens

The material from which the experimental shell specimens were manufactured was an epoxy plastic mixed from Hysol type XC9-C419 resin and type 3561 hardener. This particular material was chosen for its consistent mechanical properties and because it could be mixed, cast and cured at normal room temperatures (thus simplifying the manufacturing procedure). Prior to the manufacture of the shells, an extensive series of tests were carried out on samples of the epoxy material to determine the stress-strain characteristics under static and dynamic loading. These experiments are discussed in Appendix C.

The shell specimens were prepared using a spin-casting or centrifugal casting technique. In its most basic form, this technique involved pouring a small quantity of liquid epoxy into a cylindrical mold which was spun at high speeds (approximately 1750 rpm) so that the material was held in a thin layer on the inner surface of the cylinder as it set (see Figure 3). By coating the inner surface of the mold with a liquid releasing agent prior to casting the shell layer, adhesion between the epoxy layer and the mold surface was eliminated and it was possible to slide the hardened shell out of the mold intact. With precise balancing and centering of the mold, this method is capable of producing extremely regular shells of essentially constant wall thickness. For example, for the two near-perfect shells used in the experimental part of this work, the maximum imperfections and thickness variations in the shell walls were less than 5% of the mean wall thickness. Geometric data on these two shells is contained in Table 1a.

Two series of shells were produced with major axisymmetric geometric imperfections. For the first series, the shells were produced with regular sinusoidal profiles machined into the inner surface of an otherwise regular and uniform shell. This gave the effect of a regular axisymmetric imperfection of the median surface of the wall combined with a sinusoidal variation in wall thickness (see Figure 1b). The manufacture of these shells began with the casting of a near-perfect shell of slightly greater thickness than required for the final imperfect shell. Before this shell blank was removed from the mold, however, the mold and shell were mounted on a lathe and carefully centered and circularized. The inner surface of the shell was then machined to the desired profile by means of a tool-bit controlled by an hydraulic tracer device. This apparatus reproduced the profile of an external template onto the inner surface of the shell. The development of this system and the preparation of the templates is described in some detail in Reference 12.

The final series of shells produced for this study had matching axisymmetric profiles on both the inner and outer surfaces, giving effectively a constant thickness shell with axisymmetric imperfections of the wall mid-surface. These shells were produced using a discardable liner technique. In this method, the mold was prepared as described above. However, before the shell was cast, releasing agent was applied to the mold and a relatively thin initial layer of epoxy was cast in place. When this layer had set, the desired profile was cut into its inner surface, exactly as had been done with the previous imperfect shells and the profiled surface was coated with releasing agent. Next, the shell layer was cast and the inner surface of this layer was subsequently machined to the same profile. The shell and the profiled liner were then removed together and the liner was split away from the shell (see Figure 4). A total of five shell specimens was produced in this fashion, four with regular sinusoidal imperfections of various amplitudes and wavelengths and a fifth in which the imperfection profile consisted of a combination of three superimposed sinusoids. This last shell, because of the irregularity of its imperfection profile and because each sinusoid contained in the profile existed only as a component of a more general wave-form , was considered to have a quasi-random imperfection profile.

The ends of each shell were cast into fitted grooves on aluminum end plates using the same epoxy plastic from which the shells had been manufactured. This procedure provided a very firm and rigid mount.

3.2 Measurement of Shell Geometry

A special rig was developed to facilitate the accurate measurement of

the geometry of the shell specimens (see Figure 5). The basic measuring elements in this rig were a pair of variable transformer-type linear displacement transducers used as contact probes. These probes were mounted on an open, movable frame so that they simultaneously contacted the shell wall at the same point on its inner and outer surfaces. A motorized lead-screw arrangement moved the probes along the shell wall, parallel to the shell axis, at a steady rate. The contact probes were connected to demodulators which provided a D.C. voltage signal proportional to the displacement of the probe heads. These signals could either be monitored directly (to provide profile measurements of the inner and outer surfaces) or added electronically by means of an operational amplifier circuit to provide a differential signal proportional to the wall thickness.

The average shell wall thickness for each shell specimen was measured by integrating the thickness outputs for a number of axial traverses of the measuring rig along the shell. These integrals were converted into thickness deviation values which were used to correct the thickness readings made close to the ends of the shell with a normal screw-type micrometers.

For the shells with imperfections cut into the inner surface only, the median surface imperfection profile was related to the thickness variation of the shell so that the imperfection amplitude could be measured quite easily from an X-Y plotter trace of the thickness profile. In the case of shells with matching profiles on both surfaces of the wall, it was necessary to measure one of the wall profiles independently as well as measuring thickness. For the thickness measurements, the arrangement of the two probes and the analogue adder tends to cancel out any effects arising from minor misalignment of the shell with respect to the measuring rig or any distortion of the shell under probe forces. When monitoring the output from a single probe, however, it was absolutely essential to have the shell and measuring rig precisely aligned and adjusted for minimum contact pressure. The traces recorded from the shells used in these experiments are shown in Figures 14 to 18.

3.3 Dynamic Testing Machine

A special pneumatically driven testing machine was designed and built for the dynamic shell tests (see Figure 6).

The basic objective in designing this machine was to provide well-controlled dynamic loads at a variety of loading rates and to accurately measure the applied load and axial end-deflection of the shell during the loading-buckling cycle. Figure 7 shows a schematic drawing of the load cylinder of the testing machine. In operation, both the upper and lower chambers of this cylinder were filled with compressed gas normally to a pressure between 50 and 100 psi. If the pressure in the upper chamber were decreased by allowing the gas to escape, the resulting pressure differential across the piston caused a compressive force on the shell. The rate of the pressure drop in the upper chamber was controlled by the size of the venting orifice and by the magnitude of the original pressure. Thus, quasi-static loading rates were obtained by relatively small openings of the vent valves in the supply control plumbing, while relatively high rates were obtained by allowing the diaphragm in the main vent to rupture. A number of chokes were manufactured with different size orifices to provide variations in the venting (and hence loading) rates. The material used for the diaphragm was thin (.002 inches) mylar sheet.

Due to the high pressures involved, the flow in the venting orifices

was supersonic over most of the venting cycle so that the pressure in the upper chamber would theoretically vary with time according to

$$P(t) = P_o(1 - e^{-kt}) \qquad 3.1$$

where P_o is the initial pressure and k is a constant depending on the orifice size, chamber volume and gas properties.

By selecting initial pressures sufficiently higher than the pressures required to buckle the shells, it was possible to obtain pre-buckling loading rates that were approximately constant with time.

For all tests, a mechanical constraint system was provided to limit the axial compression of the shell. Thus, while the shells were allowed to buckle completely, large irreversible displacements were avoided and consequently the shells could be tested many times and yet continue to yield highly reproducible results.

3.4 Instrumentation

The testing machine was fitted with instruments designed to measure and record the axial loading and deflection of the shell during the loading-buckling cycle (see Figure 7).

The axial displacement was measured with an MTI model K 45A "FOTONIC SENSOR". This instrument consisted essentially of a light source and photo-cell masked from each other and mounted adjacent to the end of a divided fibre-optic light conducting probe. The opposite end of this probe was mounted close to the underside of the lower platen of the testing machine. In operation, light from the source was piped down the fibres of the probe and directed onto a small piece of reflective aluminum foil fastened to the platen. Thus, as the platen was moved with respect to the probe, the amount of light reflected back on the end of the probe and transmitted back to the photo-cell changed. Through the use of a suitable calibration curve, the output of the photo-cell could be related to the displacement of the moving platen.

A Kistler type 902A load washer was mounted between the piston shaft and the lower platen of the testing machine to measure the axial forces exerted on the shell. For dynamic loading it was necessary to correct the forces measured at this point for the inertia forces arising from the acceleration of the platen and shell end plate. For this purpose, a Kistler type 801 accelerometer was mounted at the centre of the lower platen*. The displacement and net force signal (consisting of the load washer output less the accelerometer output, suitably attenuated) were displayed on a dual-beam oscilloscope (Tektronix type 565) and the traces from each run were recorded photographically. Typical oscilloscope photographs are shown in Figures 8 and 9. The experimental buckling loads were measured directly from these photographs, with a small adjustment being made to account for the static pre-buckling load due to the weight of the upper end plate. The platen closing velocity "V" was determined from the slope of the displacement-time curve immediately preceding buckling.

---

* The accelerometer, which consisted basically of a sprung mass, exhibited some high-frequency ringing which introduced unwanted noise into the final force signal. It was found necessary to provide a low-pass electronic filter (minus 3 db at 5000 Hz) between the accelerometer and the oscilloscope used to monitor the signals.

In addition to the normal tests, several runs were made in which various shells were photographed with a high-speed movie camera during loading and buckling. The epoxy plastic material from which the shells were manufactured was translucent and birefringent so that rather than photographing the shells directly, it was convenient to use photo-elastic techniques and to photograph the 45° isoclinic patterns as they arose in the shell. This was achieved by illuminating the shell model with a powerful quartz-halogen flood lamp, the light from which passed through a polarizing filter mounted with its polarizing axis inclined at 45° to the axis of the shell (and hence at 45° to the principal stress direction). The light was reflected from a thin layer of fine aluminum powder deposited on the inner surface of the shell and thence passed through a second polarizing filter mounted on its polarizing axis perpendicular to the axis, and onto the camera lens. The camera and the flood lamp were located as close together as possible and on the same level as the centre of the shell so that the direction of the incident light and the optical axis of the lens were as close as possible to being perpendicular to shell wall. The camera used was a HYCAM 16 mm. model with a 400 foot film capacity. This instrument was capable of operating at a rate of up to 5000 full frames per second. Because of the short exposure times resulting from the very high framing rate and the light losses due to the polarizing filters, it was necessary to use the maximum possible illumination intensity and extremely sensitive film materials. Due to the large amount of heat associated with a high intensity light beam, it was necessary to use several heat absorbing (infra-red) filters immediately adjacent to the lamp to avoid damage to the first polarizing filter and to minimuze heating of the shell specimen. Further, a variable transformer was used in the power supply to the lamp so that the amount of illumination could be regulated, full intensity being used only during the actual filming. Eastman Kodak 2475 and 2485 high-speed recording films were used in these experiments. These films were processed in highly energetic developers to achieve full contrast. Normally full 400 foot spools of film were used to insure that there would be adequate time for the camera mechanism to accelerate to its full framing rate.

Through the use of the photo-elastic technique and high speed photography, it was possible to observe, in detail, the development of internal pre-buckling strains in the shell walls. A more complete description of the photo-elastic method is found in Reference 29, while a further description of the application of the high-speed movie camera in the study of buckling is found in Reference 30.

4. DISCUSSION OF RESULTS

4.1 Preliminary Theoretical Results

Figure 10a compares a series of axial load versus time curves computed for a hypothetical near-perfect shell compressed at different rates. The axial loads in this figure are expressed in non-dimensional units obtained by dividing the computed loads (P) by the classical static buckling load of the shell (P_{cl}). Similarly, the axial compression rate is given in terms of the non-dimensional parameter Vo, equal to the closing velocity of the loading platens (V) divided by the acoustic wave speed of the plastic material $c = (E/\rho)^{1/2}$. The same data is re-plotted in a different form in Figure 10b. The curve shown here is an envelope of the maximum axial loads and represents the relationship between the dynamic buckling loads and the rate parameter Vo. The results indicate that there is a substantial increase in the magnitude of the buckling loads at the higher compression rates. This is due to the effect of inertia, which

tends to retard the growth of the wall deflections.

The influence of regular axisymmetric imperfections on dynamic buckling loads is shown in Figures 11 and 12. Figure 11 contains a family of curves showing the variation of buckling strength with imperfection amplitude (for critical wavelength imperfections) while Figure 12 shows the effect of different wavelengths with a fixed amplitude. The results given in these figures indicate that the effect of imperfections on dynamic buckling loads is qualitatively quite similar to their effect on static loads. In both cases, the buckling strength may be seriously impaired by the presence of relatively shallow imperfections. Further, the theoretical results indicate that the effect of sinusoidal imperfections is much more serious when the wavelength of the imperfection profile is close to the critical wavelength for the shell in question.

When computing the theoretical buckling loads used in constructing the graphs shown here, the "independent" wave-numbers M and N were in each case chosen to provide minimum buckling loads. In the cases where the wave-number of the axisymmetric imperfection was taken to be nearly equal to the critical wave-number, it was found that the four-mode solution (that is, the case where K = 2M) provided the lowest theoretical buckling points. However, for the special case where the imperfection wave-number was substantially smaller than the critical (that is, the imperfection wavelengths were longer than critical) it was found at the higher deflection rates that the alternative five-mode solution would yield lower results. This suggests that where the imperfection wavelengths are relatively close to the critical, the geometry of the buckling deflections will be largely predetermined by the imperfection mode shape, but that in cases of highly non-optimum imperfections, buckling mode shapes will be essentially independent of the initial imperfections, and unless these imperfections are quite large, they will have a relatively small influence on the buckling strength of the shell.

A basic objective of this study has been to provide a direct comparison of experimental and theoretical results. The dynamic loading configuration chosen as being most readily adaptable to both experimental realization and theoretical modelling was compression at a constant rate of axial deflection. This corresponds to an axial deflection function of the form

$$\delta(t) = V\ t$$

Although the dynamic testing machine used in these experiments proved capable of providing reasonable constant deflection rates under most conditions, it was apparent from the experimental results that at the higher rates, the time required to accelerate the moving piston, platen and end plate became significant when compared to the total time of the test and that the axial deflection rate was considerably lower at the beginning of the test than at the buckling point. In order to determine the theoretical consequences of this situation, a number of load-time histories were computed using a deflection function of the form

$$\delta(t) = V\ (1-e^{-\gamma t})\ t$$

The results, shown in Figure 13, indicated that variations in the loading rate during the initial stages of the test have very little influence on the ultimate buckling strength of the shell. It was concluded, therefore, that the dynamic load history of the experimental shells could be adequately characterized by a single parameter, that is, the deflection rate measured in

the linear region of the deflection-time curve immediately preceding the buckling point.

4.2 Measurements of Shell Geometry

Ten shells were manufactured for this project. These included two near-perfect shells, three shells with axisymmetric sinusoidal imperfections of various wavelengths and amplitudes machined on the inner surface only, four shells with matching inner and outer surfaces (constant thickness imperfect shells) and one shell with matching inner and outer profiles which consisted of a superposition of several sinusoids of different frequencies. The characteristics of each of these shells are summarized in Table 1.

Traces of the profiles of the imperfect shells are shown in Figure 14 to 18. For shells 3 to 5, the traces were obtained from thickness measurements and represent the median surface profiles. Due to the averaging action of the probes, any overall distortion of the shell surface away from a perfect cylinder defined by the shell ends is ignored. For shells 6 to 10, the outer surface profile and thickness were measured separately along four equally-spaced generators on each shell. In Figures 16 to 18 the upper four traces show the outside surface profiles while the lower traces show thickness variations. These traces show that the periodic thickness variations of the shells were generally small when compared to either the average thickness or to the imperfection amplitude. The thickness variations that do exist are primarily due to a slight axial misalignment of the inner and outer profiles (that is, a phase mismatch) rather than a difference between the amplitudes of the profile amplitudes. The outer surface profiles shown in these figures indicate a slight inward bow of the shell walls between the end plates. This variation in radius is more apparent than real, however, as it arises largely from deflections in the wall under pressure from the outer contact probe.

The profile measurements described here demonstrate that the shell specimens used in this study were very uniform in their overall geometry and that the random imperfections and thickness variations arising from machining errors and other manufacturing faults were generally much smaller than the prescribed imperfections.

4.3 Comparison of Theory and Experiment: Dynamic Buckling Loads

An important feature of the epoxy mixture used in the manufacture of the shell specimens is that this material is capable of sustaining quite large strains without permanent deformation. Consequently, it was possible to buckle the shells repeatedly under either static or dynamic loads without damaging the material or altering the buckling strength of the shell. This meant that an extensive series of tests at different loading rates could be made with a single specimen. The experiments described in this report represent more than two hundred buckling tests. This includes 124 carefully controlled buckling strength tests (which provided the data points shown in Figure 19 through 27), four tests which were filmed with the high speed movie camera, ten tests made with restricted axial deflections (see Section 4.5) and nearly one hundred pretest runs made during the development and calibration of the testing rig.

Figure 19 shows the experimental results obtained with two near-perfect shells, plotted together with the theoretical buckling load-deflection rate curve. These 15 experimental points lie consistently between 5% and 15% below predicted

buckling loads for the entire range of axial deflection rates. Except for this small offset, which may readily be attributed to the effects of end constraints and to small residual imperfections, the agreement between theory and experiment is very good.

The results obtained from 45 tests with the three shells with axisymmetric imperfections on the inner surface only are shown in Figures 20, 21 and 22. The theoretical buckling loads of these shells were computed using the four-mode model with initial imperfections in the $\underline{W}_{20}$ cos2Mx and $\underline{W}_{11}$ cosMxcosNy modes. In each case, the axisymmetric imperfection amplitude ($\underline{W}_{20}$) and wavelength were set equal to the amplitude and wavelength of the mid-surface imperfection, while the W_{11} cosMxcosNy term served as a small asymmetric perturbation.

When comparing the theoretical and experimental results, it is apparent that although the experimental points lie within about 20% of the theoretical curve, these points indicate a more rapid increase in dynamic buckling load with deflection rate than is predicted theoretically. In several instances, the experimental buckling loads are even higher than those predicted by the somewhat idealized theoretical model. An earlier analysis of imperfect shells of this configuration[12] had shown that for the case of static buckling, the presence of small-thickness variations has a relatively minor effect on shell stiffness and stability. For the dynamic case, however, the periodic mass distribution arising from the thickness variations evidently gives rise to inertia effects which significantly increase the dynamic strength of the shells. This effect is not considered in the mathematical model which assumed constant thickness shells.

In order to eliminate this discrepancy between theory and experiment, a further series of shells was produced with matching sinusoidal imperfection profiles on both the inner and outer surfaces so that the walls were of essentially constant thickness. The theoretical and experimental results obtained with these shells are shown in Figures 23 to 27. A total of 55 data points are reported.

For the first two shells of this series (shells number 6 and 7), the wavelengths of the axisymmetric imperfections were quite close to the theoretical critical wavelengths. In both cases, the minimum theoretical buckling loads were found using the four-mode model and in each case the agreement between theoretical and experimental buckling strength is good for the entire range of compression rates encountered in the tests. The imperfection wavelength of the third shell (shell 8) was approximately half the critical wavelength (that is, the wave-number of the axisymmetric imperfection was almost twice the critical). Here again, the minimum theoretical buckling loads were obtained using the four-mode theoretical model and the agreement between predicted buckling strength and experimental results was quite good. Shell 9 had an axisymmetric sinusoidal imperfection profile with a wavelength slightly more than twice the critical. Here, the theoretical representation of the initial buckling mode was more complicated than had been encountered before. It was found that at the lower axial deflection rates, minimum theoretical buckling loads were computed using the four-mode solution but at the higher rates, lower loads could be obtained when the five-mode model was employed. Physically, this implies that the buckling mechanism would change when different loading rates were encountered. Thus, under quasi-static or gradual loading, the buckling deflection pattern would be dominated by the imperfection and would have long axial wavelengths. At higher loading rates, however, the optimum buckling deflection modes are relatively independent of the pre-buckling deflections (which, because of inertia, are comparatively

small) and assume shapes resembling those encountered in the buckling of near-perfect shells. The maximum theoretical buckling load at a given loading rate would be given by the lower of the two predictions. The theoretical curves, together with the experimental results, are shown in Figure 26.

Except for the two near-perfect shells, the shells used in the tests described above all contained regular sinusoidal imperfections. It was recognized, however, that the imperfections encountered in industrially produced shell structures would generally be random in nature with the critical axisymmetric wave-form occurring only as a component of a more general profile. In order to simulate this situation, a shell was manufactured with an imperfection profile that consisted of three superimposed sinusoids. Although this profile was basically periodic (see Figure 18) it was similar in nature to the random imperfection case in that the critical wavelength component was contained in a more general wave-form.

The experimental results obtained from 12 tests on this shell with quasi-random imperfections are shown in Figure 27. These results are compared with two theoretical models. To obtain an upper bound estimate of the dynamic buckling strength, theoretical buckling loads were computed for a hypothetical shell with a regular sinusoidal imperfection of critical wavelength whose amplitude was equal in magnitude to the Fourier component of the general profile with the equivalent wavelength. As a lower bound, a second hypothetical case was considered of a shell with a critical wavelength sinusoidal imperfection having an amplitude equal to the root mean square value of the general imperfection function. The first of these models represents the case where it is assumed that the buckling mechanism is entirely dominated by the critical wavelength component and that the other imperfections have essentially no influence on the ultimate strength, while the second model represents the opposite extreme, that is, assuming that the effect of the various imperfection components is cumulative and independent of the actual wave-form. For the imperfection profile tested, these two models give quite different results and the experimental buckling loads all lie between the two bounds.

It has been suggested[14] that the theoretical buckling strength of the axisymmetric root mean squared amplitude model would provide a useful design load for structures incorporating thin-walled cylindrical shells with generalized random imperfections. While it must be recognized that the results presented here are for a single specimen and have no statistical signifance, it has been shown that the R.M.S. lower bound does provide a safe but no unduly conservative estimate of the dynamic buckling strength of the shell.

4.4 Comparison of Theory and Experiment: Buckling Modes

According to the mathematical model of dynamic buckling developed in Section 2 of this report, the collapse of the shells is due to the combined influence of the axisymmetric and asymmetric deflections. More specifically, the numerical results suggest that for a shell with major axisymmetric imperfections, the radial wall deflections develop in two stages (see Figure 8). During the initial or pre-buckling loading, there is a gradual increase in the amplitude of the axisymmetric imperfection wave. As the buckling point is approached, the asymmetric deflections, which have hitherto been comparatively small, begin to grow rapidly so that the buckling mode has major axisymmetric and asymmetric components.

This buckling mechanism was confirmed from high speed photographs of the 45° isoclinics observed through a system of polarizing filters. As mentioned in Section 2, this was possible because of the photo-elastic nature of the epoxy plastic. A series of frames from a film taken with the high-speed move camera during a dynamic test of shell number 3 are shown in Figure 20. This sequence includes the final stages of loading, the buckling event and the early post-buckling period. The pictures illustrate that during the pre-buckled stages, the principal observable deformations are in fact axisymmetric, but that with the onset of buckling, a regular 'checker-board' type asymmetric pattern appears. Following buckling, the isoclinic patterns begin to shift their shape and eventually the diagonally oriented diamond shaped pattern typical of buckled shells emerges. Measurements made from the photographs showed that the circumferential and axial spacing of the asymmetric pattern corresponded fairly well (within about 30%) to the circumferential wavelengths of the theoretical buckling mode.

It will be recalled that during the discussion of the dynamic buckling of shell 9, it was hypothesized that at higher deflection rates the buckling modes of this shell would be largely independent of the initial imperfection wave. A number of frames from a film taken during a high-speed run with this shell are shown in Figure 29. These photographs show that while the axisymmetric pre-buckling deflections have the same wavelength as the initial imperfection, the wavelengths of the buckling deflections are generally shorter and correspond quite closely to those which would be expected for a near-perfect shell.

A quantitative comparison between experimental and theoretical waveforms is given in Table 2.

4.5 Shell Stability Under Quasi-Stepwise Loading

The dynamic loading configuration and dynamic buckling loads considered so far in this analysis are of primarily academic interest. The designer is not particularly concerned with the conditions under which buckling occurs but rather with the loads which may be imposed without incurring instability.

A typical dynamic loading situation of significance to the engineer would be the case where an axial load increases rapidly up to a value just below the critical and then remains at that level. This is equivalent, for example, to the case where a rocket engine fires and quickly achieves a thrust nearly equal to the static buckling strength of the fuselage supporting it. It is quite clear that if the ultimate axial load on the shell exceeds the static critical load, the shell will eventually buckle, regardless of its earlier loading history. What is of interest here, however, it whether or not the momentum of the dynamic pre-buckling deflections would be sufficient to carry the shell into its buckled state even though the maximum load remains below the static stability limit. This problem has been discussed a number of times in the literature (see References 18, 19, 20 and 23). Each of these studies has dealt with the case where the axial load was applied in a stepwise fashion, that is, where the axial load increased instantaneously from zero to its maximum value, and each has shown that for imperfect shells, the dynamic stability limit lies somewhat below the static critical strength of the shell. Due to limitations in the experimental apparatus, it was not possible to physically duplicate the stepwise loading case. However, the situation was approximately simulated on the dynamic testing machine by blocking the travel of the loading platen to restrict the axial deflection (and hence axial load) of the shell. At the highest piston velocities available with

the testing machine, the rise-time of the axial load was about 1.5 milliseconds. Theoretical results computed for this quasi-stepwise deflection-time configuration indicated that at experimentally realistic deflection rates, the near-perfect shells should remain unbuckled if the maximum axial load does not exceed the static critical load. These experimental results were not entirely conclusive. In about 50% of the runs made with the testing machine adjusted so that the axial travel was slightly less than that required to buckle the shell statically, the shell remained unbuckled. This suggests that the dynamic stability limit is roughly the same as the static buckling strength. A more precise experimental investigation of this probelm is beyond the capabilities of the present experimental apparatus.

5. CONCLUSIONS

The experimental data presented in this report indicate that the experimental techniques and shell manufacturing methods adopted in this study provide the most reliable and highly reproducible means of determining the dynamic axial buckling strength of thin-walled cylindrical shells hitherto available. Further, the close agreement between experimental and theoretical results for both buckling strengths and buckling modes shows that the mathematical model chosen in this analysis adquately accounts for the principal mechanisms governing the dynamic behaviour of these structures. Specifically, it may be concluded that the buckling deflection modes of real shells are similar to those employed in this model, that the change in buckling stiffness with compression rate is principally due to the effect of inertia limiting the rate of growth of radial deflections and that the dynamic buckling strength of shells is seriously impaired by the presence of geometric imperfections, especially where these imperfections are regularly spaced at intervals close to the wavelengths of important buckling modes.

These conclusions have several important implications for the structural engineer working with designs involving shell-type members. It is very clear that the amplitude and form of the wall imperfections have a major effect on the buckling strength of shells under dynamic as well as static loading. The changes in slope of buckling load versus loading rate curves indicate that the imperfection wavelengths have an especially notable influence on dynamic shell response since the wavelengths tend to dictate the deflection modes and hence influence the fundamental frequencies of the deflections.

Although the range of dynamic loading configurations and shell geometries considered in this study was restricted by limitations in the experimental apparatus, the general success of the mathematical model suggests that an analytic approach based on this model could be used very profitably to explore a broad spectrum of problems in shell design for dynamic load situations.

It has been pointed out by Professor J. Hutchinson[36] that the choice of the loading rate parameter, V/c, does not permit the results, as plotted, to be compared to other cylinder configurations. The suggested non-dimensional parameter employs the period of vibration of the classical "square-wave" mode ($T^{(1)} = 2\pi\sqrt{2}\ R/c$) and the time required for the shell to reach the critical "static" strain for buckling

$$\left(T^{(2)} = \frac{\epsilon_{cr}}{\dot{\epsilon}} = \frac{h}{R[3(1-\nu^2)]^{1/2}} \Big/ V/L\right)$$

in the form:

$$\frac{T^{(1)}}{T^{(2)}} = \frac{2\pi\sqrt{6}(1-\nu^2)^{\frac{1}{2}}R^2}{hL} \quad (V/c)$$

It would appear that this parameter is more suitable, taking into account both the shell geometry and dynamic effects.

c

REFERENCES

1. Donnell, L. H. — A New Theory for the Buckling of Thin Cylinders Under Axial Compression and Bending. Trans. ASME., Vol. 56, 1934.

2. von Karman, T.
Tsien, Hsue-Shen. — The Buckling of Thin Cylindrical Shells Under Axial Compression, Journal of the Aeronautical Sciences, Vol. 8, No. 8, June 1941.

3. Hoff, N. J.
Madsen, W. A.
Mayers, J. — Post-Buckling Equilibrium of Axially Compressed Circular Cylindrical Shells. AIAA Journal, Vol. 4, No. 1, 1966.

4. Koiter, W. T. — On the Stability of Elastic Equilibrium (in Dutch with English Summary), Thesis, Delft, Amsterdam, 1945; also available as NASA TT F-10, 833, March, 1967.

5. Koiter, W. T. — The Effect of Axisymmetric Imperfections on the Buckling of Cylindrical Shells Under Axial Compression, Proceedings of The Royal Netherlands Academy of Sciences, Amsterdam, Series B, Vol. 66, No. 5, 1963.

6. Hutchinson, J. W. — Axial Buckling of Pressurized Imperfect Cylindrical Shells, AIAA Journal, Vol. 3, No. 8, August, 1965.

7. Dym, C. L.
Hoff, N. J. — Perturbation Solutions for the Buckling Problems of Axially Compressed Thin Cylindrical Shells of Infinite or Finite Length, Trans. ASME, J. Applied Mech., Dec, 1968.

8. Danielson, D. A.
Simmonds, J. G. — Accurate Buckling Equations for Arbitrary and Cylindrical Elastic Shells, Int. J. Engr. Sci. Vol. 7, Pergamon, London, 1969.

9. Amazigo, J. C. — Buckling Under Axial Compression of Long Cylindrical Shells with Random Axisymmetric Imperfections, Quarterly of Applied Mathematics, Vol. XXVI, No. 4, Jan, 1969.

10. Hutchinson, J. W.
Tennyson, R. C.
Muggeridge, D. B. — The Effect of Local Axisymmetric Imperfection on the Buckling Behaviour of a Circular Cylindrical Shell Under Axial Compression, Paper 70-103, AIAA 8th Aerospace Sciences Meeting, New York, 1970.

11. Tennyson, R. C. — An Experimental Investigation of the Buckling of Circular Cylindrical Shells in Axial Compression Using the Photoelastic Technique, University of Toronto, UTIAS Report No. 102, 1964.

12. Muggeridge, D. B. — The Effect of Initial Axisymmetric Shape Imperfections on the Buckling Behaviour of Circular Cylindrical Shells Under Axial Compression, University of Toronto, UTIAS Report No. 148, Dec, 1969.

13. Arbocz, J. Babcock, C. D. — Experimental Investigation of the Effect of General Imperfections on the Buckling of Cylindrical Shells, Trans ASME, J. Applied Mech., Series E, Vol. 36, March 1969.

14. Tennyson, R. C. Muggeridge, D. B. Caswell, R. D. — New Design Criteria for Predicting Buckling of Cylindrical Shells Under Axial Compression. J. Spacecraft and Rockets, Vol. 8, No. 10, Oct, 1971.

15. Hoff, N. J. — Thin Shells in Aerospace Structures, Aeronautics and Astronautics, Feb, 1967.

16. Stein, M. — Some Recent Advances in the Investigation of Shell Buckling, AIAA J. Vol. 6, No.12, Dec, 1968.

17. Budiansky, B. Hutchinson, J. W. — A Survey of Some Buckling Problems, AIAA J. Vol. 4, No. 9, Sept, 1966.

18. Budiansky, B. — Dynamic Buckling of Elastic Structures: Criteria and Estimates, Dynamic Stability of Structures, Pergamon, New York, 1966.

19. Hutchinson, J. W. Budiansky, B. — Dynamic Buckling Estimates, AIAA J. Vol. 4, No.3, March 1966.

20. Danielson, D. A. — Dynamic Buckling of Imperfection Sensitive Structures from Perturbation Procedures, AIAA J. Vol. 7, No. 8, July 1969.

21. Agamirov, V. L. Vol'mir, A. S. — Behaviour of Cylindrical Shells Under Dynamic Loading by Hydrostatic Pressure or by Axial Compression, Bull. Acad. Sci. USSR, Div.Tech. Sci., Mechanics and Machine Construction No. 3, 1959. English Translation available ARS J. Supplement, Jan, 1961.

22. Coppa, A. P. Nash, W. A. — Dynamic Buckling of Shell Structures Subject to Longitudinal Impact. ASD TDR 62-744, Dec, 1962.

23. Roth, R. S. Klosner, J. M. — Non-linear Response of Cylindrical Shells with Initial Imperfections Subjected to Dynamic Axial Loads AIAA Aerospace Sciences Meeting, New York, Jan, 1964.

24. Bieniek, M. P. Fan, T. C. Lackman, L. M. — Dynamic Stability of Cylindrical Shells, AIAA J. Vol. 4, No. 3, March 1966.

25. Dym, C. L. — On The Dynamics of a Shell in a Testing Machine, Int. J. Non-Linear Mech., Vol. 4, Pergamon, London, 1969.

26. Dietz, W. K. — On the Dynamic Stability of Eccentrically Reinforced Circular Shells, Syracuse University Research Inst. Tech. Rept. No. 1620. 1245-60, Jan, 1967.

27. Lindberg, H. E. Herbert, R. E. — Dynamic Buckling of a Thin Cylindrical Shell Under Axial Impact, Poulter Res. Lab. Tech. Rept. 001-65, Feb, 1965.

28. Almroth, B. O. — Influence of Edge Conditions on the Stability of Axially Compressed Cylindrical Shells, AIAA J., Vol. 4, No. 1, Jan, 1966.

29. Tennyson, R. C. — A Review of the Theory of Photo-elasticity, UTIAS Review No. 23, Dec, 1962.

30. Tennyson, R. C. Tulk, J. D. Riciatti, R. — Analysis of the Collapse of Cylindrical Shells Using High Speed Photography. J. of the Soc. of Motion Picture and Television Engineers, June, 1971.

31. Schwieger, H. Spuida, C. — Untersuchungen über die dynamische Stabilität axial gestobener Zylinderschalen. Deutsche Forschungsund Versuchsanstalt für Festigkeit Mülheim, Nov, 1969.

32. Zimcik, D. G. — An Experimental Investigation of the Properties of Linear Visco-Elastic Solids Subjected to Dynamic Loading, B.A.Sc. Thesis, Faculty of Applied Science and Engineering, University of Toronto, March 1970.

33. Thurston, G. A. Freeland, M. A. — Buckling of Imperfect Cylinders Under Axial Compression, NASA CR-541, 1966.

34. Olson, M. D. Evensen, D. A. — Non-linear Flutter of a Circular Cylindrical Shell in Supersonic Flow, NRC Aeronautical Report LR 486, Dec, 1967. Also available as NASA TN D 4265.

35. Duncan, W. J. — Galerkin's Method in Mechanics and Differential Equations, A.R.C. R. & M. No. 1798 (3287) 1937.

36. Hutchinson, J. W. — A Note on Non-dimensional Rate Parameter, Private Communication, Harvard University, May, 1972.

APPENDIX A:

I: DERIVATION OF AIRY STRESS FUNCTION

As explained in Section 2.1, the compatibility equation for an imperfect cylindrical shell may be written as (see Equation 2.6):

$$\frac{1}{Eh}\nabla^4 f = \frac{1}{R}(w_{,xx} - \underline{w}_{,xx}) + w^2_{,xy} - \underline{w}^2_{,xy} - w_{,xx}\underline{w}_{,yy} + \underline{w}_{,xx}\underline{w}_{,yy} \qquad A.1$$

If it is assumed that the displacement function w takes the form

$$w(x,y,t) = W_o(t) + W_1(t)\cos Kx + W_{20}(t)\cos 2Mx + W_{11}(t)\cos Mx\cos Ny + W_{02}(t)\cos 2Ny \qquad A.2$$

and that the imperfection function has the form

$$\underline{w}(x,y) = \underline{W}_1\cos Kx + \underline{W}_{20}\cos 2Mx + \underline{W}_{11}\cos Mx\cos Ny + \underline{W}_{02}\cos 2Ny \qquad A.3$$

then the right-hand side of the compatibility equation may be re-written as follows:

$$\begin{aligned}\frac{1}{Eh}\nabla^4 f = \frac{1}{R}\Big\{&\Big[-K^2(W_1-\underline{W}_1)\cos Kx - 4M^2(W_{20}-\underline{W}_{20})\cos 2Mx \\ &- M^2(W_{11}-\underline{W}_{11})\cos Mx\cos Ny\Big] + M^2N^2(W^2_{11}-\underline{W}^2_{11})\sin^2 Mx\sin^2 Ny \\ &-\Big[-K^2W_1\cos Kx - 4M^2W_{20}\cos 2Mx - M^2W_{11}\cos Mx\cos Ny\Big] \\ &\Big[-N^2W_{11}\cos Mx\cos Ny - 4N^2W_{02}\cos 2Ny\Big] \\ &+\Big[-K^2\underline{W}_1\cos Kx - 4M^2\underline{W}_{20}\cos 2Mx - M^2\underline{W}_{11}\cos Mx\cos Ny\Big] \\ &\Big[-N^2\underline{W}_{11}\cos Mx\cos Ny - 4N^2\underline{W}_{02}\cos 2Ny\Big]\end{aligned} \qquad A.4$$

When the above equation is fully expanded, there are several higher order trionometric products which may be reduced using the following identities:

$$\begin{aligned}&\cos^2 Mx\cos^2 Ny - \sin^2 Mx\sin^2 Ny = \tfrac{1}{2}\cos 2Mx + \tfrac{1}{2}\cos 2Ny \\ &\cos Kx\cos Mx\cos Ny = \tfrac{1}{2}\cos(K+M)x\cos Ny + \tfrac{1}{2}\cos(K-M)x\cos Ny \\ &\cos 2Mx\cos Mx\cos Ny = \tfrac{1}{2}\cos 3Mx\cos Ny + \tfrac{1}{2}\cos Mx\cos Ny \\ &\cos Mx\cos Ny\cos 2Ny = \tfrac{1}{2}\cos Mx\cos Ny + \tfrac{1}{2}\cos Mx\cos 3Ny\end{aligned} \qquad A.5$$

On expanding and collecting terms, Equation A.4 becomes:

$$\frac{1}{Eh}\nabla^4 f = -\frac{K^2}{R}(W_1-\underline{W}_1)\cos Kx - \left[\frac{4M^2}{R}(W_{20}-\underline{W}_{20}) + \frac{M^2N^2}{2}(W_{11}^2-\underline{W}_{11}^2)\right]\cos 2Mx$$

$$-\frac{M^2N^2}{2}(W_{11}^2-\underline{W}_{11}^2)\cos 2Ny - \left[\frac{M^2}{R}(W_{11}-\underline{W}_{11}) + 2M^2N^2(W_{20}W_{11}-\underline{W}_{20}\underline{W}_{11}\right.$$

$$\left.+ W_{11}W_{02}-\underline{W}_{11}\underline{W}_{02})\right]\cos Mx\cos Ny - 2M^2N^2(W_{20}W_{11}-\underline{W}_{20}\underline{W}_{11})\cos 3Mx\cos Ny$$

$$-2M^2N^2(W_{11}W_{02}-\underline{W}_{11}\underline{W}_{02})\cos Mx\cos 3Ny$$

$$-16M^2N^2(W_{20}W_{02}-\underline{W}_{20}\underline{W}_{02})\cos 2Mx\cos 2Ny$$

$$-4K^2N^2(W_1W_{02}-\underline{W}_1\underline{W}_{02})\cos Kx\cos 2Ny - \frac{K^2N^2}{2}(W_1W_{11}-\underline{W}_1\underline{W}_{11})$$

$$\cdot\cos(K+M)x\cos Ny - \frac{K^2N^2}{2}(W_1W_{11}-\underline{W}_1\underline{W}_{11})\cos(K-M)x\cos Ny \qquad A.6$$

This equation may be satisfied if it is assumed that the stress function "f" has the form

$$f(x,y,t) = F_1(t)\cos Kx + F_2(t)\cos Kx\cos 2Ny + F_3(t)\cos(K+M)x\cos Ny$$

$$+ F_4(t)\cos(K-M)x\cos Ny + F_{20}(t)\cos 2Mx + F_{11}(t)\cos Mx\cos Ny$$

$$+ F_{02}(t)\cos 2Ny + F_{31}(t)\cos 3Mx\cos Ny + F_{13}(t)\cos Mx\cos 3Ny$$

$$+ F_{22}(t)\cos 2Mx\cos 2Ny - \frac{\Sigma_x h}{2}y^2 - \frac{\Sigma_y h}{2}x^2 \qquad A.7$$

With this premise, the left hand side of the compatibility equation becomes:

$$\frac{1}{Eh}\nabla^4 f = \frac{1}{Eh}\left[K^4F_1\cos Kx + (K^2+4N^2)^2F_2\cos Kx\cos 2Ny + ((K+M)^2+N^2)^2\right.$$

$$\cdot\ F_3\cos(K+M)x\cos Ny + ((K-M)^2+N^2)^2F_4\cos(K-M)x\cos Ny$$

$$+\ 16M^4F_{20}\cos 2Mx + (M^2+N^2)^2F_{11}\cos Mx\cos Ny + 16N^4F_{02}\cos 2Ny$$

$$+\ (9M^2+N^2)^2F_{31}\cos 3Mx\cos Ny + (M^2+9N^2)^2F_{13}\cos Mx\cos 3Ny$$

$$\left.+\ 16(M^2+N^2)^2F_{22}\cos 2Mx\cos 2Ny\right] \qquad A.8$$

For the compatibility equation to remain valid for all x and y, it is necessary to equate the coefficients related to each trigonometric expression. Thus:

cosKx coefficients:

$$\frac{K^4 F_1}{Eh} = - \frac{K^2}{R} (W_1 - \underline{W}_1)$$

cosKxcos2Ny coefficients:

$$(K^2 + 4N^2)^2 \frac{F_2}{Eh} = - 4K^2N^2 (W_1 W_{02} - \underline{W}_1 \underline{W}_{02})$$

cos(K+M)x cosNy coefficients:

$$((K+M)^2 + N^2)^2 \frac{F_3}{Eh} = - \frac{K^2N^2}{2} (W_1 W_{11} - \underline{W}_1 \underline{W}_{11})$$

cos(K-M)x cosNy coefficients:

$$((K-M)^2 + N^2)^2 \frac{F_4}{Eh} = - \frac{K^2N^2}{2} (W_1 W_{11} - \underline{W}_1 \underline{W}_{11})$$

cos2Mx coefficients:

$$16M^4 \frac{F_{20}}{Eh} = - \left[\frac{4M^2}{R} (W_{20} - \underline{W}_{20}) + \frac{M^2N^2}{2} (W_{11}^2 - \underline{W}_{11}^2) \right]$$

cosMxcosNy coefficients:

$$(M^2 + N^2)^2 \frac{F_{11}}{Eh} = -\left[\frac{M^2}{R} (W_{11} - \underline{W}_{11}) + 2M^2N^2 (W_{20}W_{11} - \underline{W}_{20}\underline{W}_{11} + W_{11}W_{02} - \underline{W}_{11}\underline{W}_{02}) \right]$$

cos2Ny coefficients:

$$16N^4 \frac{F_{02}}{Eh} = \frac{M^2N^2}{2} (W_{11}^2 - \underline{W}_{11}^2)$$

cos3MxcosNy coefficients:

$$(9M^2 + N^2)^2 \frac{F_{13}}{Eh} = 2M^2N^2 (W_{11}W_{20} - \underline{W}_{11} \underline{W}_{20})$$

cosMxcos3Ny coefficients:

$$(M^2 + 9N^2)^2 \frac{F_{13}}{Eh} = 2M^2N^2 (W_{11}W_{02} - \underline{W}_{11} \underline{W}_{02})$$

cos2Mxcos2Ny coefficients:

$$16(M^2 + N^2)^2 \quad \frac{F_{22}}{Eh} = - 16M^2N^2 \quad (W_{20}W_{02} - \underline{W}_{20}\underline{W}_{02}) \qquad A.9$$

It is a simple matter to re-write this set of equations as expressions for the stress function coefficients F_1, F_2, etc. (see Equation 2.11). The stress function f(x,y,t) is thus completely determined by the displacement field w(x,y,t) and uniform stresses (Σ_x and Σ_y) existing in the shell.

II: SOLUTION OF EQUILIBRIUM EQUATION

The equilibrium equation introduced in Section 2.1 is as follows (see Equation 2.7):

$$\frac{Eh^3}{12(1-\nu^2)} \nabla^4 (w-\underline{w}) + \frac{1}{R} \; f_{,xx}(-w_{,xx})f_{,yy} - w_{,yy}f_{,xx} + 2w_{,xy}f_{,xy} + \rho h w_{,tt} = 0 \qquad A.10$$

If the trigonometric series representation of the deflection and stress functions given above are substituted into the left hand side of this equation, one obtains the expression,

$$\frac{Eh}{12(1-\nu^2)} \Big[K^4(W_1 - \underline{W}_1)\cos Kx + 16M^4 (W_{20} - \underline{W}_{20}) \cos 2Mx$$

$$+ (M^2+N^2)^2 (W_{11} - \underline{W}_{11})\cos Mx\cos Ny + 16N^2 W_{02}\cos 2Ny \Big] - \frac{1}{R} \Big[K^2 F_1 \cos Kx$$

$$+ K^2 F_2 \cos Kx\cos 2Ny + (K+M)^2 F_3 \cos(K+M)x \cos Ny + (K-M)^2 F_4 \cos(K-M)x \cos Ny$$

$$+ 4M^2 F_{20}\cos 2Mx + M^2 F_{11}\cos Mx\cos Ny + 9M^2 F_{31}\cos 3Mx\cos Ny + M^2 F_{13}\cos Mx\cos 3Ny$$

$$+ 4M^2 F_{22}\cos 2x\cos 2Ny + \Sigma_y h \Big] - \Big[K^2 W_1 \cos Kx + 4M^2 W_{20}\cos 2Mx$$

$$+ M^2 W_{11}\cos Mx\cos Ny \Big] \Big[4N^2 F_2 \cos Kx\cos 2Ny + N^2 F_3 \cos(K+M)x \cos Ny$$

$$+ N^2 F_4 \cos(K-M)x \cos Ny + 4N^2 F_{02}\cos 2Ny + N^2 F_{11}\cos Mx\cos Ny$$

$$+ N^2 F_{31}\cos 3Mx\cos Ny + 9N^2 F_{13}\cos Mx\cos 3Ny + 4N^2 F_{22}\cos 2Mx\cos 2Ny + \Sigma_x h \Big]$$

$$- \Big[N^2 W_{11}\cos Mx\cos Ny + 4N^2 W_{02}\cos 2Ny \Big] \Big[K^2 F_1 \cos Kx + K^2 F_2 \cos Kx\cos 2Ny$$

$$+ (K+M)^2 F_3 \cos(K+M)x \cos Ny + (K-M)^2 F_4 \cos(K-M)x \cos Ny + 4M^2 F_{20}\cos 2Mx$$

$$+ M^2 F_{11}\cos Mx\cos Ny + 9M^2 F_{31}\cos 3Mx\cos Ny + M^2 F_{13}\cos Mx\cos 3Ny$$

$$+ 4M^2 F_{22}\cos 2Mx\cos 2Ny + \Sigma_y h \Big] + 2 \Big[MNW_{11}\sin Mx\sin Ny \Big] \Big[2KNF_2 \sin Kx\sin 2Ny$$

$$+ (K+M)NF_3 \sin(K+M)x \sin Ny + (K-M)NF_4 \sin(K-M)\sin Ny$$

$$+ MNF_{11}\sin Mx\sin Ny + 3MNF_{31}\sin 3Mx\sin Ny + 3MNF_{13}\sin Mx\sin 3Ny$$

$$+ 4MNF_{22}\sin 2Mx\sin 2Ny\Big] + \rho h\ddot{W}_1\cos Kx + \rho h\ddot{W}_{20}\cos 2Mx + \rho h\ddot{W}_{11}\cos Mx\cos Ny$$

$$+ \rho h\ddot{W}_{02}\cos 2Ny + \rho h\ddot{W}_o = 0 \qquad \text{A.11}$$

If Equation A.11 is expanded and the trigonometric coefficients collected, it then becomes:

$$\left[\frac{Eh^3}{12(1-\nu^2)}K^4(W_1 - \underline{W}_1) - \frac{K^2}{R}F_1 - K^2W_1\Sigma_x h + \rho hW_1\right]\cos Kx$$

$$+ \left[\frac{4Eh^3}{3(1-\nu^2)}M^4(W_{20} - \underline{W}_{20}) - \frac{4M^2}{R}F_{20} - 4M^2W_{20}\Sigma_x h + \rho h\ddot{W}_{20}\right]\cos 2Mx$$

$$+ \left[\frac{Eh^3}{12(1-\nu^2)}(M^2+N^2)^2(W_{11} - \underline{W}_{11}) - \frac{M^2}{R}F_{11} - M^2W_{11}\Sigma_x h - N^2W_{11}\Sigma_y h + \rho h\ddot{W}_{11}\right]\cos Mx \cdot \cos Ny$$

$$+ \left[\frac{4Eh}{3(1-\nu^2)}N^4(W_{02} - \underline{W}_{02}) - 4N^2W_{02}\Sigma_y h + \rho hW_{02}\right]\cos 2Ny$$

$$- \left[\frac{K^2}{R}F_2 + 4K^2N^2(W_1F_{02} + W_{02}F_1)\right]\cos Kx\cos 2Ny - \frac{(K-M)^2}{R}F_4\cos(K-M)x\cos Ny$$

$$- (M^2 + (K-M)^2)N^2W_{11}F_4\cos Mx\cos(K-M)x\cos^2 Ny - M^2N^2W_{11}F_{11}\cos 2Mx$$

$$+ 2(K-M)MN^2W_{11}F_{11}\sin Mx\sin(K-M)x\sin^2 Ny - \frac{(K+M)^2}{R}F_3\cos(K+M)x\cos Ny$$

$$- \frac{9M^2}{R}F_{31}\cos 3Mx\cos Ny - \left[\frac{4M^2}{R}F_{22} + 16M^2N^2W_{20}F_{02} + 16M^2N^2W_{02}F_{20}\right]\cos 2Mx\cos 2Ny$$

$$- \frac{M^2F_{13}}{R}\cos Mx\cos 3Ny - 4K^2N^2W_1F_2\cos^2 Kx\cos 2Ny - 16M^2N^2W_{20}F_{22}\cos^2 2Mx\cos 2Ny$$

$$- ((K+M)^2 + M^2)N^2W_{11}F_3\cos Mx\cos(K+M)x\cos^2 Ny - M^2N^2W_{11}F_{11}\cos 2Ny$$

$$- 10M^2N^2W_{11}F_{31}\cos Mx\cos 3Mx\cos^2 Ny + 2(K+M)MN^2W_{11}F_3\sin Mx\sin(K+M)x\sin^2 Ny$$

$$+ 6M^2N^2W_{11}F_{31}\sin Mx\sin 3Mx\sin^2 Ny - K^2N^2W_1F_3\cos Kx\cos(K+M)x\cos Ny$$

$$- K^2N^2W_1F_{31}\cos Kx\cos 3Mx\cos Ny - 4M^2N^2W_{20}F_{31}\cos 2Mx\cos 3Mx\cos Ny$$

$$- 4M^2N^2W_{20}F_3\cos 2Mx\cos(K+M)x\cos Ny - K^2N^2W_1F_4\cos Kx\cos(K-M)x\cos Ny$$

$$
\begin{aligned}
&- K^2N^2\,(W_1F_{11} + W_{11}F_1)\cos Mx\cos Kx\cos Ny - 4M^2N^2W_{20}F_4\cos 2Mx\cos(K-M)x\,\cos Ny \\
&- 4M^2N^2\,(W_{11}F_{20} + W_{20}F_{11})\,\cos Mx\cos 2Mx\cos Ny + (4K^2N^2W_1F_{22} + 16M^2N^2W_{20}F_2) \\
&\cdot \cos Kx\cos 2Mx\cos 2Ny - 9K^2N^2W_1F_{13}\cos Kx\cos Mx\cos 3Ny \\
&- 36M^2N^2W_{20}F_{13}\cos Mx\cos 2Mx\cos 3Ny - (M^2N^2W_{11}F_2 + K^2N^2W_{11}F_2) \\
&\cdot \cos Mx\cos Kx\cos Ny\cos 2Ny - 8M^2N^2W_{11}F_{22}\cos Mx\cos 2Mx\cos Ny\cos 2Ny \\
&+ 4KMN^2W_{11}F_2\sin Mx\sin Kx\sin Ny\sin 2Ny + 8M^2N^2W_{11}F_{22}\sin Mx\sin 2Mx\sin Ny\sin 2Ny \\
&- 4M^2N^2(W_{02}F_{11} + W_{11}F_{02})\cos Mx\cos Ny\cos 2Ny - 4(K-M)N^2W_{02}F_4\cos(K-M)x\,\cos Ny \\
&\qquad\qquad\qquad\qquad\qquad\qquad\qquad\qquad\qquad\qquad\qquad\qquad\qquad\qquad \cdot \cos 2Ny \\
&- 10M^2N^2W_{11}F_{13}\cos^2 Mx\cos Ny\cos 3Ny + 6M^2N^2W_{11}F_{13}\sin^2 Mx\sin Ny\sin 3Ny \\
&- 4(K+M)^2N^2W_{02}F_3\cos(K+M)x\,\cos Ny\cos 2Ny - 36M^2N^2W_{02}F_{31}\cos 3Mx\cos Ny\cos 2Ny \\
&- 4K^2N^2W_{02}F_2\cos Kx\cos^2 2Ny - 16M^2N^2W_{02}F_{22}\cos 2Mx\cos^2 2Ny \\
&- 4M^2N^2W_{02}F_{13}\cos Mx\cos 2Ny\cos 3Ny - \frac{\Sigma_y h}{R} + \rho h\ddot{W}_o = 0
\end{aligned}
\qquad \text{A.12}
$$

Although it would be possible to apply the Galerkin procedure to the above expression and evaluate the integrals (Equations 2.12 to 2.15) directly, it is possible to achieve identical results with considerably less effort by rearranging this expression in a form that avoids multiples of the trigonometric terms and by using the orthogonality property:

$$\int_o^{2\pi} \cos i\,x\,\cos j\,x\,dx = 0 \text{ if } i \neq j \qquad \text{A.13}$$

This rearrangement of expression A.12 involves the use of the following trigonometric identities:

$$
\begin{aligned}
\cos A\ \cos B &= \tfrac{1}{2}\cos(A+B)x + \tfrac{1}{2}\cos(A-B)x \\
\sin A\ \sin B &= \tfrac{1}{2}\cos(A-B)x - \tfrac{1}{2}\cos(A+B)x
\end{aligned}
\qquad \text{A.14}
$$

After these transformations have been made and the terms collected according to their trigonometric coefficients, the equilibrium expression becomes:

$$\left[\frac{Eh^3}{12(1-\nu^2)} K^4 (W_1 - \underline{W}_1) - \frac{K^2}{R} F_1 - K^2 W_1 \Sigma_x h - \frac{K^2N^2}{4} (W_{11}F_3 + W_{11}F_4 + 8W_{02}F_2) \right.$$

$$\left. + \rho h \ddot{W}_1 \right] \cos Kx + \left[\frac{4Eh^3}{3(1-\nu^2)} M^4 (W_{20} - \underline{W}_{20}) - \frac{4M^2}{R} F_{20} - 4M^2 W_{20} \Sigma_x h - M^2N^2 (W_{11}F_{11} \right.$$

$$\left. + W_{11}F_{31} + 8W_{02}F_{22}) + \rho h \ddot{W}_{20} \right] \cos 2Mx + \left[\frac{Eh^3}{12(1-\nu^2)} (M^2+N^2)^2 (W_{11} - \underline{W}_{11}) \right.$$

$$- \frac{M^2}{R} F_{11} - M^2 W_{11} \Sigma_x h - N^2 W_{11} \Sigma_y h - 2M^2N^2 (W_{20}(F_{11} + F_{31}) + W_{11}(F_{20} + F_{02})$$

$$\left. + W_{02} (F_{11} + F_{13})) - \frac{K^2N^2}{2} W_1 (F_3 + F_4) + \rho h \ddot{W}_{11} \right] \cos Mx \cos Ny$$

$$+ \left[\frac{4Eh^3}{3(1-\nu^2)} N^4 (W_{02} - \underline{W}_{02}) - 4N^2 W_{02} \Sigma_y h - M^2N^2 (W_{11}(F_{11} + F_{13}) + 8W_{20}F_{22}) \right.$$

$$\left. - 2K^2N^2 W_1 F_2 + \rho h \ddot{W}_{02} \right] \cos 2Ny + \left[\; . \; . \; . \; \right] \cos 3Mx \cos Ny$$

$$+ \left[\; . \; . \; . \; \right] \cos (M+K)x \cos Ny + \; . \; . \; . \; - \frac{\Sigma_y h}{R} + \rho h \ddot{W}_o = 0 \qquad \text{A.15}$$

Applying the Galerkin procedure to this equation is equivalent to simply equating the coefficients of the appropriate trigonometric terms to zero. This results in Equations 2.17 to 2.21 of the main text.

APPENDIX B

COMPUTER LISTINGS AND OUTPUTS

This section contains a listing of the computer programs used to integrate the set of time-dependent differential Equations 2.17 to 2.21 and a set of sample outputs. The program is written in Fortran IV language and is designed to run on the IBM 1130 computer. The subroutine RKGIL referred to in this program is a fourth-order Runge-Kutta integration algorithm supplied by IBM as part of the standard scientific systems package for this machine. Two versions of the program and two versions of the subroutine NYST are given here, one for use when considering the general five-mode displacement function and one for use with the four-mode approximation.

FIVE MODE MODEL

```
// FOR
* LIST SOURCE PROGRAM
* IOCS (1132 PRINTER,CARD,DISK)
* ONE WORD INTEGERS
C     FIVE MODE (THREE WAVENUMBER) RUNGE KUTTA SCHEME
C
C * * * * * * * * * * * * * * * * * * * * * * * * * * * * * * * * * * * * * * *
C     ITN              NO. OF WAVENUMBER COMBINATIONS PROVIDED
C     ISHEL            SHELL NUMBER
C     C,A,B            AXIAL + CIRCUMFERENTIAL WAVENUMBERS (=K,M,N)
C     L                SHELL LENGTH
C     R                SHELL RADIUS
C     H                SHELL THICKNESS
C     W1,WTO WOO,WOT   IMPERFECTION AMPLITUDES (W1,W20,W11,W02
C                      MODES RESPECTIVELY)
C     Y(1)...Y(5)      RADIAL DEFLECTIONS
C     Y(6)...Y(10)     TIME DERIVATIVES OF Y(1) ETC.
C     T                TIME PARAMETER (TIME/ONE-DIM. WAVESPEED)
C     TR               REAL TIME
C     VO               AXIAL VELOCITY PARAMETER
C                      (VELOCITY/ONE-DIM.WAVESPEED)
C     DISP             AXIAL DISPLACEMENT OF SHELL END
C     PAX              AXIAL LOAD
C     PCR              CLASSICAL AXIAL BUCKLING LOAD
C     SIGEX            AXIAL STRESS
C    AS,BS,DEL         STARTING POINT, END POINT AND INCREMENT
C                      FOR RUNGE-KUTTA CYCLE
C
      EXTERNAL NYST
      DIMENSION Y(10),P(5)
```

```
C       THREE WAVE-NUMBER RUNGE-KUTTA SCHEME
        READ(2,200) ITN
        DO 2 I=1,ITN
        READ (2,201) A,B
 200    FORMAT (I10)
 201    FORMAT (2F10.5)
        ISHEL = 9
        C= 2.282
        H=0.01746
        R=3.900
        W1=-0.00294
        WTO=0.0
        WOO=0.00001
        WOT=0.0
        VO=0.0001
        DO 1 J=1,5
        STD=0.0
        P(2)=VO
        P(3)=A
        P(4)=B
        WRITE (3,100) ISHEL,VO,W1,WTO,WOO,WOT,C,A,B
 100    FORMAT (10H1SHELL NO.,I3,/,4H VO=,F7.5,4H W1=,F8.5,5H W20=,F8.5,5H
       1 W11=,F8.5,5H W02=,F8.5,3H K=,F6.3,3H M=,F6.3,3H N=,F6.3,//,5X,4HT
       2IME,8X,5HWO(T),7X,5HW1(T),6X,6HW20(T),6X,6HW11(T),6X,6HW02(T),7X,4
       3HP(T),5X,8HP(T)/PCL,/)
        Y(1)=W1
        Y(2)=WTO
        Y(3)=WOO
        Y(4)=WOT
        Y(5)=0.0
        Y(6)=0.0
        Y(7)=0.0
        Y(8)=0.0
        Y(9)=0.0
        Y(10)=0.0
        SIGEX=0.0
        AS=0.0
        BS=7.0
        DEL=1.75
        DO 6 K = 1,1000
        CALL RKGIL(Y,10,AS,BS,DEL,NYST,P)
        T=P(1)
        SIGEX=P(5)
        PAX=2477000.*R*H*SIGEX
        PCR=1555000.*H*H
        PND=PAX/PCR
        TR=T/70000.
        WRITE (3,101) TR,Y(5),Y(1),Y(2),Y(3),Y(4),PAX,PND
 101    FORMAT (1X,6(F9.5,3X),F9.3,3X,F9.5)
        IF (STD-PAX-20.) 5,1,1
   5    AS=BS
        STD=PAX
        CALL DATSW(1,KK)
        GO TO (1,6),KK
   6    BS=AS+7.
   1    VO=VO+0.0001000001
   2    CONTINUE
        CALL EXIT
```

```
      SUBROUTINE NYST (M,T,Y,YDOT,P)
C     SUBROUTINE NYST   FIVE MODE MODEL
C     F1,F2...          STRESS FUNCTION COEFFICIENTS
C     NU                POISSON'S RATIO
C     SIGEX             AXIAL STRESS
C     SIGWY             CIRCUMFERENTIAL STRESS
C
      DIMENSION Y(10),YDOT(10),P(5)
      VO=P(2)
      A=P(3)
      B=P(4)
      C=2.282
      H=0.01746
      R=3.900
      W1=-0.00294
      WTO=0.0
      WOO=0.00001
      WOT=0.0
      NU=0.40
      Z=2.52
      L=11.0
      F1=-(Y(1)-W1)/(R*C*C)
      F2=-4.*C*C*B*B*(Y(1)*Y(4)-W1*WOT)/(C*C+4.*B*B)**2
      F3=-C*C*B*B*(Y(1)*Y(3)-W1*WOO)/(2.*((C+A)**2+B*B)**2)
      F4=-C*C*B*B*(Y(1)*Y(3)-W1*WOO)/(2.*((C-A)**2+B*B)**2)
      F20=-(4./R*(Y(2)-WTO)+.5*B*B*(Y(3)**2-WOO**2))/(16.*A*A)
      F11=-(A*A/R*(Y(3)-WOO)+2.*A*A*B*B*(Y(2)*Y(3)-WTO*WOO+Y(3)*Y(4)-WOO
     1*WOT))/(A*A+B*B)**2
      F02=-A*A*(Y(3)**2-WOO**2)/(32.*B*B)
      F31=-2.*A*A*B*B*(Y(2)*Y(3)-WTO*WOO)/(9.*A*A+B*B)**2
      F13=-2.*A*A*B*B*(Y(3)*Y(4)-WOO*WOT)/(A*A+9.*B*B)**2
      F22=-A*A*B*B*(Y(2)*Y(4)-WTO*WOT)/(A*A+B*B)**2
      DISP=VO*T
      SIGEX=NU*SIGWY+DISP/L-.25*C*C*(Y(1)**2-W1*W1)-A*A*(Y(2)**2-WTO**2+
     10.125*(Y(3)**2-WOO**2))
      SIGWY=NU*SIGEX-B*B*(Y(4)**2-WOT**2+.125*(Y(3)**2-WOO**2))-Y(5)/R
      YDOT(1)=Y(6)
      YDOT(6)=-H*H/(4.*Z)*C**4*(Y(1)-W1)+C*C/R*F1+.25*C*C*B*B*(Y(3)*(F3+
     1F4)+8.*Y(4)*F2)+C*C*Y(1)*SIGEX
      YDOT(2)=Y(7)
      YDOT(7)=-4.*H*H/Z*A**4*(Y(2)-WTO)+4.*A*A/R*F20+A*A*B*B*(Y(3)*(F11+
     1F31)+8.*Y(4)*F22)+4.*A*A*Y(2)*SIGEX
      YDOT(3)=Y(8)
      YDOT(8)=-H*H/(4.*Z)*(A*A+B*B)**2*(Y(3)-WOO)+A*A/R*F11+2.*A*A*B*B*(
     1Y(2)*(F11+F31)+Y(3)*(F20+F02)+Y(4)*(F11+F13))+.5*C*C*B*B*Y(1)*(F3+
     2F4)+A*A*Y(3)*SIGEX+B*B*Y(3)*SIGWY
      YDOT(4)=Y(9)
      YDOT(9)=-4.*H*H/Z*B**4*(Y(4)-WOT)+A*A*B*B*(Y(3)*(F11+F13)+8.*Y(2)*

     1F22)+2.*B*C*B*C*Y(1)*F2+4.*B*B*Y(4)*SIGWY
      YDOT(5)=Y(10)
      YDOT(10)=SIGWY/R
      P(1)=T
      P(5)=SIGEX
      RETURN
      END
```

SAMPLE RESULTS (5 MODE MODEL)

SHELL NO. 9
V0=0.00010 W1=-0.00294 W20= 0.00000 W11= 0.00001 W02= 0.00000 K= 2.282 M= 3.450 N= 3.450

TIME	W0(T)	W1(T)	W20(T)	W11(T)	W02(T)	P(T)	P(T)/PCL
0.00010	-0.00000	-0.00294	-0.00000	0.00001	-0.00000	10.724	0.02262
0.00020	-0.00000	-0.00297	-0.00000	0.00001	-0.00000	21.424	0.04519
0.00030	-0.00000	-0.00299	-0.00000	0.00001	-0.00000	32.134	0.06778
0.00040	-0.00000	-0.00299	-0.00000	0.00001	-0.00000	42.864	0.09042
0.00050	-0.00000	-0.00301	-0.00000	0.00001	-0.00000	53.574	0.11301
0.00060	-0.00000	-0.00303	-0.00000	0.00001	-0.00000	64.271	0.13558
0.00070	-0.00000	-0.00304	-0.00000	0.00001	-0.00000	74.994	0.15820
0.00080	-0.00000	-0.00305	-0.00000	0.00001	-0.00000	85.718	0.18082
0.00090	-0.00000	-0.00308	-0.00000	0.00001	-0.00000	96.415	0.20338
0.00100	-0.00000	-0.00310	-0.00000	0.00001	-0.00000	107.121	0.22597
0.00110	-0.00000	-0.00310	-0.00000	0.00001	-0.00000	117.849	0.24860
0.00120	-0.00000	-0.00312	-0.00000	0.00001	-0.00000	128.560	0.27119
0.00130	-0.00000	-0.00315	-0.00000	0.00001	-0.00000	139.253	0.29375
0.00140	-0.00000	-0.00316	-0.00000	0.00001	-0.00000	149.970	0.31636
0.00150	-0.00000	-0.00316	-0.00000	0.00001	-0.00000	160.695	0.33898
0.00160	-0.00000	-0.00319	-0.00000	0.00001	-0.00000	171.392	0.36155
0.00170	-0.00000	-0.00321	-0.00000	0.00001	-0.00000	182.091	0.38412
0.00180	-0.00000	-0.00322	-0.00000	0.00001	-0.00000	192.815	0.40674
0.00190	-0.00000	-0.00323	-0.00000	0.00001	-0.00000	203.529	0.42934
0.00200	-0.00000	-0.00326	-0.00000	0.00001	-0.00000	214.220	0.45189
0.00210	-0.00000	-0.00328	-0.00000	0.00001	-0.00000	224.926	0.47448
0.00220	-0.00000	-0.00329	-0.00000	0.00001	-0.00000	235.651	0.49710
0.00230	-0.00000	-0.00331	-0.00000	0.00002	-0.00000	246.354	0.51968
0.00240	-0.00000	-0.00334	-0.00000	0.00002	-0.00000	257.043	0.54223
0.00250	-0.00000	-0.00335	-0.00000	0.00002	-0.00000	267.757	0.56483
0.00260	-0.00000	-0.00336	-0.00000	0.00002	-0.00000	278.477	0.58745
0.00270	-0.00000	-0.00339	-0.00000	0.00002	-0.00000	289.170	0.61000
0.00280	-0.00000	-0.00342	-0.00000	0.00002	-0.00000	299.861	0.63256
0.00290	-0.00000	-0.00343	-0.00000	0.00002	-0.00000	310.580	0.65517
0.00300	-0.00000	-0.00344	-0.00000	0.00003	-0.00000	321.293	0.67777
0.00310	-0.00000	-0.00347	-0.00000	0.00003	-0.00000	331.978	0.70031

0.00320	-0.00000	-0.00350	-0.00000	0.00003	-0.00000	342.674	0.72287
0.00330	-0.00000	-0.00351	-0.00000	0.00003	-0.00000	353.394	0.74548
0.00340	-0.00000	-0.00353	-0.00000	0.00004	-0.00000	364.098	0.76806
0.00350	-0.00000	-0.00356	-0.00000	0.00004	-0.00000	374.779	0.79060
0.00360	-0.00000	-0.00358	-0.00000	0.00004	-0.00000	385.478	0.81317
0.00370	-0.00000	-0.00359	-0.00000	0.00005	-0.00000	396.197	0.83578
0.00380	-0.00000	-0.00361	-0.00000	0.00006	-0.00000	406.893	0.85834
0.00390	-0.00000	-0.00365	-0.00000	0.00007	-0.00000	417.571	0.88087
0.00400	-0.00000	-0.00367	-0.00000	0.00008	-0.00000	428.272	0.90344
0.00410	-0.00000	-0.00368	-0.00000	0.00009	-0.00000	438.987	0.92604
0.00420	-0.00000	-0.00371	-0.00000	0.00011	-0.00000	449.676	0.94859
0.00430	-0.00000	-0.00374	-0.00000	0.00013	-0.00000	460.351	0.97111
0.00440	-0.00000	-0.00376	-0.00000	0.00016	-0.00000	471.050	0.99368
0.00450	-0.00000	-0.00377	-0.00000	0.00021	-0.00000	481.758	1.01627
0.00460	-0.00000	-0.00380	-0.00001	0.00028	-0.00000	492.434	1.03879
0.00470	-0.00000	-0.00384	-0.00002	0.00038	-0.00000	503.090	1.06127
0.00480	-0.00000	-0.00386	-0.00005	0.00053	-0.00000	513.750	1.08376
0.00490	-0.00000	-0.00387	-0.00013	0.00078	-0.00000	524.345	1.10611
0.00500	-0.00000	-0.00390	-0.00036	0.00120	-0.00001	534.589	1.12772
0.00510	-0.00001	-0.00394	-0.00099	0.00201	-0.00003	542.868	1.14518
0.00520	-0.00005	-0.00394	-0.00288	0.00384	-0.00008	536.191	1.13110
0.00530	-0.00023	-0.00383	-0.00749	0.00911	-0.00023	434.342	0.91624

SHELL NO. 9
VO=0.00020 W1=-0.00294 W20= 0.00000 W11= 0.00001 W02= 0.00000 K= 2.282 M= 3.450 N= 3.450

TIME	WO(T)	W1(T)	W20(T)	W11(T)	W02(T)	P(T)	P(T)/PCL
0.00010	-0.00000	-0.00295	-0.00000	0.00001	-0.00000	21.449	0.04524
0.00020	-0.00000	-0.00300	-0.00000	0.00001	-0.00000	42.847	0.09038
0.00030	-0.00000	-0.00304	-0.00000	0.00001	-0.00000	64.265	0.13556
0.00040	-0.00000	-0.00304	-0.00000	0.00001	-0.00000	85.724	0.18083
0.00050	-0.00000	-0.00308	-0.00000	0.00001	-0.00000	107.142	0.22601
0.00060	-0.00000	-0.00314	-0.00000	0.00001	-0.00000	128.532	0.27114
0.00070	-0.00000	-0.00316	-0.00000	0.00001	-0.00000	149.971	0.31636
0.00080	-0.00000	-0.00317	-0.00000	0.00001	-0.00000	171.416	0.36160
0.00090	-0.00000	-0.00323	-0.00000	0.00001	-0.00000	192.807	0.40672
0.00100	-0.00000	-0.00327	-0.00000	0.00001	-0.00000	214.205	0.45186

0.00110	-0.00000	-0.00329	-0.00000	0.00001	-0.00000	235.653	0.49711
0.00120	-0.00000	-0.00332	-0.00000	0.00002	-0.00000	257.075	0.54230
0.00130	-0.00000	-0.00338	-0.00000	0.00002	-0.00000	278.449	0.58739
0.00140	-0.00000	-0.00342	-0.00000	0.00002	-0.00000	299.857	0.63255
0.00150	-0.00000	-0.00344	-0.00000	0.00002	-0.00000	321.301	0.67778
0.00160	-0.00000	-0.00348	-0.00000	0.00003	-0.00000	342.699	0.72292
0.00170	-0.00000	-0.00355	-0.00000	0.00003	-0.00000	364.065	0.76799
0.00180	-0.00000	-0.00358	-0.00000	0.00004	-0.00000	385.478	0.81316
0.00190	-0.00000	-0.00360	-0.00000	0.00005	-0.00000	406.911	0.85838
0.00200	-0.00000	-0.00366	-0.00000	0.00006	-0.00000	428.288	0.90347
0.00210	-0.00000	-0.00373	-0.00000	0.00008	-0.00000	449.645	0.94853
0.00220	-0.00000	-0.00376	-0.00000	0.00011	-0.00000	471.055	0.99369
0.00230	-0.00000	-0.00379	-0.00000	0.00015	-0.00000	492.472	1.03887
0.00240	-0.00000	-0.00385	-0.00000	0.00021	-0.00000	513.826	1.08392
0.00250	-0.00000	-0.00392	-0.00001	0.00033	-0.00000	535.157	1.12891
0.00260	-0.00000	-0.00396	-0.00004	0.00053	-0.00000	556.511	1.17396
0.00270	-0.00000	-0.00399	-0.00014	0.00090	-0.00000	577.746	1.21876
0.00280	-0.00001	-0.00406	-0.00053	0.00166	-0.00002	598.058	1.26160
0.00290	-0.00004	-0.00413	-0.00220	0.00346	-0.00006	607.863	1.28229
0.00300	-0.00020	-0.00406	-0.00860	0.00900	-0.00021	473.649	0.99916

SHELL NO. 9
VO=0.00030 W1=-0.00294 W20= 0.00000 W11= 0.00001 W02= 0.00000 K= 2.282 M= 3.450 N= 3.450

TIME	WO(T)	W1(T)	W20(T)	W11(T)	W02(T)	P(T)	P(T)/PCL
0.00010	-0.00000	-0.00296	-0.00000	0.00001	-0.00000	32.174	0.06787
0.00020	-0.00000	-0.00304	-0.00000	0.00001	-0.00000	64.269	0.13557
0.00030	-0.00000	-0.00309	-0.00000	0.00001	-0.00000	96.393	0.20334
0.00040	-0.00000	-0.00310	-0.00000	0.00001	-0.00000	128.578	0.27123
0.00050	-0.00000	-0.00316	-0.00000	0.00001	-0.00000	160.703	0.33900
0.00060	-0.00000	-0.00325	-0.00000	0.00001	-0.00000	192.780	0.40667
0.00070	-0.00000	-0.00328	-0.00000	0.00001	-0.00000	224.926	0.47448
0.00080	-0.00000	-0.00331	-0.00000	0.00002	-0.00000	257.091	0.54233
0.00090	-0.00000	-0.00339	-0.00000	0.00002	-0.00000	289.171	0.61001
0.00100	-0.00000	-0.00347	-0.00000	0.00002	-0.00000	321.244	0.67766
0.00110	-0.00000	-0.00351	-0.00000	0.00003	-0.00000	353.395	0.74548
0.00120	-0.00000	-0.00355	-0.00000	0.00004	-0.00000	385.527	0.81327
0.00130	-0.00000	-0.00365	-0.00000	0.00005	-0.00000	417.572	0.88087

0.00140	-0.00000	-0.00373	-0.00000	0.00006	-0.00000	449.634	0.94850
0.00150	-0.00000	-0.00377	-0.00000	0.00009	-0.00000	481.772	1.01630
0.00160	-0.00000	-0.00383	-0.00000	0.00014	-0.00000	513.870	1.08401
0.00170	-0.00000	-0.00394	-0.00000	0.00022	-0.00000	545.873	1.15152
0.00180	-0.00000	-0.00403	-0.00001	0.00037	-0.00000	577.885	1.21905
0.00190	-0.00000	-0.00408	-0.00006	0.00069	-0.00000	609.904	1.28659
0.00200	-0.00000	-0.00415	-0.00029	0.00138	-0.00001	641.452	1.35314
0.00210	-0.00002	-0.00427	-0.00152	0.00307	-0.00005	666.990	1.40702
0.00220	-0.00017	-0.00430	-0.00813	0.00844	-0.00020	555.348	1.17151

SHELL NO. 9
VO=0.00040 W1=-0.00294 W20= 0.00000 W11= 0.00001 W02= 0.00000 K= 2.282 M= 3.450 N= 3.450

TIME	WO(T)	W1(T)	W20(T)	W11(T)	W02(T)	P(T)	P(T)/PCL
0.00010	-0.00000	-0.00296	-0.00000	0.00001	-0.00000	42.898	0.09049
0.00020	-0.00000	-0.00307	-0.00000	0.00001	-0.00000	85.691	0.18076
0.00030	-0.00000	-0.00315	-0.00000	0.00001	-0.00000	128.517	0.27110
0.00040	-0.00000	-0.00316	-0.00000	0.00001	-0.00000	171.426	0.36162
0.00050	-0.00000	-0.00324	-0.00000	0.00001	-0.00000	214.257	0.45197
0.00060	-0.00000	-0.00336	-0.00000	0.00002	-0.00000	257.013	0.54217
0.00070	-0.00000	-0.00342	-0.00000	0.00002	-0.00000	299.857	0.63255
0.00080	-0.00000	-0.00346	-0.00000	0.00002	-0.00000	342.737	0.72300
0.00090	-0.00000	-0.00357	-0.00000	0.00003	-0.00000	385.501	0.81321
0.00100	-0.00000	-0.00370	-0.00000	0.00005	-0.00000	428.229	0.90335
0.00110	-0.00000	-0.00376	-0.00000	0.00007	-0.00000	471.058	0.99370
0.00120	-0.00000	-0.00382	-0.00000	0.00010	-0.00000	513.891	1.08405
0.00130	-0.00000	-0.00395	-0.00000	0.00017	-0.00000	556.592	1.17413
0.00140	-0.00000	-0.00410	-0.00000	0.00031	-0.00000	599.248	1.26411
0.00150	-0.00000	-0.00418	-0.00004	0.00061	-0.00000	641.952	1.35420
0.00160	-0.00000	-0.00426	-0.00022	0.00132	-0.00001	684.287	1.44351
0.00170	-0.00002	-0.00441	-0.00145	0.00320	-0.00005	720.610	1.52013
0.00180	-0.00020	-0.00449	-0.00952	0.00968	-0.00023	564.213	1.19021

SHELL NO. 9
VO=0.00050 W1=-0.00294 W20= 0.00000 W11= 0.00001 W02= 0.00000 K= 2.282 M= 3.450 N= 3.450

TIME	WO(T)	W1(T)	W20(T)	W11(T)	W02(T)	P(T)	P(T)/PCL
0.00010	-0.00000	-0.00297	-0.00000	0.00001	-0.00000	53.623	0.11311
0.00020	-0.00000	-0.00310	-0.00000	0.00001	-0.00000	107.111	0.22595
0.00030	-0.00000	-0.00320	-0.00000	0.00001	-0.00000	160.637	0.33886
0.00040	-0.00000	-0.00323	-0.00000	0.00001	-0.00000	214.269	0.45200
0.00050	-0.00000	-0.00332	-0.00000	0.00002	-0.00000	267.802	0.56493
0.00060	-0.00000	-0.00348	-0.00000	0.00002	-0.00000	321.231	0.67764
0.00070	-0.00000	-0.00357	-0.00000	0.00003	-0.00000	374.759	0.79055
0.00080	-0.00000	-0.00362	-0.00000	0.00004	-0.00000	428.346	0.90359
0.00090	-0.00000	-0.00376	-0.00000	0.00006	-0.00000	481.789	1.01633
0.00100	-0.00000	-0.00394	-0.00000	0.00010	-0.00000	535.147	1.12889
0.00110	-0.00000	-0.00405	-0.00000	0.00018	-0.00000	588.614	1.24168
0.00120	-0.00000	-0.00414	-0.00001	0.00036	-0.00000	642.104	1.35452
0.00130	-0.00000	-0.00431	-0.00006	0.00077	-0.00000	695.330	1.46680
0.00140	-0.00001	-0.00453	-0.00042	0.00188	-0.00001	747.469	1.57679
0.00150	-0.00006	-0.00468	-0.00341	0.00530	-0.00011	771.311	1.62708
0.00160	-0.00067	-0.00427	-0.01782	0.01836	0.00002	169.845	0.35829

SHELL NO. 9
VO=0.00010 W1=-0.00294 W20= 0.00000 W11= 0.00001 W02= 0.00000 K= 2.282 M= 3.384 N= 3.450

TIME	WO(T)	W1(T)	W20(T)	W11(T)	W02(T)	P(T)	P(T)/PCL
0.00010	-0.00000	-0.00294	-0.00000	0.00001	-0.00000	10.724	0.02262
0.00020	-0.00000	-0.00297	-0.00000	0.00001	-0.00000	21.424	0.04519
0.00030	-0.00000	-0.00299	-0.00000	0.00001	-0.00000	32.134	0.06778
0.00040	-0.00000	-0.00299	-0.00000	0.00001	-0.00000	42.864	0.09042
0.00050	-0.00000	-0.00301	-0.00000	0.00001	-0.00000	53.574	0.11301
0.00060	-0.00000	-0.00303	-0.00000	0.00001	-0.00000	64.271	0.13558
0.00070	-0.00000	-0.00304	-0.00000	0.00001	-0.00000	74.994	0.15820
0.00080	-0.00000	-0.00305	-0.00000	0.00001	-0.00000	85.718	0.18082
0.00090	-0.00000	-0.00308	-0.00000	0.00001	-0.00000	96.415	0.20338
0.00100	-0.00000	-0.00310	-0.00000	0.00001	-0.00000	107.121	0.22597
0.00110	-0.00000	-0.00310	-0.00000	0.00001	-0.00000	117.849	0.24860
0.00120	-0.00000	-0.00312	-0.00000	0.00001	-0.00000	128.560	0.27119

0.00130	-0.00000	-0.00315	-0.00000	0.00001	-0.00000	139.253	0.29375
0.00140	-0.00000	-0.00316	-0.00000	0.00001	-0.00000	149.970	0.31636
0.00150	-0.00000	-0.00316	-0.00000	0.00001	-0.00000	160.695	0.33898
0.00160	-0.00000	-0.00319	-0.00000	0.00001	-0.00000	171.392	0.36155
0.00170	-0.00000	-0.00321	-0.00000	0.00001	-0.00000	182.091	0.38412
0.00180	-0.00000	-0.00322	-0.00000	0.00001	-0.00000	192.815	0.40674
0.00190	-0.00000	-0.00323	-0.00000	0.00001	-0.00000	203.529	0.42934
0.00200	-0.00000	-0.00326	-0.00000	0.00001	-0.00000	214.220	0.45189
0.00210	-0.00000	-0.00328	-0.00000	0.00001	-0.00000	224.926	0.47448
0.00220	-0.00000	-0.00329	-0.00000	0.00001	-0.00000	235.651	0.49710
0.00230	-0.00000	-0.00331	-0.00000	0.00002	-0.00000	246.354	0.51968
0.00240	-0.00000	-0.00334	-0.00000	0.00002	-0.00000	257.043	0.54223
0.00250	-0.00000	-0.00335	-0.00000	0.00002	-0.00000	267.757	0.56483
0.00260	-0.00000	-0.00336	-0.00000	0.00002	-0.00000	278.477	0.58745
0.00270	-0.00000	-0.00339	-0.00000	0.00002	-0.00000	289.170	0.61000
0.00280	-0.00000	-0.00342	-0.00000	0.00002	-0.00000	299.861	0.63256
0.00290	-0.00000	-0.00343	-0.00000	0.00002	-0.00000	310.580	0.65517
0.00300	-0.00000	-0.00344	-0.00000	0.00003	-0.00000	321.293	0.67777
0.00310	-0.00000	-0.00347	-0.00000	0.00003	-0.00000	331.978	0.70031
0.00320	-0.00000	-0.00350	-0.00000	0.00003	-0.00000	342.674	0.72287
0.00330	-0.00000	-0.00351	-0.00000	0.00003	-0.00000	353.394	0.74548
0.00340	-0.00000	-0.00353	-0.00000	0.00004	-0.00000	364.098	0.76806
0.00350	-0.00000	-0.00356	-0.00000	0.00004	-0.00000	374.779	0.79060
0.00360	-0.00000	-0.00358	-0.00000	0.00004	-0.00000	385.478	0.81317
0.00370	-0.00000	-0.00359	-0.00000	0.00005	-0.00000	396.197	0.83578
0.00380	-0.00000	-0.00361	-0.00000	0.00006	-0.00000	406.893	0.85834
0.00390	-0.00000	-0.00365	-0.00000	0.00006	-0.00000	417.571	0.88087
0.00400	-0.00000	-0.00367	-0.00000	0.00008	-0.00000	428.272	0.90344
0.00410	-0.00000	-0.00368	-0.00000	0.00009	-0.00000	438.987	0.92604
0.00420	-0.00000	-0.00371	-0.00000	0.00011	-0.00000	449.676	0.94859
0.00430	-0.00000	-0.00374	-0.00000	0.00013	-0.00000	460.351	0.97111
0.00440	-0.00000	-0.00376	-0.00000	0.00016	-0.00000	471.051	0.99368
0.00450	-0.00000	-0.00377	-0.00000	0.00021	-0.00000	481.759	1.01627
0.00460	-0.00000	-0.00380	-0.00001	0.00027	-0.00000	492.435	1.03879
0.00470	-0.00000	-0.00384	-0.00002	0.00037	-0.00000	503.093	1.06128
0.00480	-0.00000	-0.00386	-0.00005	0.00051	-0.00000	513.758	1.08377
0.00490	-0.00000	-0.00387	-0.00012	0.00075	-0.00000	524.369	1.10616
0.00500	-0.00000	-0.00390	-0.00032	0.00115	-0.00001	534.690	1.12793
0.00510	-0.00001	-0.00394	-0.00089	0.00188	-0.00002	543.490	1.14649
0.00520	-0.00004	-0.00394	-0.00254	0.00351	-0.00007	541.139	1.14153
0.00530	-0.00018	-0.00387	-0.00682	0.00803	-0.00019	462.076	0.97475

SHELL NO. 9

VO=0.00020 W1=-0.00294 W20= 0.00000 W11= 0.00001 W02= 0.00000 K= 2.282 M= 3.384 N= 3.450

TIME	WO(T)	W1(T)	W20(T)	W11(T)	W02(T)	P(T)	P(T)/PCL
0.00010	-0.00000	-0.00295	-0.00000	0.00001	-0.00000	21.449	0.04524
0.00020	-0.00000	-0.00300	-0.00000	0.00001	-0.00000	42.847	0.09038
0.00030	-0.00000	-0.00304	-0.00000	0.00001	-0.00000	64.265	0.13556
0.00040	-0.00000	-0.00304	-0.00000	0.00001	-0.00000	85.724	0.18083
0.00050	-0.00000	-0.00308	-0.00000	0.00001	-0.00000	107.142	0.22601
0.00060	-0.00000	-0.00314	-0.00000	0.00001	-0.00000	128.532	0.27114
0.00070	-0.00000	-0.00316	-0.00000	0.00001	-0.00000	149.971	0.31636
0.00080	-0.00000	-0.00317	-0.00000	0.00001	-0.00000	171.416	0.36160
0.00090	-0.00000	-0.00323	-0.00000	0.00001	-0.00000	192.807	0.40672
0.00100	-0.00000	-0.00327	-0.00000	0.00001	-0.00000	214.205	0.45186
0.00110	-0.00000	-0.00329	-0.00000	0.00001	-0.00000	235.653	0.49711
0.00120	-0.00000	-0.00332	-0.00000	0.00002	-0.00000	257.075	0.54230
0.00130	-0.00000	-0.00338	-0.00000	0.00002	-0.00000	278.449	0.58739
0.00140	-0.00000	-0.00342	-0.00000	0.00002	-0.00000	299.857	0.63255
0.00150	-0.00000	-0.00344	-0.00000	0.00002	-0.00000	321.301	0.67778
0.00160	-0.00000	-0.00348	-0.00000	0.00003	-0.00000	342.699	0.72292
0.00170	-0.00000	-0.00355	-0.00000	0.00003	-0.00000	364.065	0.76799
0.00180	-0.00000	-0.00358	-0.00000	0.00004	-0.00000	385.478	0.81316
0.00190	-0.00000	-0.00360	-0.00000	0.00005	-0.00000	406.911	0.85838
0.00200	-0.00000	-0.00366	-0.00000	0.00006	-0.00000	428.288	0.90347
0.00210	-0.00000	-0.00373	-0.00000	0.00008	-0.00000	449.645	0.94853
0.00220	-0.00000	-0.00376	-0.00000	0.00010	-0.00000	471.055	0.99369
0.00230	-0.00000	-0.00379	-0.00000	0.00014	-0.00000	492.473	1.03887
0.00240	-0.00000	-0.00385	-0.00000	0.00021	-0.00000	513.827	1.08392
0.00250	-0.00000	-0.00392	-0.00001	0.00032	-0.00000	535.159	1.12892
0.00260	-0.00000	-0.00396	-0.00003	0.00051	-0.00000	556.519	1.17398
0.00270	-0.00000	-0.00399	-0.00012	0.00086	-0.00000	577.781	1.21883
0.00280	-0.00000	-0.00406	-0.00047	0.00156	-0.00001	598.310	1.26214
0.00290	-0.00003	-0.00413	-0.00190	0.00317	-0.00005	611.218	1.28937
0.00300	-0.00016	-0.00409	-0.00756	0.00795	-0.00018	516.302	1.08914

SHELL NO. 9
VO=0.00030 W1=-0.00294 W20= 0.00000 W11= 0.00001 W02= 0.00000 K= 2.282 M= 3.384 N= 3.450

TIME	WO(T)	W1(T)	W20(T)	W11(T)	W02(T)	P(T)	P(T)/PCL
0.00010	-0.00000	-0.00296	-0.00000	0.00001	-0.00000	32.174	0.06787
0.00020	-0.00000	-0.00304	-0.00000	0.00001	-0.00000	64.269	0.13557
0.00030	-0.00000	-0.00309	-0.00000	0.00001	-0.00000	96.393	0.20334
0.00040	-0.00000	-0.00310	-0.00000	0.00001	-0.00000	128.578	0.27123
0.00050	-0.00000	-0.00316	-0.00000	0.00001	-0.00000	160.703	0.33900
0.00060	-0.00000	-0.00325	-0.00000	0.00001	-0.00000	192.780	0.40667
0.00070	-0.00000	-0.00328	-0.00000	0.00001	-0.00000	224.926	0.47448
0.00080	-0.00000	-0.00331	-0.00000	0.00002	-0.00000	257.091	0.54233
0.00090	-0.00000	-0.00339	-0.00000	0.00002	-0.00000	289.171	0.61001
0.00100	-0.00000	-0.00347	-0.00000	0.00002	-0.00000	321.244	0.67766
0.00110	-0.00000	-0.00351	-0.00000	0.00003	-0.00000	353.395	0.74548
0.00120	-0.00000	-0.00355	-0.00000	0.00004	-0.00000	385.527	0.81327
0.00130	-0.00000	-0.00365	-0.00000	0.00005	-0.00000	417.572	0.88087
0.00140	-0.00000	-0.00373	-0.00000	0.00006	-0.00000	449.635	0.94850
0.00150	-0.00000	-0.00377	-0.00000	0.00009	-0.00000	481.772	1.01630
0.00160	-0.00000	-0.00383	-0.00000	0.00013	-0.00000	513.870	1.08401
0.00170	-0.00000	-0.00394	-0.00000	0.00021	-0.00000	545.874	1.15152
0.00180	-0.00000	-0.00403	-0.00001	0.00036	-0.00000	577.889	1.21906
0.00190	-0.00000	-0.00408	-0.00005	0.00066	-0.00000	609.921	1.28663
0.00200	-0.00000	-0.00415	-0.00025	0.00129	-0.00001	641.569	1.35339
0.00210	-0.00002	-0.00427	-0.00130	0.00282	-0.00004	668.829	1.41090
0.00220	-0.00014	-0.00433	-0.00694	0.00748	-0.00017	599.033	1.26366

SHELL NO. 9
VO=0.00040 W1=-0.00294 W20= 0.00000 W11= 0.00001 W02= 0.00000 K= 2.282 M= 3.384 N= 3.450

TIME	WO(T)	W1(T)	W20(T)	W11(T)	W02(T)	P(T)	P(T)/PCL
0.00010	-0.00000	-0.00296	-0.00000	0.00001	-0.00000	42.898	0.09049
0.00020	-0.00000	-0.00307	-0.00000	0.00001	-0.00000	85.691	0.18076
0.00030	-0.00000	-0.00315	-0.00000	0.00001	-0.00000	128.517	0.27110
0.00040	-0.00000	-0.00316	-0.00000	0.00001	-0.00000	171.426	0.36162
0.00050	-0.00000	-0.00324	-0.00000	0.00001	-0.00000	214.257	0.45197
0.00060	-0.00000	-0.00336	-0.00000	0.00002	-0.00000	257.013	0.54217

0.00070	-0.00000	-0.00342	-0.00000	0.00002	-0.00000	299.857	0.63255
0.00080	-0.00000	-0.00346	-0.00000	0.00002	-0.00000	342.737	0.72300
0.00090	-0.00000	-0.00357	-0.00000	0.00003	-0.00000	385.502	0.81321
0.00100	-0.00000	-0.00370	-0.00000	0.00005	-0.00000	428.229	0.90335
0.00110	-0.00000	-0.00376	-0.00000	0.00007	-0.00000	471.058	0.99370
0.00120	-0.00000	-0.00382	-0.00000	0.00010	-0.00000	513.891	1.08405
0.00130	-0.00000	-0.00395	-0.00000	0.00017	-0.00000	556.592	1.17413
0.00140	-0.00000	-0.00410	-0.00000	0.00030	-0.00000	599.251	1.26412
0.00150	-0.00000	-0.00418	-0.00003	0.00058	-0.00000	641.965	1.35423
0.00160	-0.00000	-0.00426	-0.00019	0.00124	-0.00000	684.386	1.44371
0.00170	-0.00002	-0.00441	-0.00122	0.00293	-0.00004	722.493	1.52410
0.00180	-0.00016	-0.00452	-0.00801	0.00852	-0.00020	627.941	1.32464

SHELL NO. 9

VO=0.00050 W1=-0.00294 W20= 0.00000 W11= 0.00001 W02= 0.00000 K= 2.282 M= 3.384 N= 3.450

TIME	WO(T)	W1(T)	W20(T)	W11(T)	W02(T)	P(T)	P(T)/PCL
0.00010	-0.00000	-0.00297	-0.00000	0.00001	-0.00000	53.623	0.11311
0.00020	-0.00000	-0.00310	-0.00000	0.00001	-0.00000	107.111	0.22595
0.00030	-0.00000	-0.00320	-0.00000	0.00001	-0.00000	160.637	0.33886
0.00040	-0.00000	-0.00323	-0.00000	0.00001	-0.00000	214.269	0.45200
0.00050	-0.00000	-0.00332	-0.00000	0.00002	-0.00000	267.802	0.56493
0.00060	-0.00000	-0.00348	-0.00000	0.00002	-0.00000	321.231	0.67764
0.00070	-0.00000	-0.00357	-0.00000	0.00003	-0.00000	374.759	0.79055
0.00080	-0.00000	-0.00362	-0.00000	0.00004	-0.00000	428.346	0.90359
0.00090	-0.00000	-0.00376	-0.00000	0.00006	-0.00000	481.789	1.01633
0.00100	-0.00000	-0.00394	-0.00000	0.00010	-0.00000	535.147	1.12889
0.00110	-0.00000	-0.00405	-0.00000	0.00018	-0.00000	588.615	1.24168
0.00120	-0.00000	-0.00414	-0.00000	0.00034	-0.00000	642.108	1.35453
0.00130	-0.00000	-0.00431	-0.00005	0.00073	-0.00000	695.354	1.46685
0.00140	-0.00000	-0.00453	-0.00036	0.00174	-0.00001	747.735	1.57735
0.00150	-0.00005	-0.00469	-0.00281	0.00476	-0.00009	781.054	1.64764
0.00160	-0.00052	-0.00443	-0.01716	0.01645	-0.00012	240.121	0.50653

FOUR MODE MODEL

```
// FOR
* IOCS (1132 PRINTER,CARD,DISK)
* LIST SOURCE PROGRAM
* ONE WORD INTEGERS
C       FOUR MODE (TWO WAVENUMBER) RUNGE KUTTA SCHEME
C
C * * * * * * * * * * * * * * * * * * * * * * * * * * * * * * * * * * * * * *
C      A,B               AXIAL + CIRCUMFERENTIAL WAVENUMBERS (=M,N)
C      ITN               NO. OF WAVENUMBER COMBINATIONS PROVIDED
C      ISHEL             SHELL NUMBER
C      L                 SHELL LENGTH
C      R                 SHELL RADIUS
C      H                 SHELL THICKNESS
C      WTO,WOO,WOT       IMPERFECTION AMPLITUDES (W20,W11,W02 MODES
C                        RESPECTIVELY)
C      Y(1)...Y(5)       RADIAL DEFLECTIONS
C      Y(6)...Y(10)      TIME DERIVATIVES OF Y(1) ETC.
C      T                 TIME PARAMETER (TIME/ONE-DIM. WAVESPEED)
C      TR                REAL TIME
C      VO                AXIAL VELOCITY PARAMETER
C                        (VELOCITY/ONE-DIM.WAVESPEED)
C      DISP              AXIAL DISPLACEMENT OF SHELL END
C      SIGEX             AXIAL STRESS
C      PAX               AXIAL LOAD
C      PCR               CLASSICAL AXIAL BUCKLING LOAD
C     AS,BS,DEL          STARTING POINT, END POINT AND INCREMENT
C                        FOR RUNGE-KUTTA CYCLE
C
      EXTERNAL MYST
      DIMENSION Y(10),P(5)
      READ(2,200) ITN
      DO 2 I=1,ITN
      READ (2,201) A,B
  200 FORMAT (I10)
  201 FORMAT (2F10.5)
      ISHEL = 1
      H=0.0172
      R=3.874
      WTO=0.0
      WOO=0.00001
      WOT=0.0
      VO=0.0001
      DO 1 J=1,5
      STD=0.0
      P(2)=VO
      P(3)=A
      P(4)=B
      WRITE (3,100) ISHEL ,VO,WTO,WOO,WOT,A,B
  100 FORMAT (10H1SHELL NO.,I3,/,4H VO=,F7.5,5H W20=,F8.5,5H W11=,F8.5,
     15H W02=,F8.5,3H M=,F6.3,3H N=,F6.3,//,5X,4HTIME,8X,5HW0(T),6X,6HW2
     20(T),6X,6HW11(T),6X,6HW02(T),7X,4HP(T),5X,8HP(T)/PCL,/)
```

```
      Y(1)=0.0
      Y(2)=WTO
      Y(3)=WOO
      Y(4)=WOT
      Y(5)=0.0
      Y(6)=0.0
      Y(7)=0.0
      Y(8)=0.0
      Y(9)=0.0
      Y(10)=0.0
      SIGEX=0.0
      AS=0.0
      BS=7.0
      DEL=1.75
      DO 6 K=1,1000
      CALL RKGIL(Y,10,AS,BS,DEL,MYST,P)
      T=P(1)
      SIGEX=P(5)
      PAX=2477000.*R*H*SIGEX
      PCR=1555000.*H*H
      PND=PAX/PCR
      TR=T/70000.
      WRITE(3,101)TR,Y(5),Y(2),Y(3),Y(4),PAX,PND
  101 FORMAT (1X,5(F9.5,3X),F9.3,3X,F9.5)
      IF (STD-PAX-20.) 5,1,1
    5 AS=BS
      STD=PAX
      CALL DATSW (1,KK)
      GO TO (1,6),KK
    6 BS=AS+7.0
    1 VO=VO+0.0001000001
    2 CONTINUE
      CALL EXIT
      END

FEATURES SUPPORTED
 ONE WORD INTEGERS
 IOCS

CORE REQUIREMENTS FOR
 COMMON       0  VARIABLES     82  PROGRAM     456

END OF COMPILATION
```

```
      SUBROUTINE MYST(M,T,Y,YDOT,P)
C     SUBOUTINE MYST     FOUR MODE MODEL
C     F1,F2...           STRESS FUNCTION COEFFICIENTS
C     NU                 POISSON'S RATIO
C     SIGEX              AXIAL STRESS
C     SIGWY              CIRCUMFERENTIAL STRESS
C
      DIMENSION Y(10),YDOT(10),P(5)
      VO=P(2)
      A=P(3)
      B=P(4)
      H=0.0172
      R=3.874
      WTO=0.0
      WOO=0.00001
      WOT=0.0
      NU=0.40
      Z=3.0*(1.0-NU**2)
      L=11.0
      F20=-(4./R*(Y(2)-WTO)+.5*B*B*(Y(3)**2-WOO**2))/(16.*A*A)
      F11=-(A*A/R*(Y(3)-WOO)+2.*A*A*B*B*(Y(2)*Y(3)-WTO*WOO+Y(3)*Y(4)-WOO
     1*WOT))/(A*A+B*B)**2
      F02=-A*A*(Y(3)**2-WOO**2)/(32.*B*B)
      F31=-2.*A*A*B*B*(Y(2)*Y(3)-WTO*WOO)/(9.*A*A+B*B)**2
      F13=-2.*A*A*B*B*(Y(3)*Y(4)-WOO*WOT)/(A*A+9.*B*B)**2
      F22=-A*A*B*B*(Y(2)*Y(4)-WTO*WOT)/(A*A+B*B)**2
      DISP=VO*T
      SIGEX=NU*SIGWY+DISP/L-A*A*(Y(2)**2-WTO**2+.125*(Y(3)**2-WOO**2))
      SIGWY=NU*SIGEX-B*B*(Y(4)**2-WOT**2+.125*(Y(3)**2-WOO**2))-Y(5)/R
      YDOT(1)=0.0
      YDOT(6)=0.0
      YDOT(2)=Y(7)
      YDOT(7)=-4.*H*H/Z*A**4*(Y(2)-WTO)+4.*A*A/R*F20+A*A*B*B*(Y(3)*(F11+
     1F31)+8.*Y(4)*F22)+4.*A*A*Y(2)*SIGEX
      YDOT(3)=Y(8)
      YDOT(8)=-H*H/(4.*Z)*(A*A+B*B)**2*(Y(3)-WOO)+A*A/R*F11+2.*A*A*B*B*(
     1Y(2)*(F11+F31)+Y(3)*(F20+F02)+Y(4)*(F11+F13))+A*A*Y(3)*SIGEX+B*B*Y
     2(3)*SIGWY
      YDOT(4)=Y(9)
      YDOT(9)=-4.*H*H/Z*B**4*(Y(4)-WOT)+A*A*B*B*(Y(3)*(F11+F13)+8.*Y(2)*
     1F22)+4.*B*B*Y(4)*SIGWY
      YDOT(5)=Y(10)
      YDOT(10)=SIGWY/R
      P(1)=T
      P(5)=SIGEX
      RETURN
      END
```

SAMPLE RESULTS (4 MODE MODEL)

SHELL NO. 1
VO=0.00010 W20= 0.00000 W11= 0.00001 W02= 0.00000 M= 3.410 N= 3.410

TIME	W0(T)	W20(T)	W11(T)	W02(T)	P(T)	P(T)/PCL
0.00010	-0.00000	-0.00000	0.00001	-0.00000	10.503	0.02283
0.00020	-0.00000	-0.00000	0.00001	-0.00000	21.006	0.04566
0.00030	-0.00000	-0.00000	0.00001	-0.00000	31.509	0.06849
0.00040	-0.00000	-0.00000	0.00001	-0.00000	42.012	0.09132
0.00050	-0.00000	-0.00000	0.00001	-0.00000	52.515	0.11415
0.00060	-0.00000	-0.00000	0.00001	-0.00000	63.018	0.13698
0.00070	-0.00000	-0.00000	0.00001	-0.00000	73.521	0.15981
0.00080	-0.00000	-0.00000	0.00001	-0.00000	84.025	0.18265
0.00090	-0.00000	-0.00000	0.00001	-0.00000	94.528	0.20548
0.00100	-0.00000	-0.00000	0.00001	-0.00000	105.031	0.22831
0.00110	-0.00000	-0.00000	0.00001	-0.00000	115.534	0.25114
0.00120	-0.00000	-0.00000	0.00001	-0.00000	126.037	0.27397
0.00130	-0.00000	-0.00000	0.00001	-0.00000	136.540	0.29680
0.00140	-0.00000	-0.00000	0.00001	-0.00000	147.043	0.31963
0.00150	-0.00000	-0.00000	0.00001	-0.00000	157.547	0.34247
0.00160	-0.00000	-0.00000	0.00001	-0.00000	168.050	0.36530
0.00170	-0.00000	-0.00000	0.00001	-0.00000	178.553	0.38813
0.00180	-0.00000	-0.00000	0.00001	-0.00000	189.056	0.41096
0.00190	-0.00000	-0.00000	0.00001	-0.00000	199.559	0.43379
0.00200	-0.00000	-0.00000	0.00001	-0.00000	210.062	0.45662
0.00210	-0.00000	-0.00000	0.00002	-0.00000	220.565	0.47945
0.00220	-0.00000	-0.00000	0.00002	-0.00000	231.069	0.50229
0.00230	-0.00000	-0.00000	0.00002	-0.00000	241.572	0.52512
0.00240	-0.00000	-0.00000	0.00002	-0.00000	252.075	0.54795
0.00250	-0.00000	-0.00000	0.00002	-0.00000	262.578	0.57078
0.00260	-0.00000	-0.00000	0.00002	-0.00000	273.081	0.59361
0.00270	-0.00000	-0.00000	0.00002	-0.00000	283.584	0.61644
0.00280	-0.00000	-0.00000	0.00003	-0.00000	294.087	0.63927
0.00290	-0.00000	-0.00000	0.00003	-0.00000	304.590	0.66210
0.00300	-0.00000	-0.00000	0.00003	-0.00000	315.093	0.68494
0.00310	-0.00000	-0.00000	0.00004	-0.00000	325.596	0.70777
0.00320	-0.00000	-0.00000	0.00004	-0.00000	336.099	0.73060
0.00330	-0.00000	-0.00000	0.00005	-0.00000	346.603	0.75343
0.00340	-0.00000	-0.00000	0.00005	-0.00000	357.106	0.77626
0.00350	-0.00000	-0.00000	0.00006	-0.00000	367.609	0.79909
0.00360	-0.00000	-0.00000	0.00007	-0.00000	378.111	0.82192
0.00370	-0.00000	-0.00000	0.00008	-0.00000	388.614	0.84475
0.00380	-0.00000	-0.00000	0.00010	-0.00000	399.116	0.86758
0.00390	-0.00000	-0.00000	0.00012	-0.00000	409.618	0.89041
0.00400	-0.00000	-0.00000	0.00015	-0.00000	420.120	0.91324
0.00410	-0.00000	-0.00000	0.00019	-0.00000	430.619	0.93606
0.00420	-0.00000	-0.00000	0.00025	-0.00000	441.116	0.95888
0.00430	-0.00000	-0.00001	0.00034	-0.00000	451.606	0.98168
0.00440	-0.00000	-0.00004	0.00048	-0.00000	462.078	1.00445
0.00450	-0.00000	-0.00010	0.00070	-0.00000	472.501	1.02710
0.00460	-0.00000	-0.00027	0.00107	-0.00001	482.723	1.04932
0.00470	-0.00001	-0.00075	0.00175	-0.00002	491.821	1.06910
0.00480	-0.00003	-0.00216	0.00321	-0.00007	492.640	1.07088
0.00490	-0.00015	-0.00606	0.00718	-0.00022	431.792	0.93861

SHELL NO. 1
V0=0.00020 W20= 0.00000 W11= 0.00001 W02= 0.00000 M= 3.410 N= 3.410

TIME	W0(T)	W20(T)	W11(T)	W02(T)	P(T)	P(T)/PCL
0.00010	-0.00000	-0.00000	0.00001	-0.00000	21.006	0.04566
0.00020	-0.00000	-0.00000	0.00001	-0.00000	42.012	0.09132
0.00030	-0.00000	-0.00000	0.00001	-0.00000	63.018	0.13698
0.00040	-0.00000	-0.00000	0.00001	-0.00000	84.025	0.18265
0.00050	-0.00000	-0.00000	0.00001	-0.00000	105.031	0.22831
0.00060	-0.00000	-0.00000	0.00001	-0.00000	126.037	0.27397
0.00070	-0.00000	-0.00000	0.00001	-0.00000	147.044	0.31963
0.00080	-0.00000	-0.00000	0.00001	-0.00000	168.050	0.36530
0.00090	-0.00000	-0.00000	0.00001	-0.00000	189.056	0.41096
0.00100	-0.00000	-0.00000	0.00001	-0.00000	210.062	0.45662
0.00110	-0.00000	-0.00000	0.00002	-0.00000	231.069	0.50229
0.00120	-0.00000	-0.00000	0.00002	-0.00000	252.075	0.54795
0.00130	-0.00000	-0.00000	0.00002	-0.00000	273.081	0.59361
0.00140	-0.00000	-0.00000	0.00002	-0.00000	294.087	0.63927
0.00150	-0.00000	-0.00000	0.00003	-0.00000	315.094	0.68494
0.00160	-0.00000	-0.00000	0.00004	-0.00000	336.100	0.73060
0.00170	-0.00000	-0.00000	0.00004	-0.00000	357.106	0.77626
0.00180	-0.00000	-0.00000	0.00006	-0.00000	378.112	0.82192
0.00190	-0.00000	-0.00000	0.00007	-0.00000	399.118	0.86758
0.00200	-0.00000	-0.00000	0.00010	-0.00000	420.123	0.91325
0.00210	-0.00000	-0.00000	0.00013	-0.00000	441.127	0.95890
0.00220	-0.00000	-0.00000	0.00019	-0.00000	462.128	1.00456
0.00230	-0.00000	-0.00001	0.00030	-0.00000	483.122	1.05019
0.00240	-0.00000	-0.00003	0.00047	-0.00000	504.093	1.09578
0.00250	-0.00000	-0.00011	0.00081	-0.00000	524.974	1.14117
0.00260	-0.00000	-0.00041	0.00148	-0.00001	545.304	1.18536
0.00270	-0.00003	-0.00167	0.00300	-0.00006	559.575	1.21638
0.00280	-0.00014	-0.00688	0.00745	-0.00021	483.799	1.05166

SHELL NO. 1
V0=0.00030 W20= 0.00000 W11= 0.00001 W02= 0.00000 M= 3.410 N= 3.410

TIME	W0(T)	W20(T)	W11(T)	W02(T)	P(T)	P(T)/PCL
0.00010	-0.00000	-0.00000	0.00001	-0.00000	31.509	0.06849
0.00020	-0.00000	-0.00000	0.00001	-0.00000	63.018	0.13698
0.00030	-0.00000	-0.00000	0.00001	-0.00000	94.528	0.20548
0.00040	-0.00000	-0.00000	0.00001	-0.00000	126.037	0.27397
0.00050	-0.00000	-0.00000	0.00001	-0.00000	157.547	0.34247
0.00060	-0.00000	-0.00000	0.00001	-0.00000	189.056	0.41096
0.00070	-0.00000	-0.00000	0.00001	-0.00000	220.566	0.47945
0.00080	-0.00000	-0.00000	0.00002	-0.00000	252.075	0.54795
0.00090	-0.00000	-0.00000	0.00002	-0.00000	283.584	0.61644
0.00100	-0.00000	-0.00000	0.00003	-0.00000	315.094	0.68494
0.00110	-0.00000	-0.00000	0.00004	-0.00000	346.603	0.75343
0.00120	-0.00000	-0.00000	0.00005	-0.00000	378.112	0.82192
0.00130	-0.00000	-0.00000	0.00007	-0.00000	409.621	0.89042
0.00140	-0.00000	-0.00000	0.00010	-0.00000	441.129	0.95891
0.00150	-0.00000	-0.00000	0.00015	-0.00000	472.636	1.02740
0.00160	-0.00000	-0.00000	0.00024	-0.00000	504.136	1.09587
0.00170	-0.00000	-0.00001	0.00041	-0.00000	535.617	1.16430
0.00180	-0.00000	-0.00008	0.00077	-0.00000	567.010	1.23254
0.00190	-0.00000	-0.00039	0.00158	-0.00001	597.780	1.29943
0.00200	-0.00003	-0.00207	0.00363	-0.00007	618.704	1.34491
0.00210	-0.00024	-0.01052	0.01051	-0.00028	423.683	0.92098

SHELL NO. 1
VO=0.00050 W20= 0.00000 W11= 0.00001 W02= 0.00000 M= 3.410 N= 3.410

TIME	W0(T)	W20(T)	W11(T)	W02(T)	P(T)	P(T)/PCL
0.00010	-0.00000	-0.00000	0.00001	-0.00000	52.515	0.11415
0.00020	-0.00000	-0.00000	0.00001	-0.00000	105.031	0.22831
0.00030	-0.00000	-0.00000	0.00001	-0.00000	157.547	0.34247
0.00040	-0.00000	-0.00000	0.00001	-0.00000	210.062	0.45662
0.00050	-0.00000	-0.00000	0.00002	-0.00000	262.578	0.57078
0.00060	-0.00000	-0.00000	0.00002	-0.00000	315.094	0.68494
0.00070	-0.00000	-0.00000	0.00003	-0.00000	367.609	0.79909
0.00080	-0.00000	-0.00000	0.00005	-0.00000	420.125	0.91325
0.00090	-0.00000	-0.00000	0.00008	-0.00000	472.639	1.02740
0.00100	-0.00000	-0.00000	0.00014	-0.00000	525.152	1.14155
0.00110	-0.00000	-0.00000	0.00028	-0.00000	577.654	1.25568
0.00120	-0.00000	-0.00003	0.00058	-0.00000	630.103	1.36969
0.00130	-0.00000	-0.00021	0.00137	-0.00001	682.157	1.48285
0.00140	-0.00003	-0.00167	0.00365	-0.00006	726.532	1.57931
0.00150	-0.00028	-0.01277	0.01232	-0.00030	439.403	0.95516

SHELL NO. 1
VO=0.00040 W20= 0.00000 W11= 0.00001 W02= 0.00000 M= 3.410 N= 3.410

TIME	W0(T)	W20(T)	W11(T)	W02(T)	P(T)	P(T)/PCL
0.00010	-0.00000	-0.00000	0.00001	-0.00000	42.012	0.09132
0.00020	-0.00000	-0.00000	0.00001	-0.00000	84.025	0.18265
0.00030	-0.00000	-0.00000	0.00001	-0.00000	126.037	0.27397
0.00040	-0.00000	-0.00000	0.00001	-0.00000	168.050	0.36530
0.00050	-0.00000	-0.00000	0.00001	-0.00000	210.062	0.45662
0.00060	-0.00000	-0.00000	0.00002	-0.00000	252.075	0.54795
0.00070	-0.00000	-0.00000	0.00002	-0.00000	294.087	0.63927
0.00080	-0.00000	-0.00000	0.00003	-0.00000	336.100	0.73060
0.00090	-0.00000	-0.00000	0.00004	-0.00000	378.112	0.82192
0.00100	-0.00000	-0.00000	0.00006	-0.00000	420.124	0.91325
0.00110	-0.00000	-0.00000	0.00009	-0.00000	462.136	1.00457
0.00120	-0.00000	-0.00000	0.00015	-0.00000	504.145	1.09589
0.00130	-0.00000	-0.00000	0.00027	-0.00000	546.144	1.18719
0.00140	-0.00000	-0.00003	0.00054	-0.00000	588.103	1.27840
0.00150	-0.00000	-0.00016	0.00115	-0.00000	629.814	1.36906
0.00160	-0.00002	-0.00104	0.00274	-0.00004	668.291	1.45271
0.00170	-0.00014	-0.00706	0.00793	-0.00022	602.650	1.31002

APPENDIX C: DYNAMIC PROPERTIES OF EPOXY PLASTIC

In Chapter 3 of the main text, it was explained that because of the particular requirements of the spin-casting technique, the shell specimens were manufactured from an epoxy plastic material. However, a well recognized feature of polymer solids such as epoxies is that their stress-strain characteristics are normally rate dependent, and that in extreme cases, their response to dynamically applied loads can differ very signficantly from their static behaviour.

The visco-elastic properties of the epoxy mixture used in the manufacture of the shell specimens were determined in a series of tests which employed three experimental approaches. The first and simplest technique involved the use of a small pneumatic testing rig in which several small samples of the material were tested in tension and compression at strain rates varying from the quasi-static up to 1.5×10^{-2} sec^{-1}. In the second series of experiments, considerably higher strain rates were achieved with a split Hopkinson bar apparatus, while by the third method, material properties were determined from the transmission characteristics of high-frequency stress waves initiated by an explosion. The first two sets of experiments were performed by the author, while the third was conducted by Zimcik[32].

The techniques and principles employed in the first series of tests were quite conventional and straightforward. The loading elements of the testing machine consisted of a pair of pneumatic cylinders so that the loading rate of the machine corresponded to the rate at which the cylinders were pressurized. Strain was measured by small foil resistance strain gauges bonded directly to the sample while the load was measured by a simple strain gauge load cell mounted in series with the sample piece between the platens of the testing machine. The strain gauges on the sample and the load cell were connected to bridge circuits, the output signals from which were displayed on a dual beam oscilloscope. The results obtained with this arrangement are shown in Figure 31.

The split Hopkinson bar technique used to measure material properties at medium and high strain rates was somewhat more complicated in concept than the tests described above. The apparatus consisted essentially of two slender bars (15 inches long, .375 inches in diameter) mounted in tandem on a common axis with a small (.5 inches long by .375 inches in diameter) sample of the material sandwiched between them (see Figure 30).

In operation, the free end of one of the bars (termed the weigh bar) was struck by a projectile fired from a large air gun so that a compressive one-dimensional stress wave propagated down the bar and through the sample into the downstream or anvil bar. Foil resistance-type strain gauges were mounted on each bar close to the sample interfaces to measure the incoming, reflected and transmitted stress waves. The strain signals were displayed on an oscilloscope and recorded photographically. By assuming that the stress waves were essentially one-dimensional (due to the geometry of the bars) it was possible to calculate the particle velocities in the two bars from the waveforms and hence to derive the strain rate and strain from the relative velocities and displacements of the two bar-sample interfaces. The sample stress was taken as being equal to the average of the stresses in the two bars.

The mathematical model used to calculate the strains was developed as follows. An element of bar of length Δx is shown below. The axial stresses and displacements are represented by $\sigma(x,t)$ and $u(x,t)$ respectively, while the

mass density of the bar material is represented by ρ.

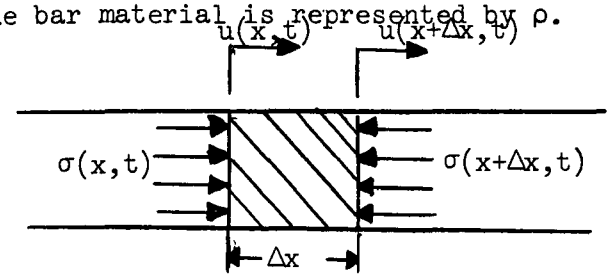

The unbalanced force on the element will be equal to the mass times acceleration of the element, so that in the limit, as Δx approaches zero we may write

$$\frac{\partial \sigma(x,t)}{\partial x} = - \frac{\rho \partial^2 u(x,t)}{\partial t^2} \qquad C.1$$

If it is assumed that the material is linearly elastic, that is

$$\sigma(x,t) = E\epsilon(x,t) = \frac{E\partial u(x,t)}{\partial x} \qquad C.2$$

then C.1 becomes

$$\frac{E}{\rho} \frac{\partial^2 u}{\partial x^2} + \frac{\partial^2 u}{\partial t^2} = 0 \qquad C.3$$

This is a wave equation with the solution

$$u(x,t) = f(x + ct) + g(x-ct) \qquad C.4$$

where $c = \sqrt{\frac{E}{\rho}}$

If we consider the case of a stress wave of magnitude Σ moving to the right along a previously undisturbed bar, we have

$$\sigma(x,t) = E\, g'\,(x-ct) = 0 \qquad C.5$$

in the undisturbed region and

$$\sigma(x,t) = \Sigma(x,t) = E\, g'(x-ct) \qquad C.6$$

behind the wave front. The particle velocity behind the wave front is

$$v(x,t) = \frac{\partial u}{\partial t}\,(x,t) = - c\, g'(x-ct)$$

so that

$$\Sigma(x,t) = \rho c v(x,t) \qquad C.7$$

When the stress wave encounters an interface at X between two different materials, a more complicated situation arises with displacements due to the incident wave $g_A(x\text{-}ct)$, a reflected wave $f_A(x + ct)$ and a wave transmitted into the new material $u_B(x,t)$. At the interfaces, continuity demands that the displacements and velocities in two materials be equal, that is,

$$g_A\,(X\text{-}ct) + f_A(X + ct) = u_B(X,t) \qquad C.8$$

$$-cg_A'(X\text{-}ct) + cf_A'\,(X + ct) = \frac{\partial u_B}{\partial t}\,(X,t) \qquad C.9$$

Also, the equilibrium condition specifies that the stresses in both materials be equal:

$$E\,(g_A'\,(X\text{-}ct) + f_A'\,(X\text{-}ct)) = \sigma_B\,(X,t) \qquad C.10$$

An important design feature of the split Hopkinson bar apparatus is that the incident stress wave is of essentially constant magnitude for the duration of the pulse. If this stress level is written Σ_A, then

$$g_A'\,(X\text{-}ct) = \frac{\Sigma_A}{E} \qquad C.11$$

If this stress level is known and the total stress level at the interface is determined from strain gauge measurements, we can write

$$f_A'\,(x\text{-}ct) = \frac{\sigma_I\,(X,t)}{E} - \Sigma_A \qquad C.12$$

The stress at the interface σ_I is, of course, equal to σ_B.

Thus, the velocity in material B adjacent to the interface is

$$\frac{\partial u_B}{\partial t}\,(X,t) = \frac{c}{E}\,(\sigma\,(X,t) - 2\Sigma_A) = \frac{(\sigma\,(X,t) - 2\Sigma_A)}{\rho c} \qquad C.13$$

At the sample-anvil bar interface, waves transmitted from the sample into the bar are entering an undisturbed medium so that it is possible to use Equation C.7, written here as

$$\frac{\partial u_B}{\partial t}\,(X + \ell,t) = \frac{\sigma\,(X + \ell,t)}{\rho c} \qquad C.14$$

The sample strain rate is then

$$\dot{\epsilon}(t) = \frac{1}{\ell}\left[\frac{\partial u_B}{\partial t}(x,t) - \frac{\partial u_B}{\partial t}(X+\ell,t)\right] \qquad C.15$$

and the sample strain at time T is

$$\epsilon(T) = \int_0^T \dot{\epsilon}(t)\,dt \qquad C.16$$

It should be noted that these equations make no assumptions as to the material properties of the sample itself and are applicable regardless of any energy dissipation or internal reflections within the sample piece. For practical reasons, it was impossible to measure the bar strains precisely at the interfaces as was implied in the above derivation. If, however, it is assumed that there is negligible dispersion or attenuation in the steel bars between the ends and the strain gauge stations (a distance of approximately 3/8 of an inch), the equations remain completely applicable.

An attractive feature of the split Hopkinson bar technique is that the instrumentation is carried entirely on the apparatus, so that the test specimens are very simple and economical to produce. Nevertheless, several sample pieces were specially cast with small strain gauges embedded directly at their centre. Comparison between the internal strains measured directly by this technique and the strains calculated from the wave data indicated that the one-dimensional wave analysis outlined above was capable of producing quite accurate results.

A full description of the third experimental method used in determining dynamic stress-strain properties of the epoxy material is contained in Reference 32. Briefly, this method was based on an analysis of the wave transmission properties of the material. A long slender sample was mounted in linear bearings, which permitted axial motion, and loaded impulsively at one end by a small explosive charge. Strain gauges mounted at the mid-point of the bar were used to measure the strain pulse as it travelled back and forth along the bar and was reflected at the free ends. Each of these strain pulses was represented mathematically as a Fourier series so that by comparing the magnitude of the Fourier components of each pulse, it was possible to determine the attenuation coefficient and phase velocity of a strain wave as a function of frequency. This data was used to determine the constitutive properties of the material in terms of a complex Young's Modulus $(E_1 + iE_2)$ where E_1 is the elastic stiffness and E_2 is representative of the energy dissipation in the material.

These three experiments were complemented by earlier work done by Tennyson[11], in which measurements of the static modulus and Poisson's ratio were made.

Sample results from the three dynamic experiments are plotted together in Figure 32, while the results from the first low strain rate series are shown in Figure 31. The results from the wave transmission experiment are plotted as a straight line. This must not be taken to imply that this experiment predicts completely linear behaviour at all stress levels, but rather it simply reflects the fact that at the strain levels encountered here and because of the nature of the analysis procedure, no information on yield

points or non-linear behaviour was obtained.

During the course of the dynamic shell buckling tests, the maximum pre-buckling strains were of the order of 4×10^{-3}, while the maximum pre-buckling strain rates were approximately 2.5 sec^{-1} and the maximum buckling strain rates equal to about 4 sec^{-1}. This range of strains corresponds to a region of the stress-strain diagrams where the results obtained with all three experimental methods are in good agreement. It was decided, therefore, that the material could be considered as being linearly elastic with a Young's modulus of 4.05×10^{5} psi over the entire range of strain rates encountered in the shell buckling tests. It was also assumed that the statically determined Poisson's ratio of 0.4 would remain constant under these conditions.

TABLE 1

SERIES I: NEAR-PERFECT SHELLS

Shell No.	Length (in.)	Radius (in.)	Thickness (in.)	P_{cl} (lbs.)
1	11.0	3.92	.0174	472
2	11.0	3.98	.0180	503

SERIES II: SHELLS WITH AXISYMMETRIC SINUSOIDAL IMPERFECTIONS AND THICKNESS VARIATIONS

					Imperfection			Geometry	
Shell No.	Length (in.)	Radius (in.)	Thickness (in.)	P_{cl} (lbs.)	Amplitude (in.)	μ	Wavelength (in.)	Wave-number K	K/K_{cr}
3	11.0	3.97	.0130	264	.00042	.0322	.924	3.40	.868
4	11.0	3.95	.0202	637	.00037	.0185	.924	3.40	1.066
5	11.0	3.93	.0168	422	.00112	.0676	.786	4.00	1.152

SERIES III: SHELLS WITH AXISYMMETRIC SINUSOIDAL IMPERFECTIONS AND CONSTANT WALL THICKNESS

					Imperfection			Geometry	
Shell No.	Length (in.)	Radius (in.)	Thickness (in.)	P_{cl} (lbs.)	Amplitude (in.)	μ	Wavelength (in.)	Wave-number K	K/K_{cr}
6	11.0	3.90	.0189	554	.00234	.124	.786	4.00	1.218
7	11.0	3.90	.0193	579	.00124	.064	.924	3.40	1.052
8	9.5	3.92	.0181	508	.00203	.112	.486	6.47	1.932
9	11.0	3.90	.0175	474	.00294	.168	2.756	1.141	0.334

SERIES IV: SHELL WITH QUASI-RANDOM AXISYMMETRIC IMPERFECTION AND CONSTANT WALL THICKNESS

Shell No.	Length (in.)	Radius (in.)	Thickness (in.)	P_{cl} (lbs.)
10	11.0	3.90	.0160	396

TABLE 2

COMPARISON OF THEORETICAL AND EXPERIMENTAL BUCKLING WAVELENGTHS

SHELL 3 (Figure 28)

AXISYMMETRIC MODE (W(t) cos2Mx)

Theoretical Wavelength (inches)	Experimental Wavelength (inches)
.924	.93

ASYMMETRIC MODE (W(t) cosMxcosNy)

Theoretical Wavelengths (inches)		Experimental Wavelength (inches)	
Axial	Circumferential	Axial	Circumferential
1.85	1.62	2.0	2.1

SHELL 9 (Figure 29)

AXISYMMETRIC MODEL (W(t) cosKx)

Theoretical Wavelength (inches)	Experimental Wavelength (inches)
2.756	2.3

ASYMMETRIC MODE (W(t)cosMxcosNy)

Theoretical Wavelengths (inches)		Experimental Wavelengths (inches)	
Axial	Circumferential	Axial	Circumferential
1.96	1.96	1.7	1.3

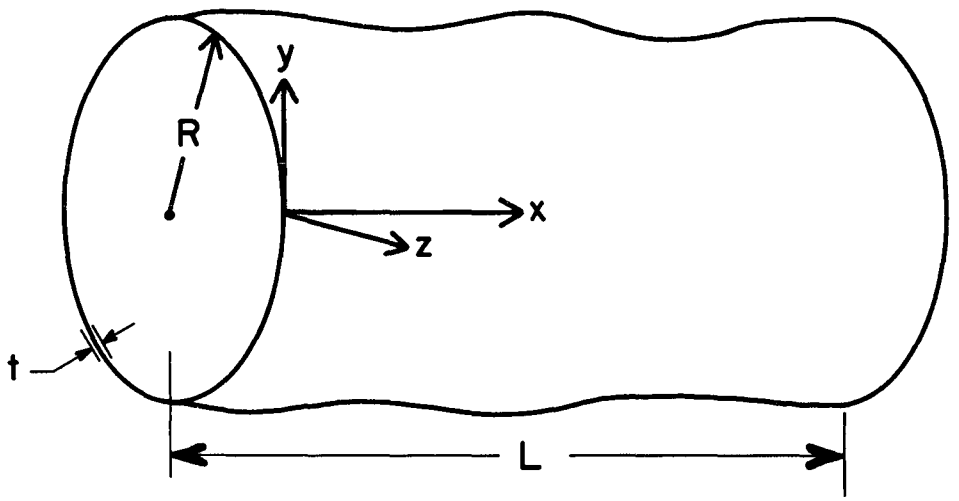

FIG. 1(a) SHELL GEOMETRY

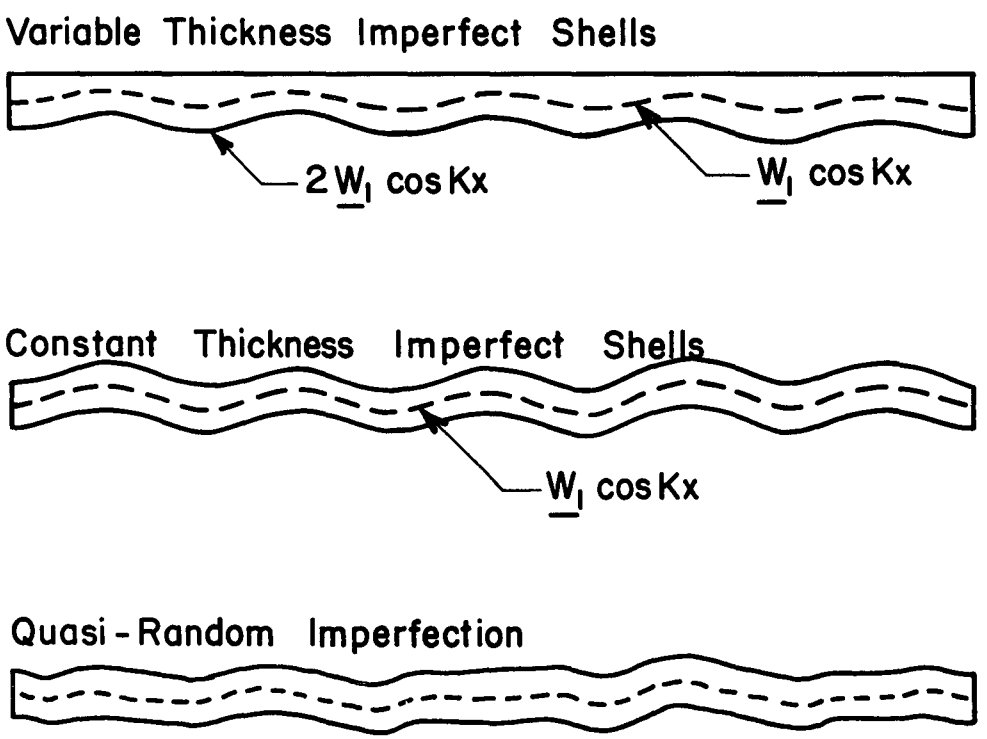

FIG. 1(b) IMPERFECTION GEOMETRIES

FIG. 2 COMPUTER GENERATED RADIAL DISPLACEMENTS & AXIAL LOADS VERSUS TIME

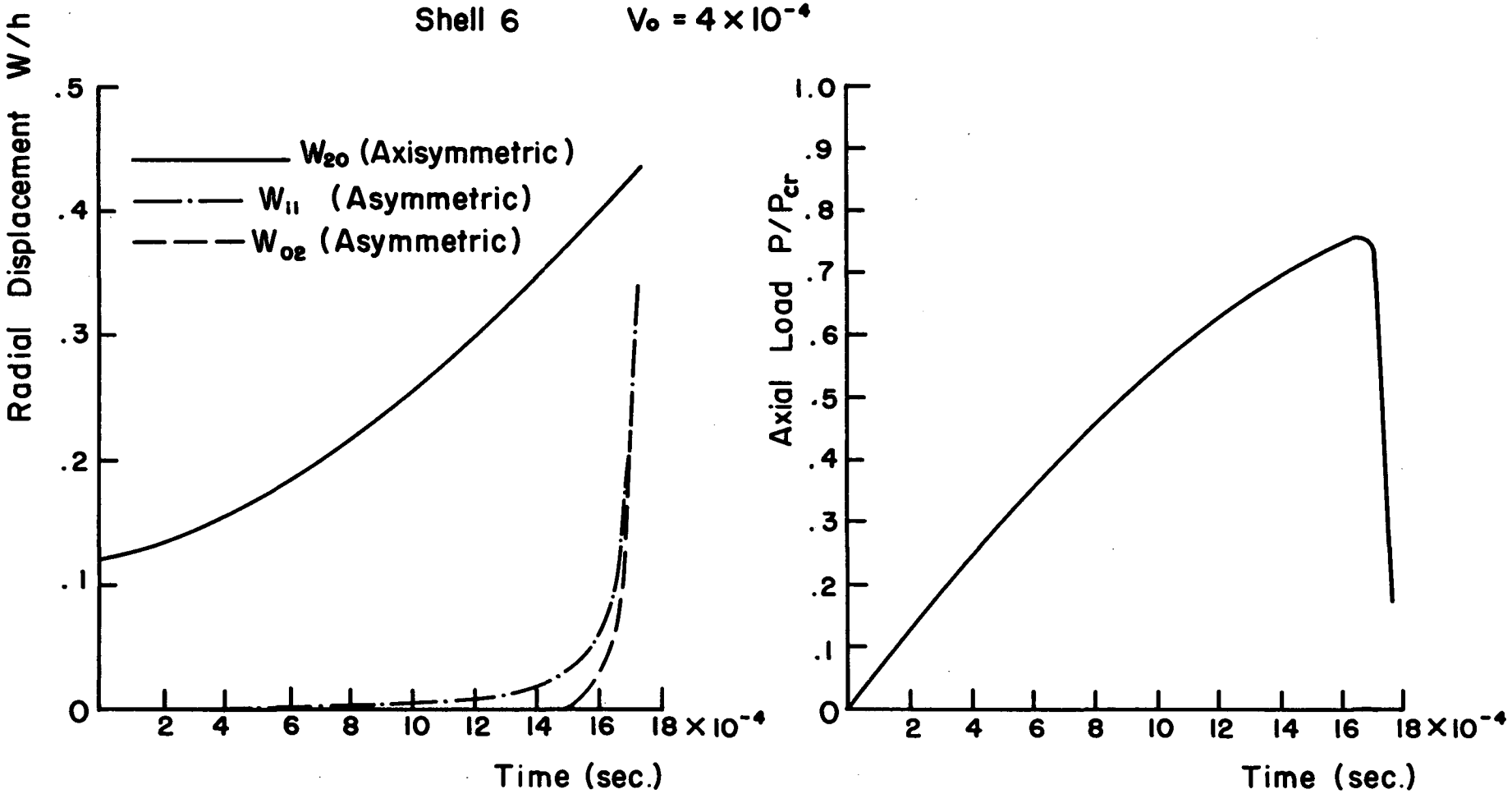

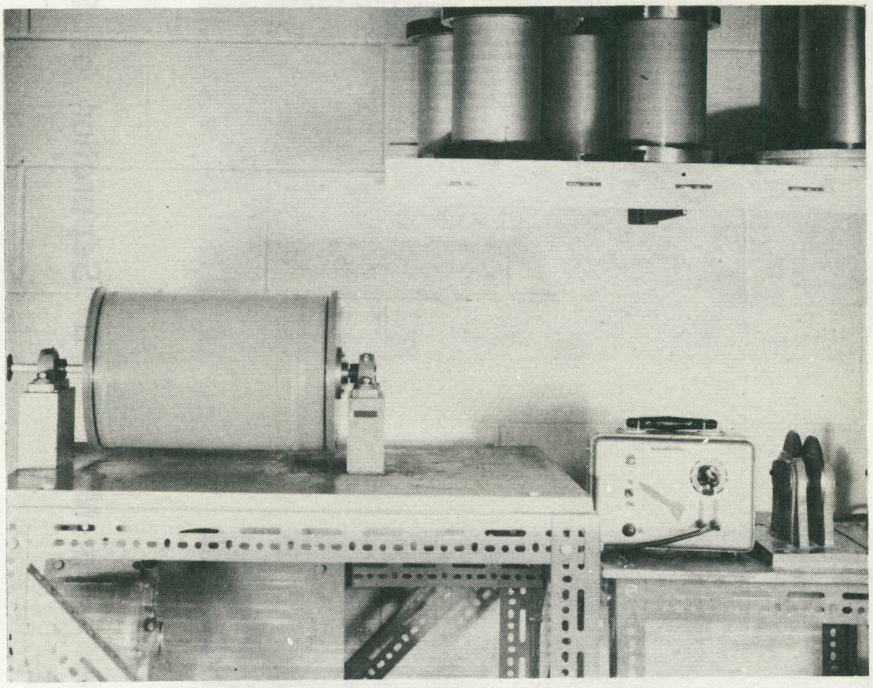

FIG. 3 APPARATUS FOR SPIN-CASTING PHOTOELASTIC SHELLS

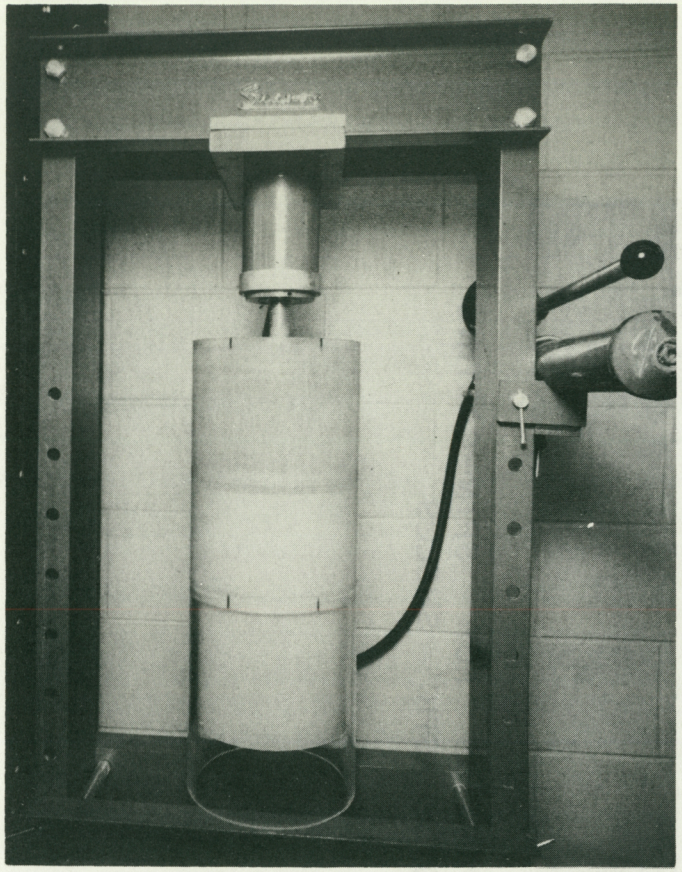

(a) Extraction of Shell and Liner from Mold

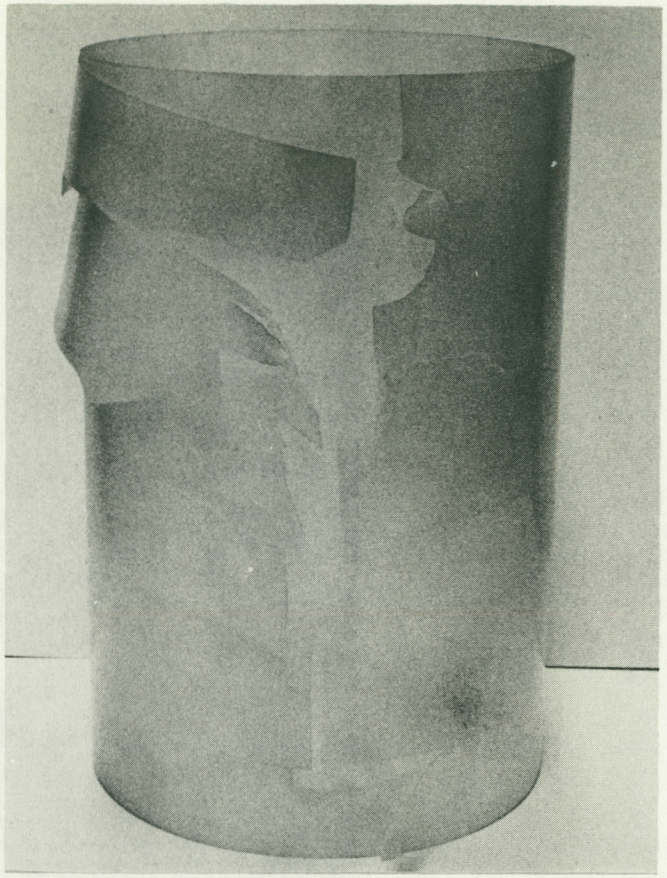

(b) Separation of Shell and Liner

FIG. 4 STEPS IN THE MANUFACTURING OF CONSTANT-THICKNESS IMPERFECT SHELLS

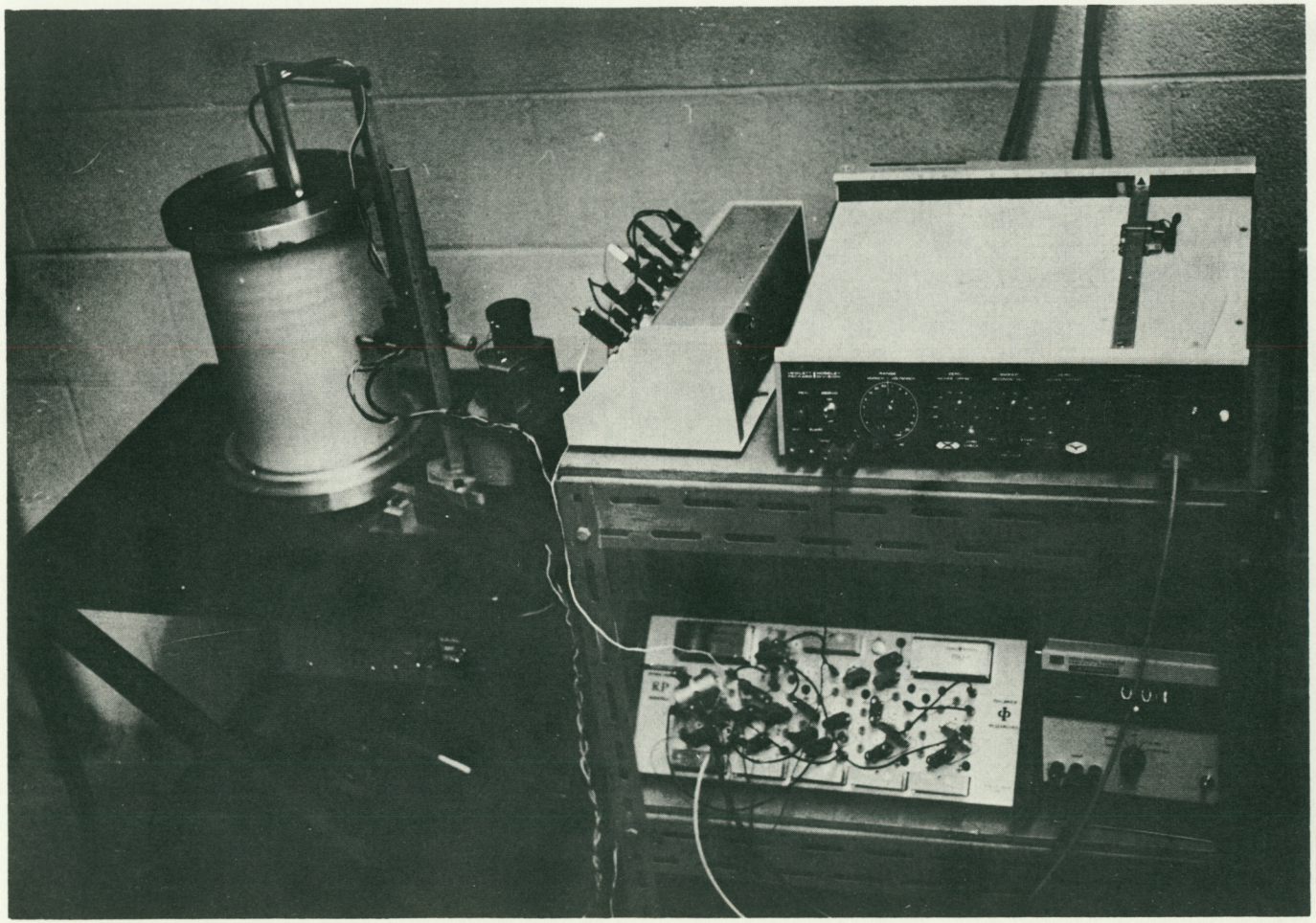

FIG. 5 PHOTOGRAPH OF PROFILE MEASURING APPARATUS

FIG. 6 **TESTING MACHINE AND INSTRUMENTATION**

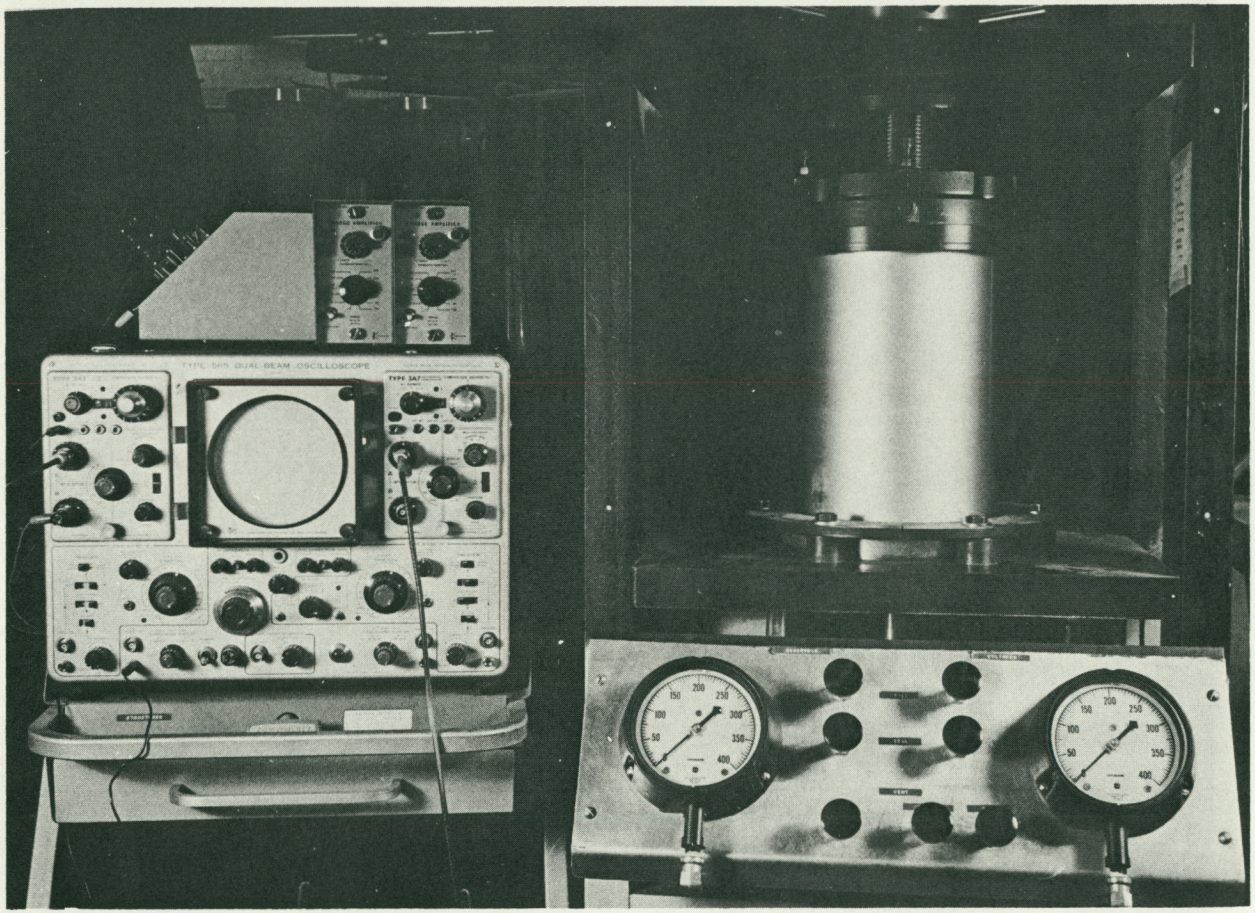

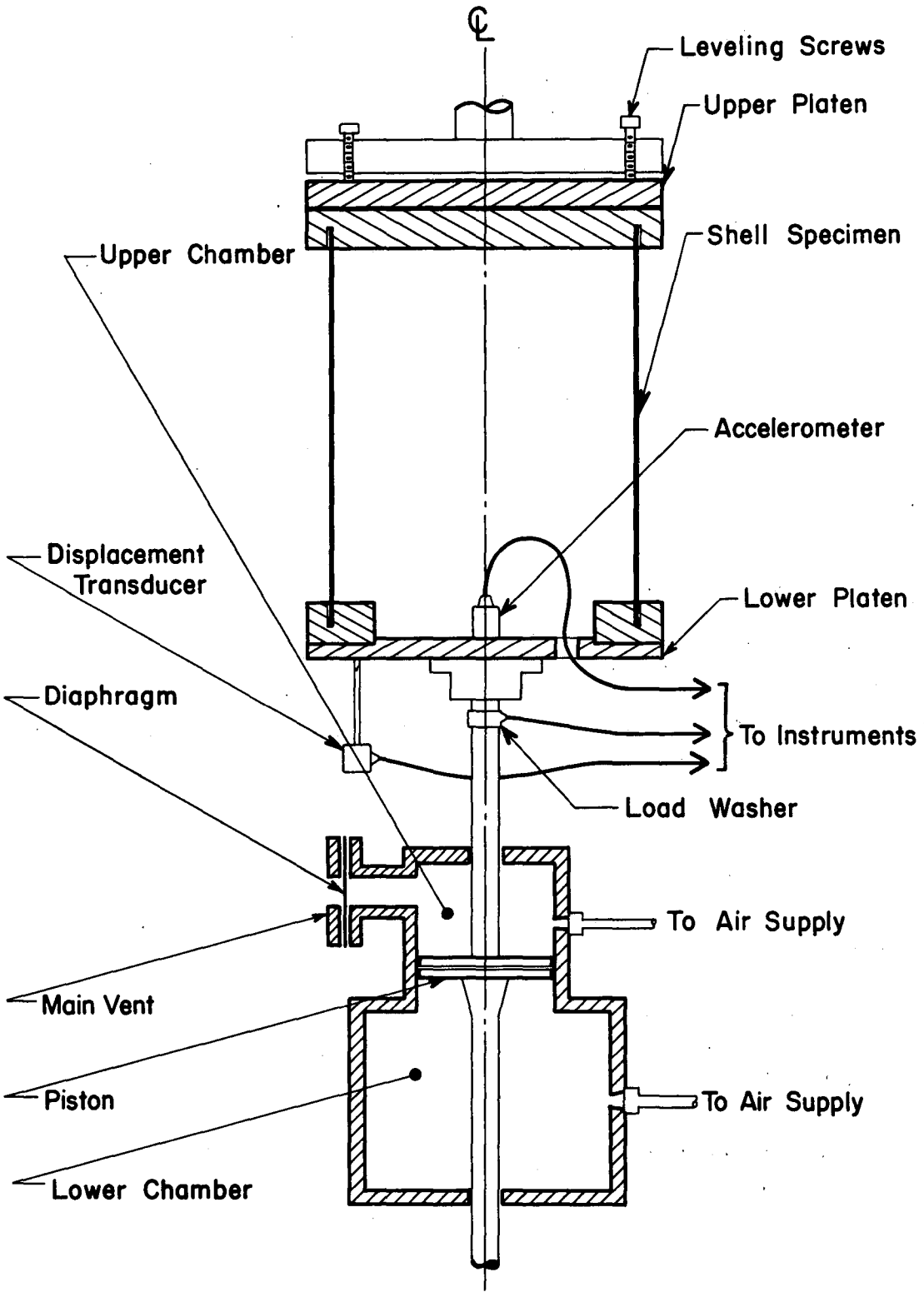

FIG. 7 SCHEMATIC VIEW OF TESTING MACHINE

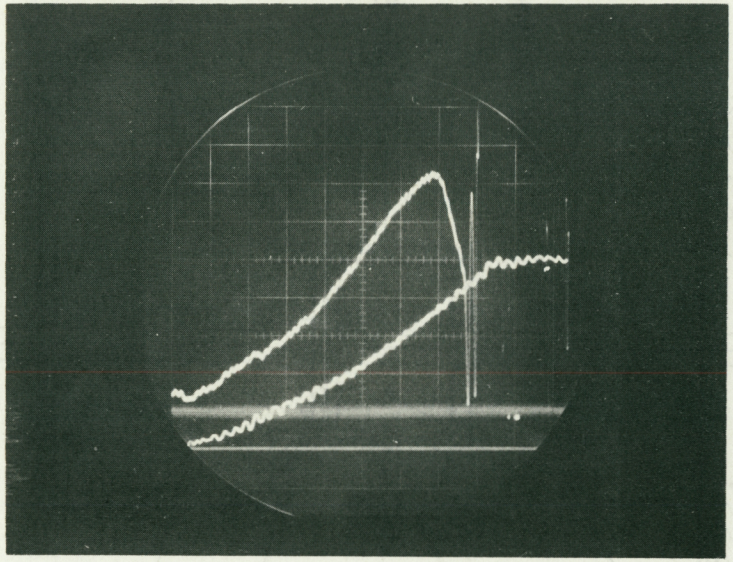

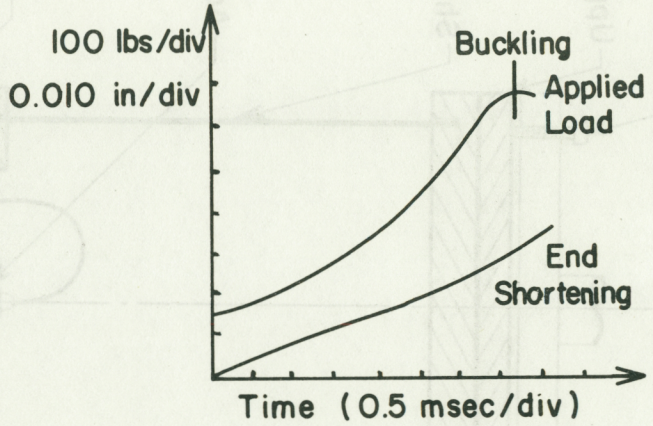

FIG. 8 DYNAMIC OUTPUTS OF END SHORTENING & AXIAL LOAD

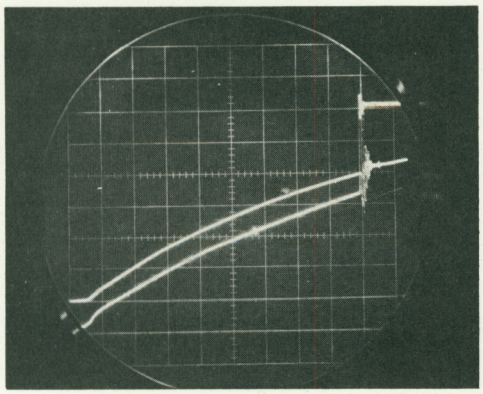

100 msec/div.

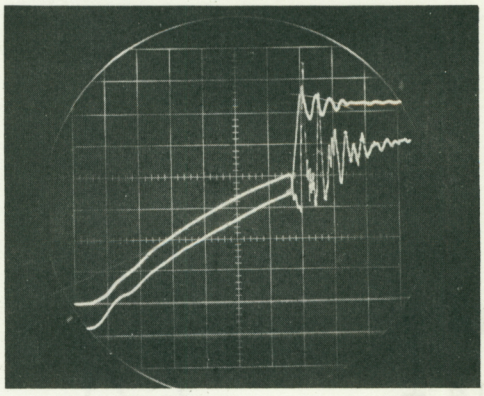

10 msec/div.

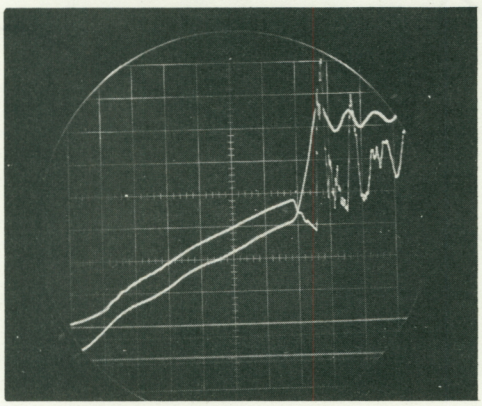

5 msec/div.

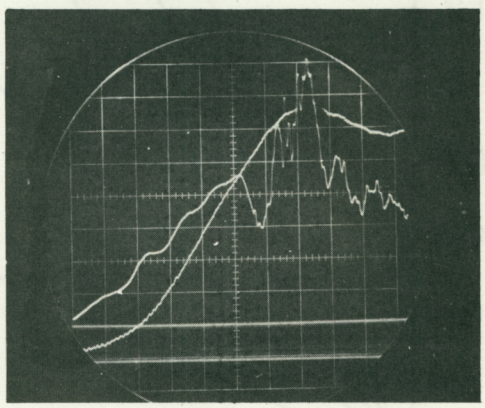

1 msec/div.

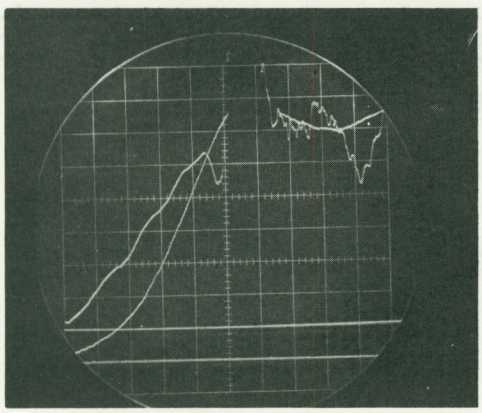

1 msec/div.

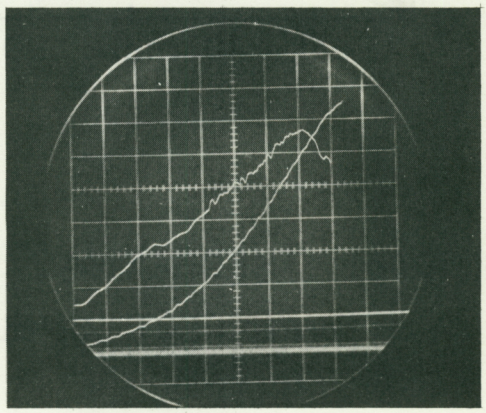

.5 msec/div.

FIG. 9 OSCILLOSCOPE PHOTOGRAPHS FROM A TYPICAL TEST SERIES (SHELL 8)

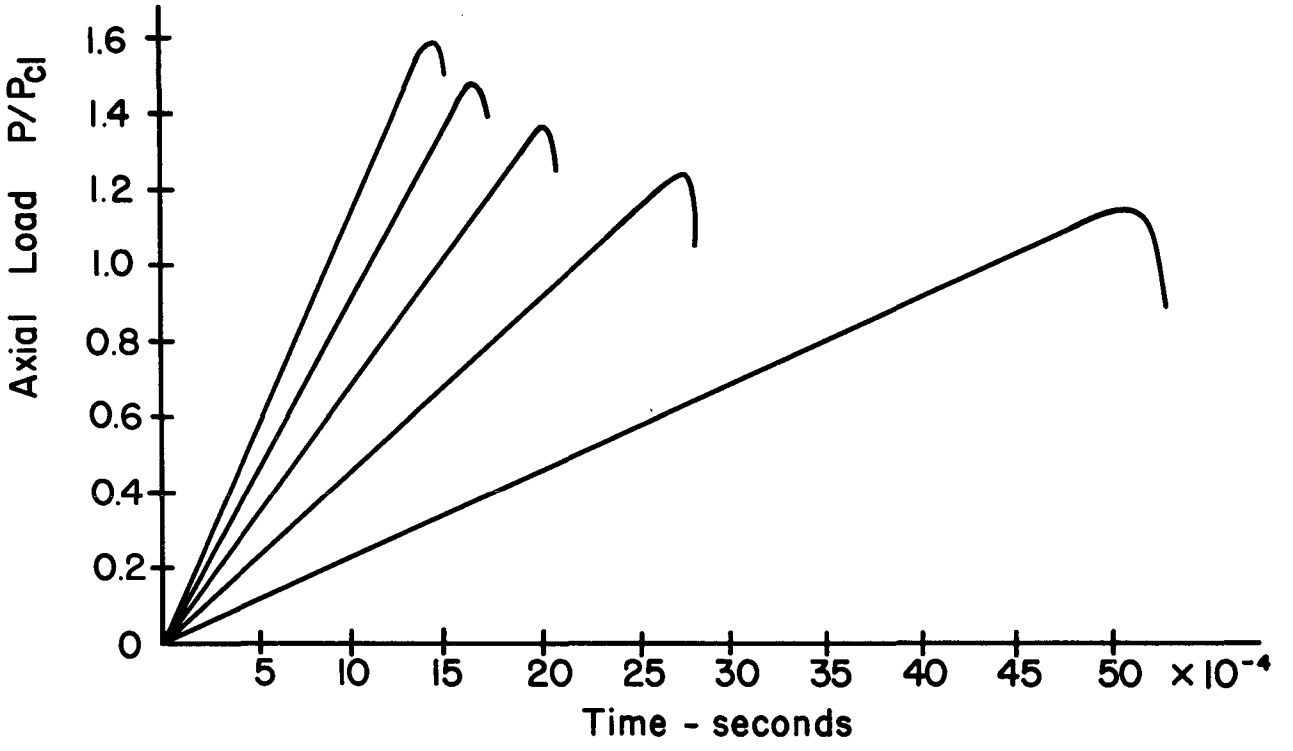

FIG. 10(a) THEORETICAL AXIAL LOADS VS TIME
PERFECT SHELL MODEL

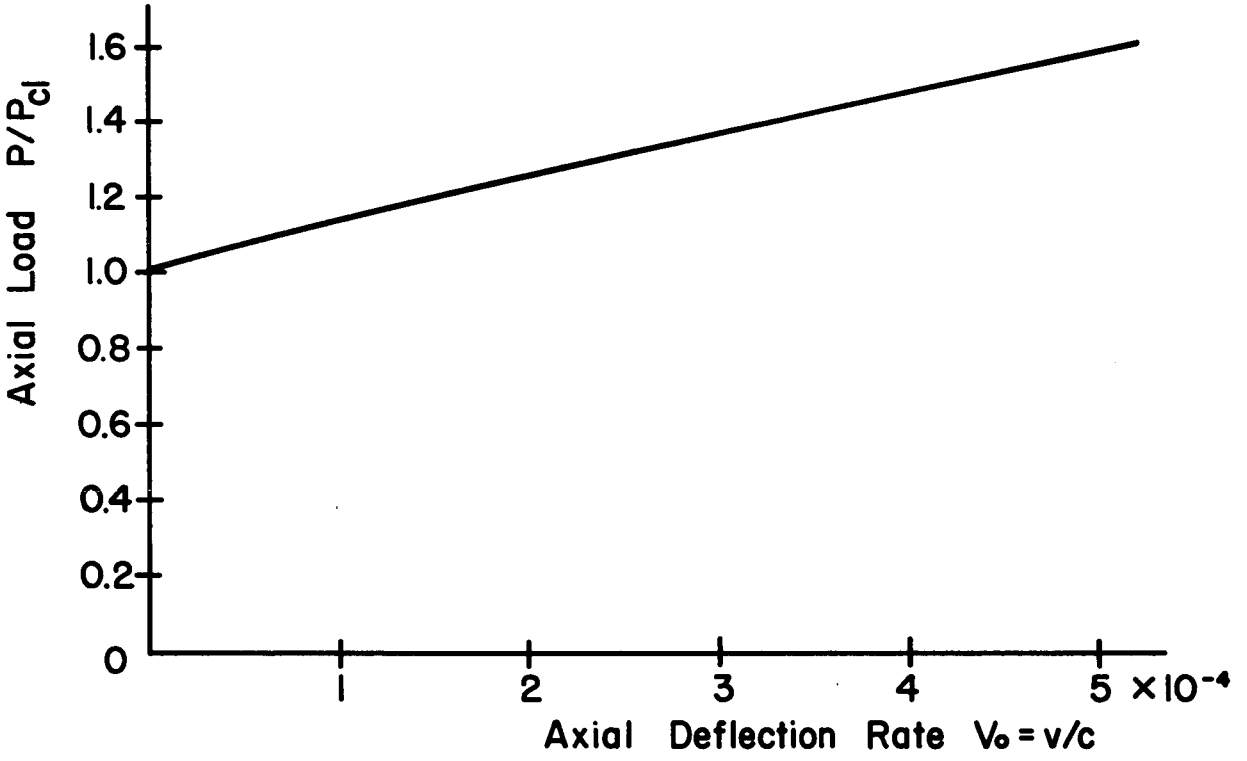

FIG. 10(b) THEORETICAL BUCKLING LOADS VS DEFLECTION RATE

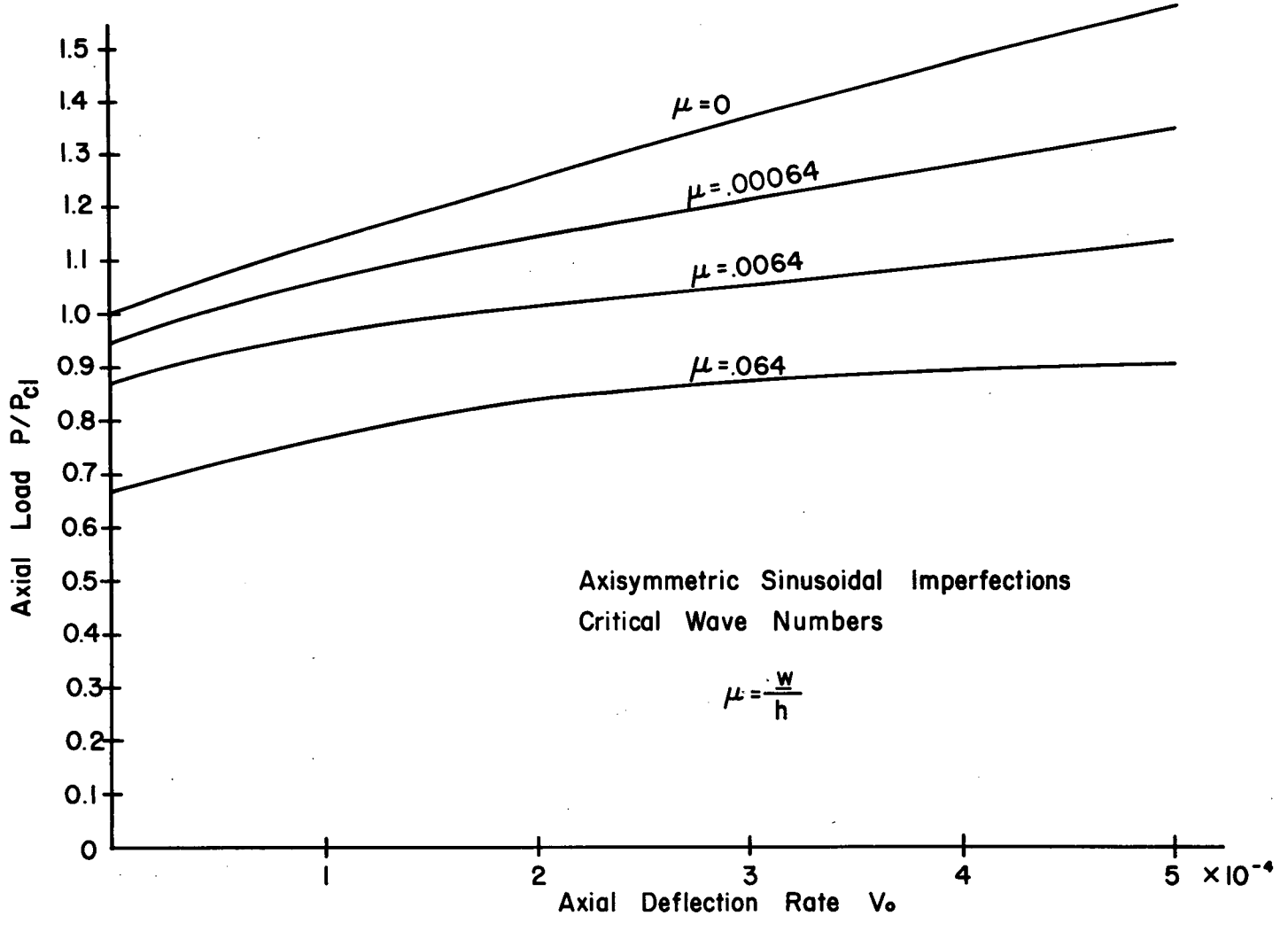

FIG. 11 VARIATION IN DYNAMIC BUCKLING LOADS WITH IMPERFECTION AMPLITUDE

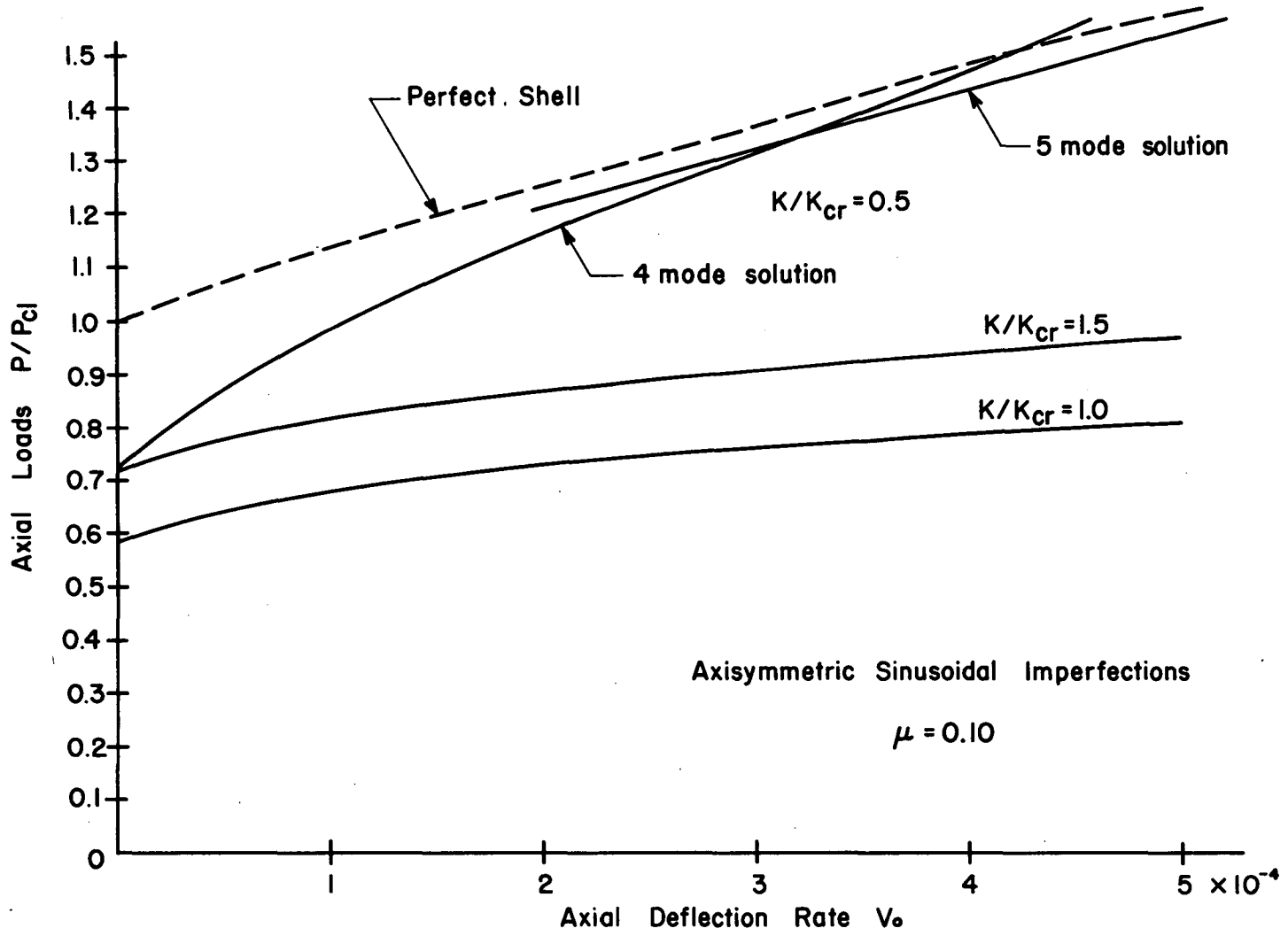

FIG. 12 VARIATION IN DYNAMIC BUCKLING LOADS WITH IMPERFECTION WAVENUMBER

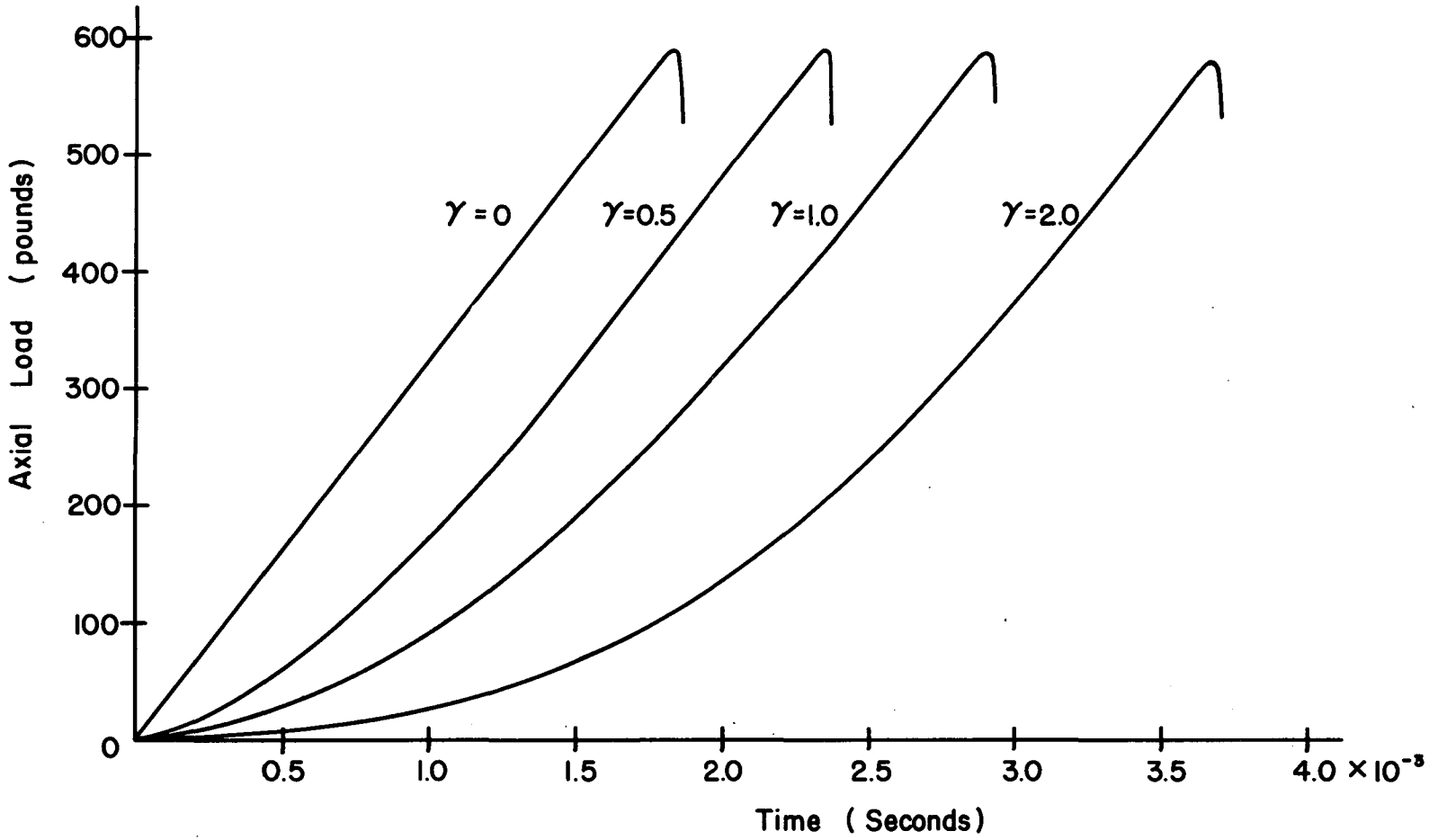

FIG. 13 THEORETICAL AXIAL LOADS FOR NON-LINEAR AXIAL DEFLECTION RATES $\delta(t) = V_o(1-e^{-\gamma t})t$

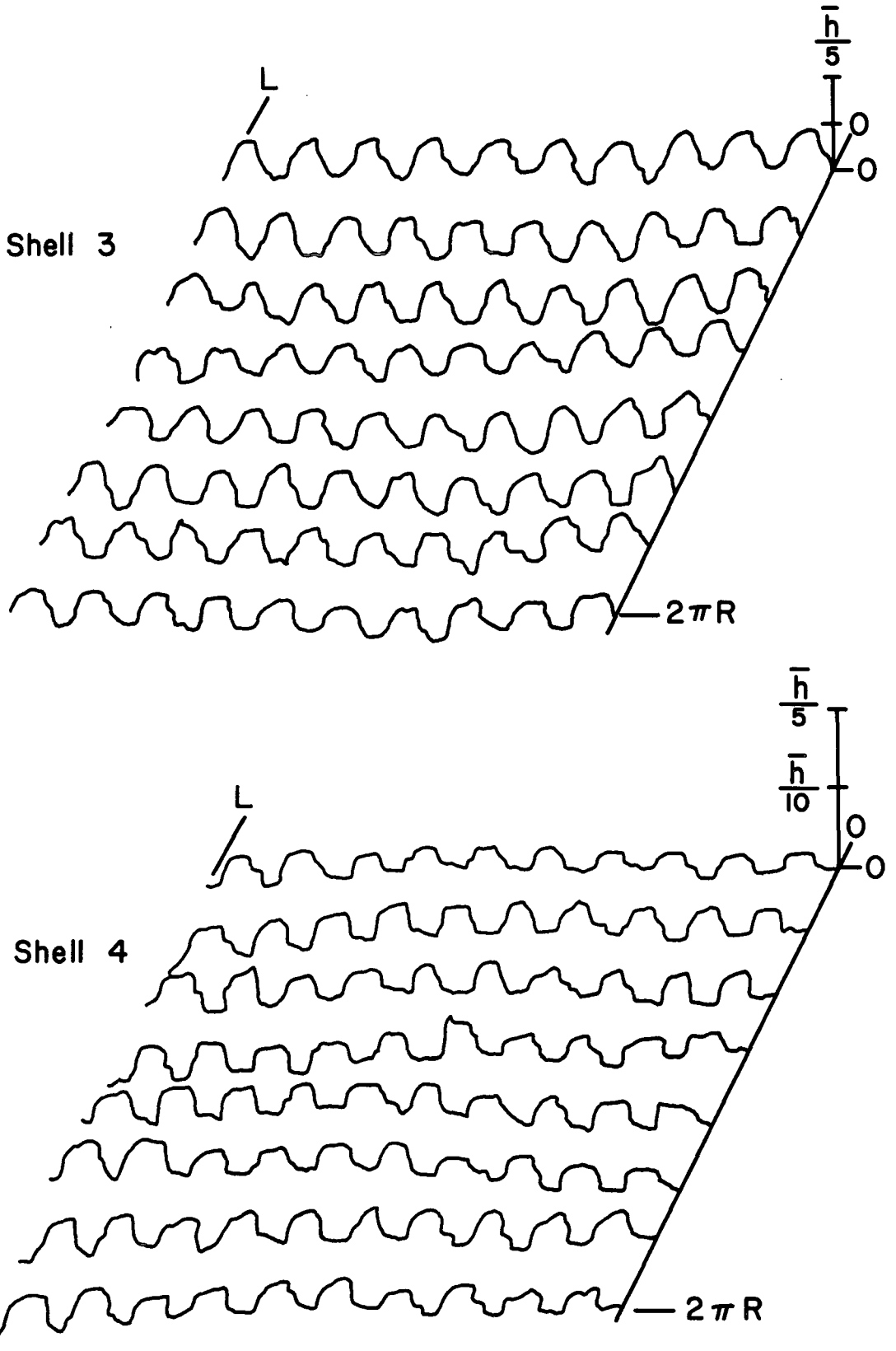

FIG. 14 SHELL MEDIAN SURFACE PROFILES

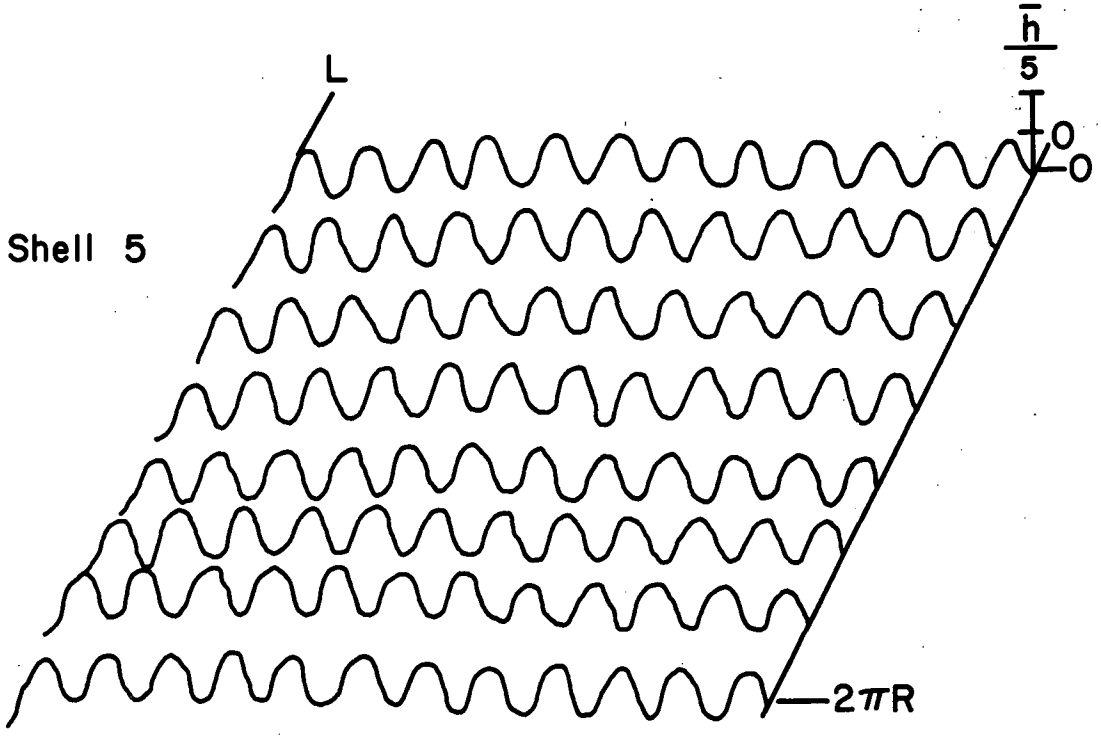

FIG. 15 SHELL MEDIAN SURFACE PROFILES

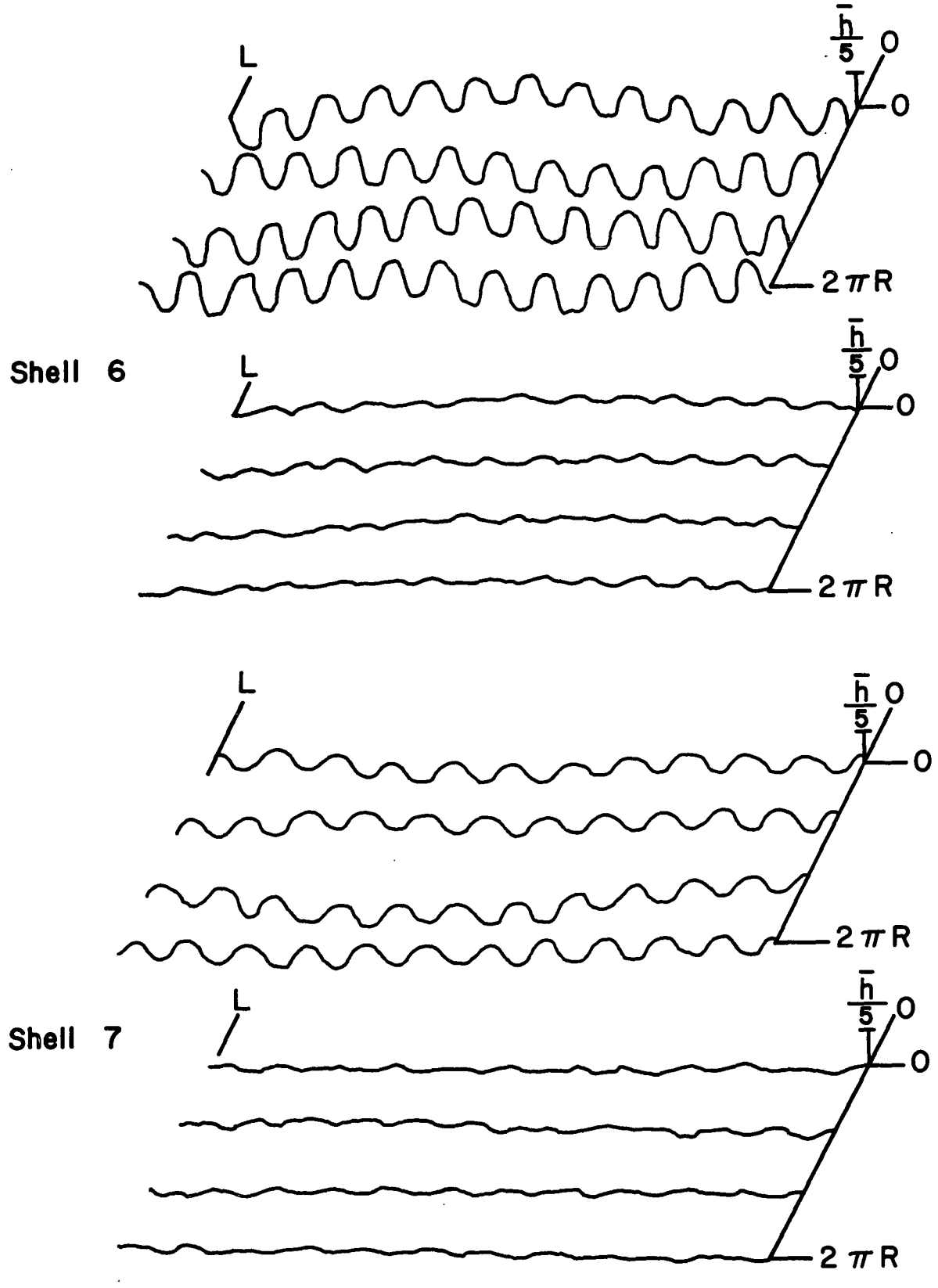

FIG. 16 SHELL WALL & THICKNESS PROFILES

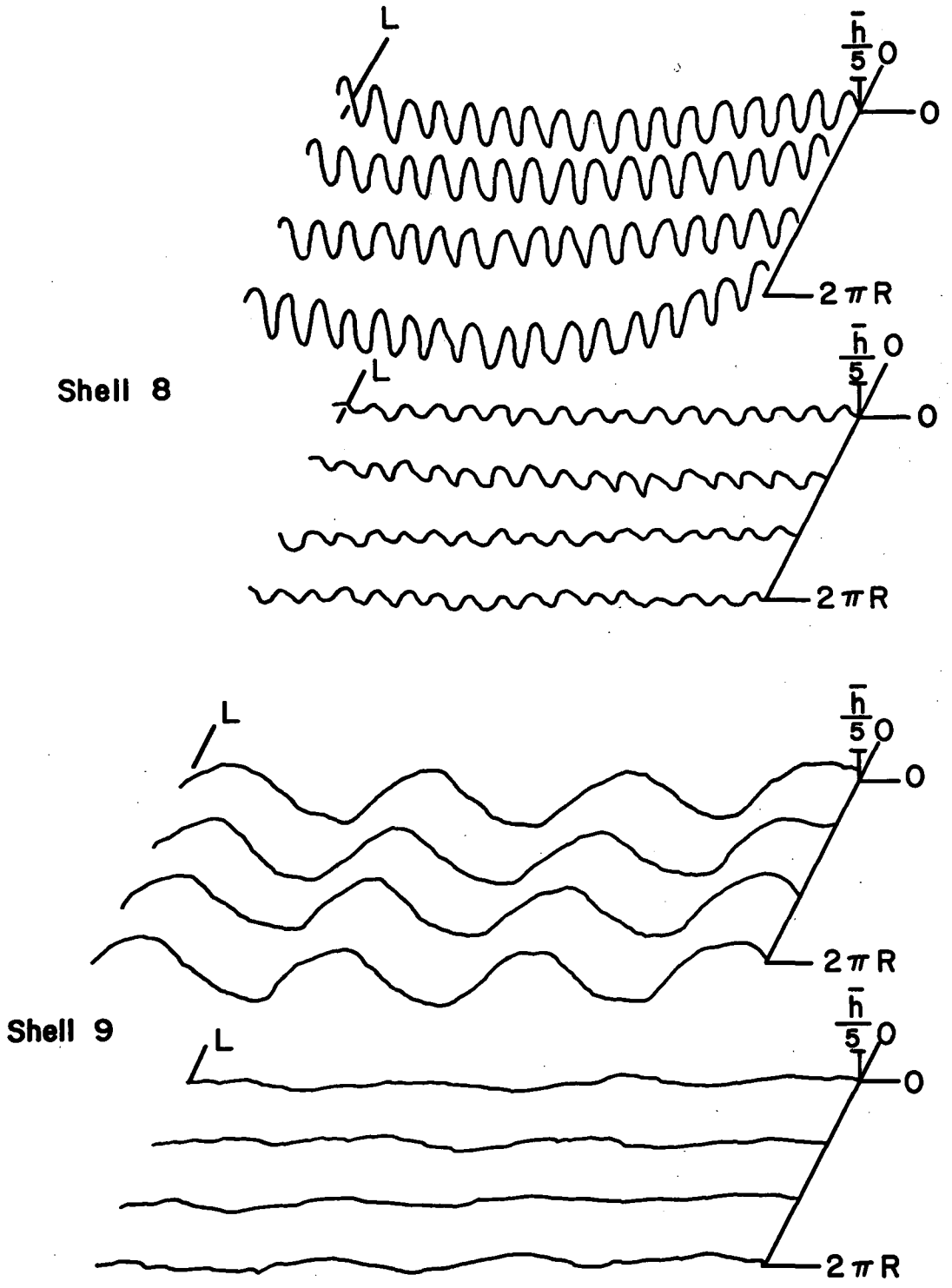

FIG. 17 SHELL WALL & THICKNESS PROFILES

Shell 10

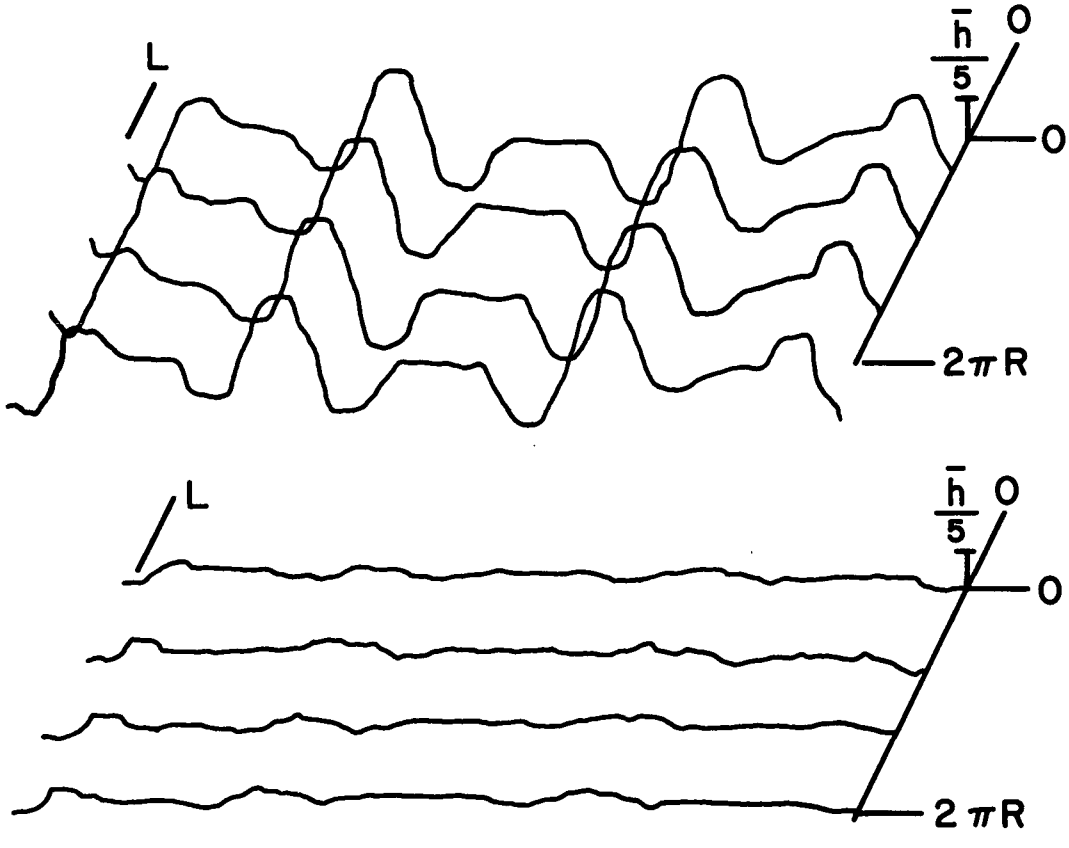

FIG. 18 SHELL WALL & THICKNESS PROFILES

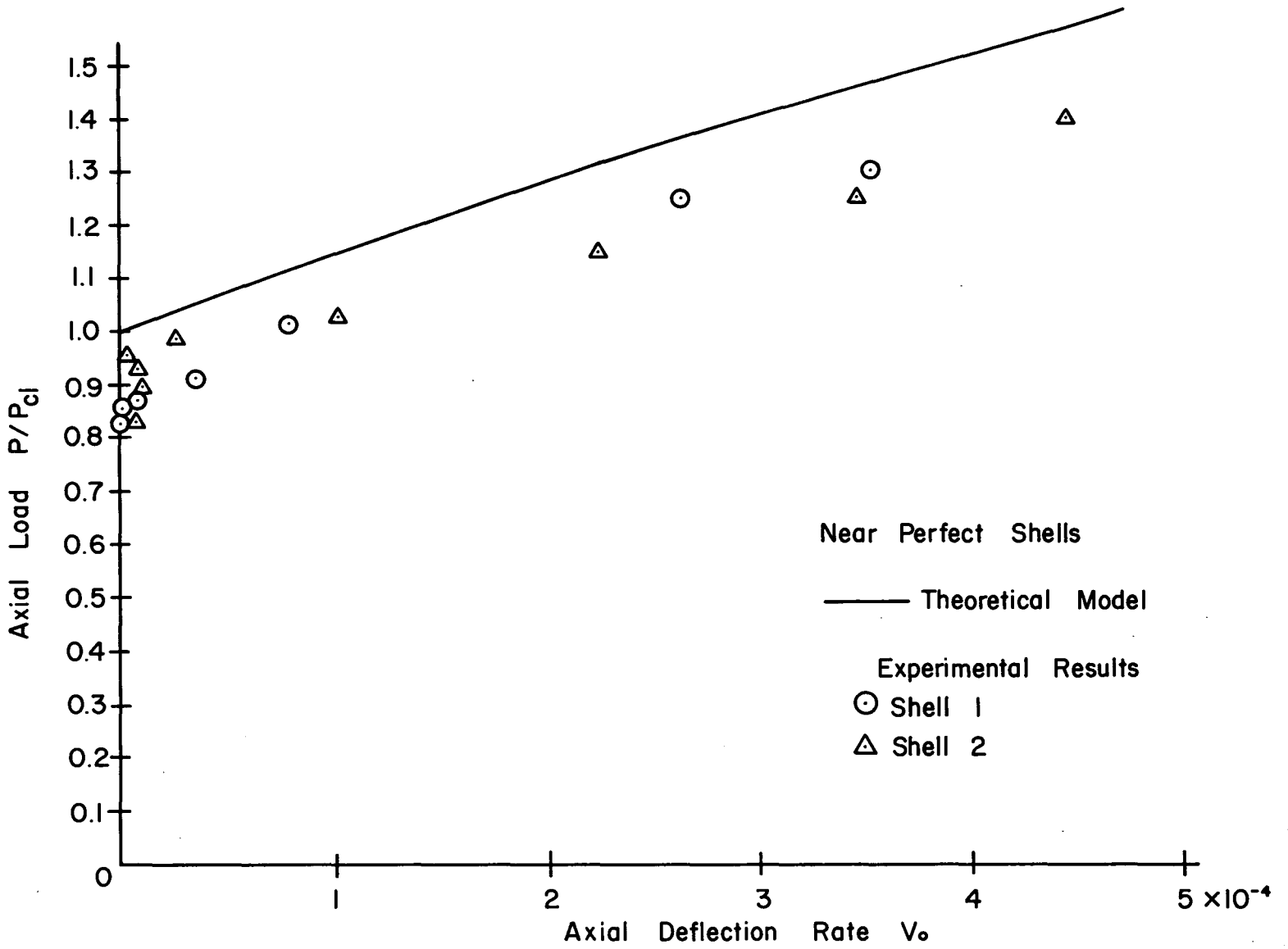

FIG. 19 DYNAMIC BUCKLING LOADS VS AXIAL DEFLECTION RATE

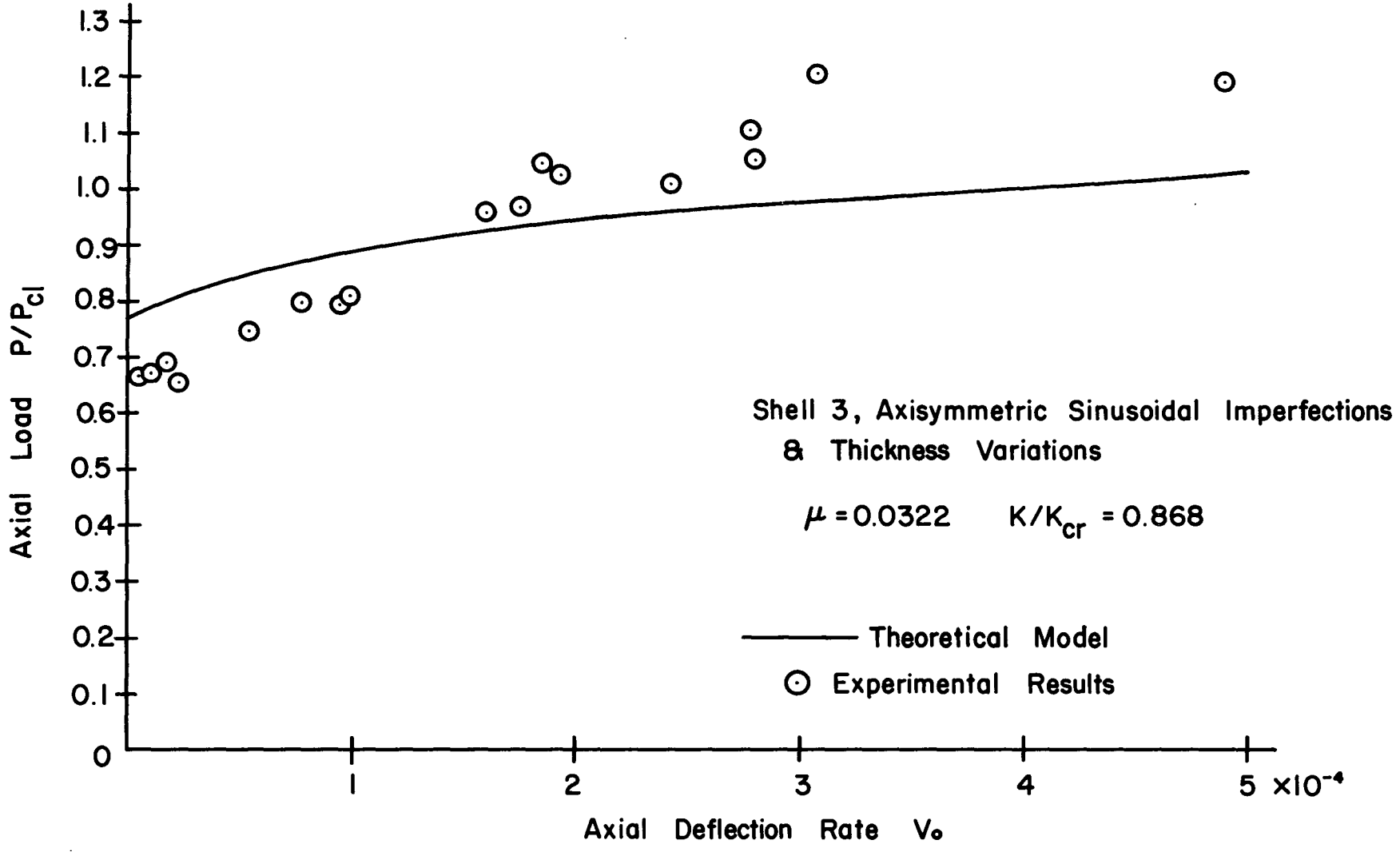

FIG. 20 DYNAMIC BUCKLING LOADS VS AXIAL DEFLECTION RATE

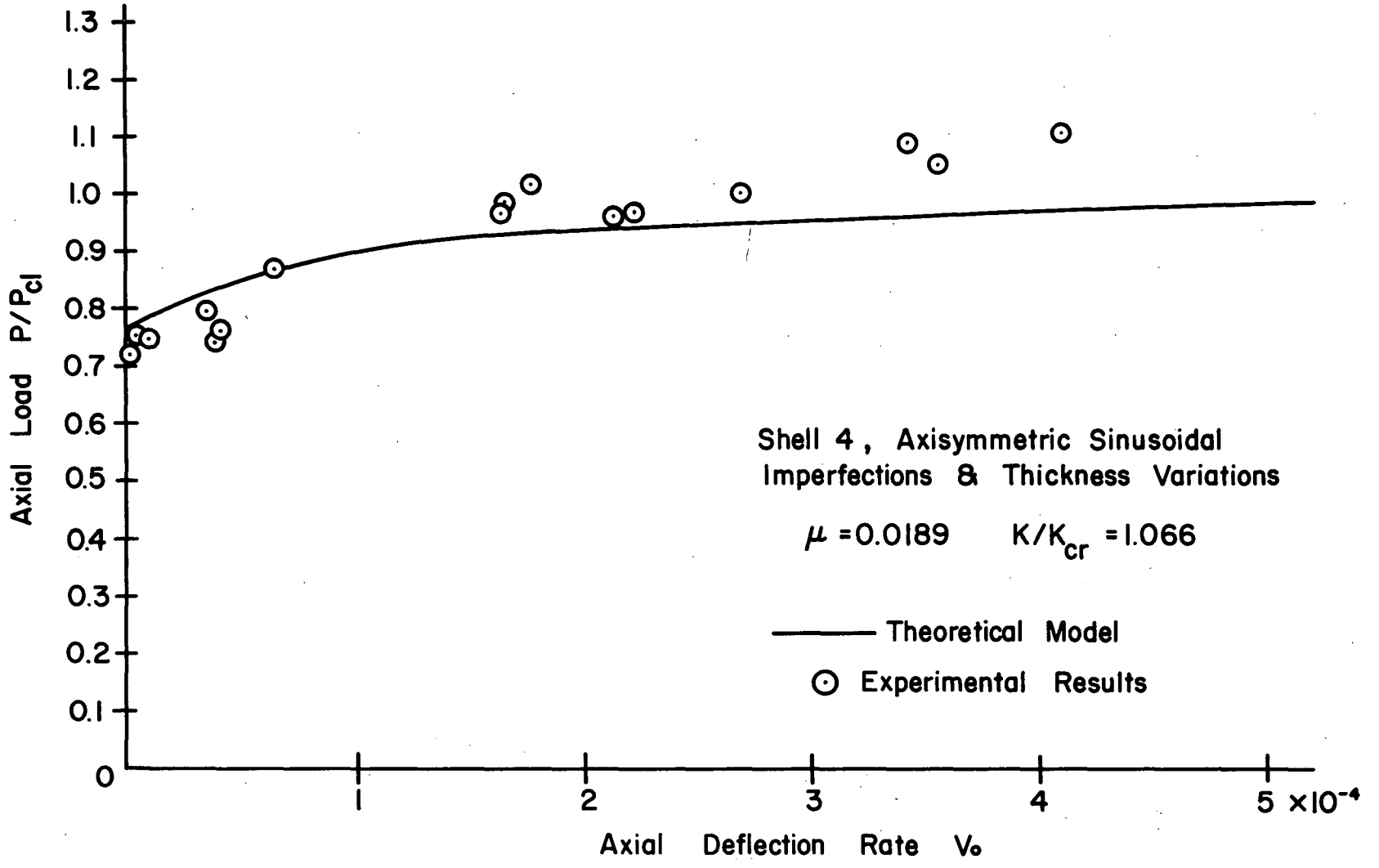

FIG. 21 DYNAMIC BUCKLING LOADS VS AXIAL DEFLECTION RATE

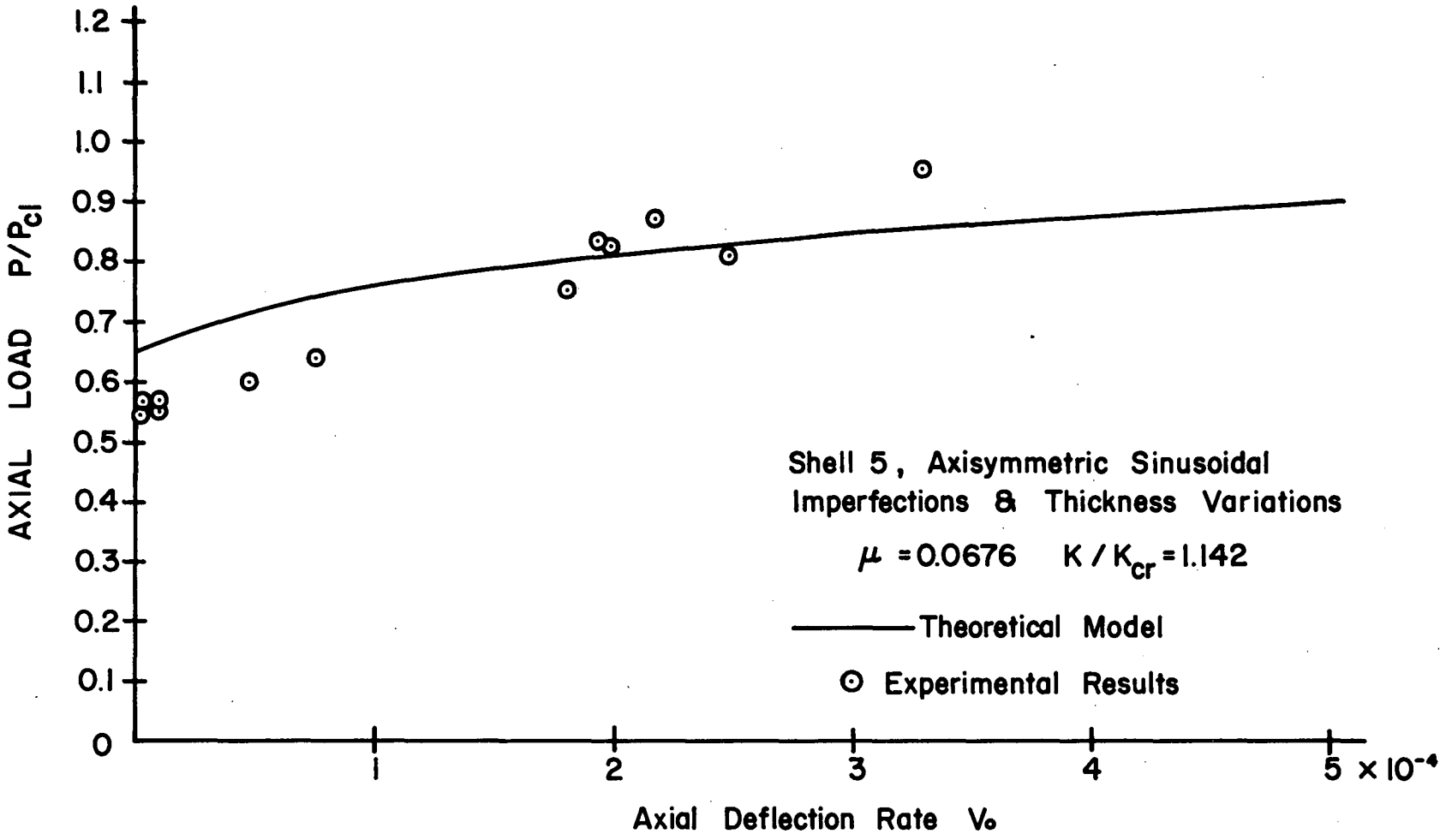

FIG. 22 DYNAMIC BUCKLING LOADS VS AXIAL DEFLECTION RATE

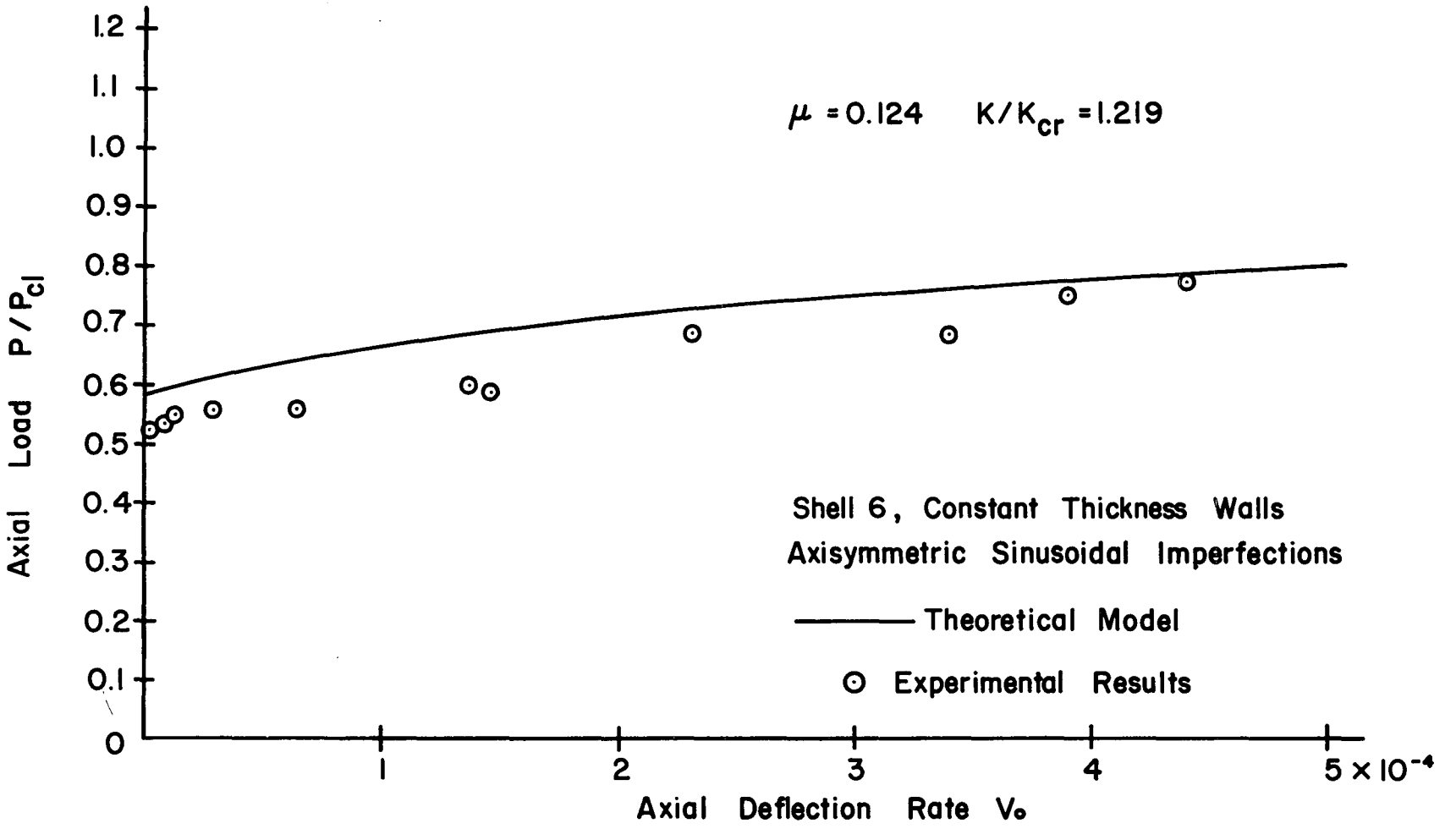

FIG. 23 DYNAMIC BUCKLING LOADS VS AXIAL DEFLECTION RATE

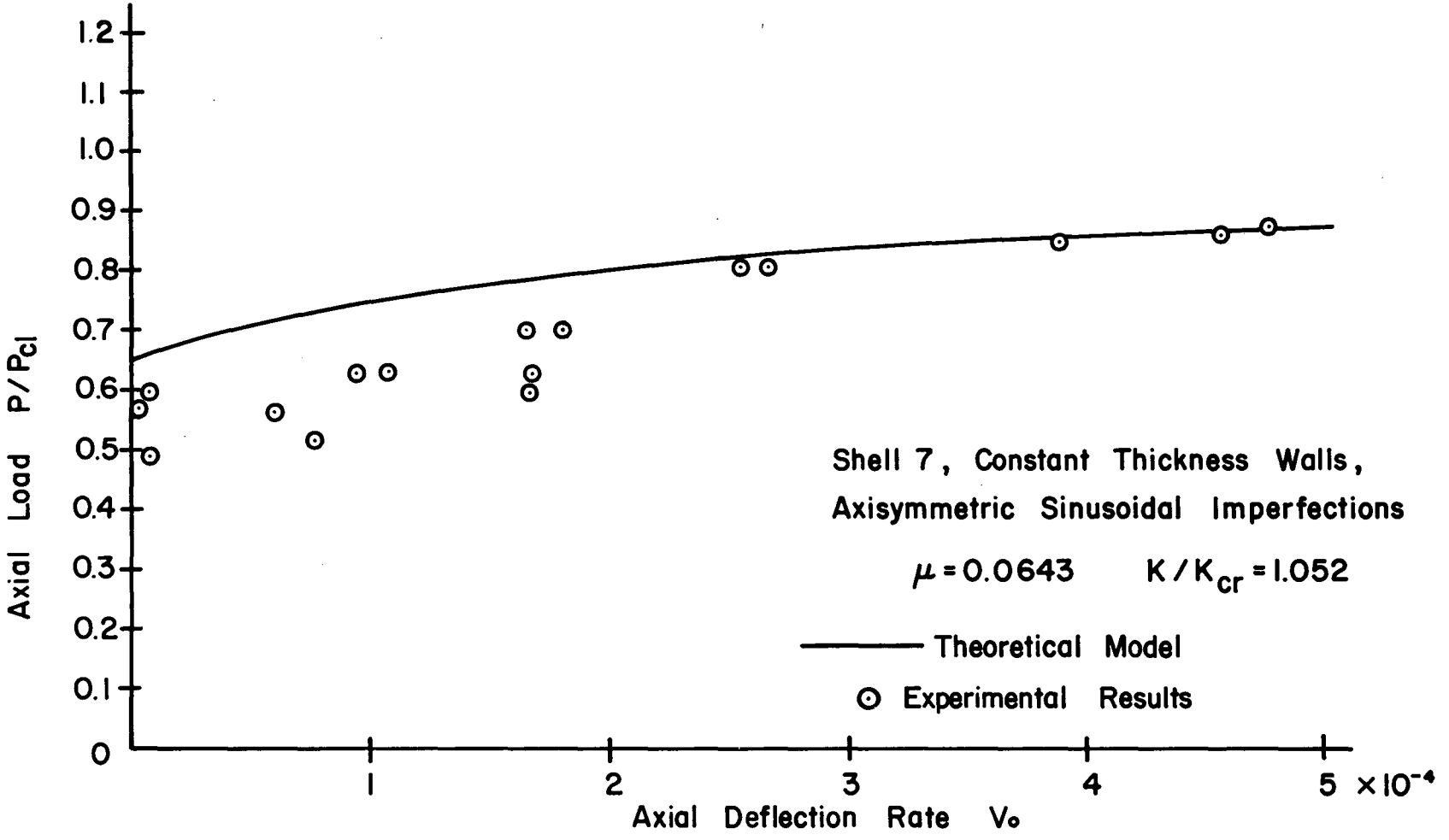

FIG. 24 DYNAMIC BUCKLING LOADS VS AXIAL DEFLECTION RATE

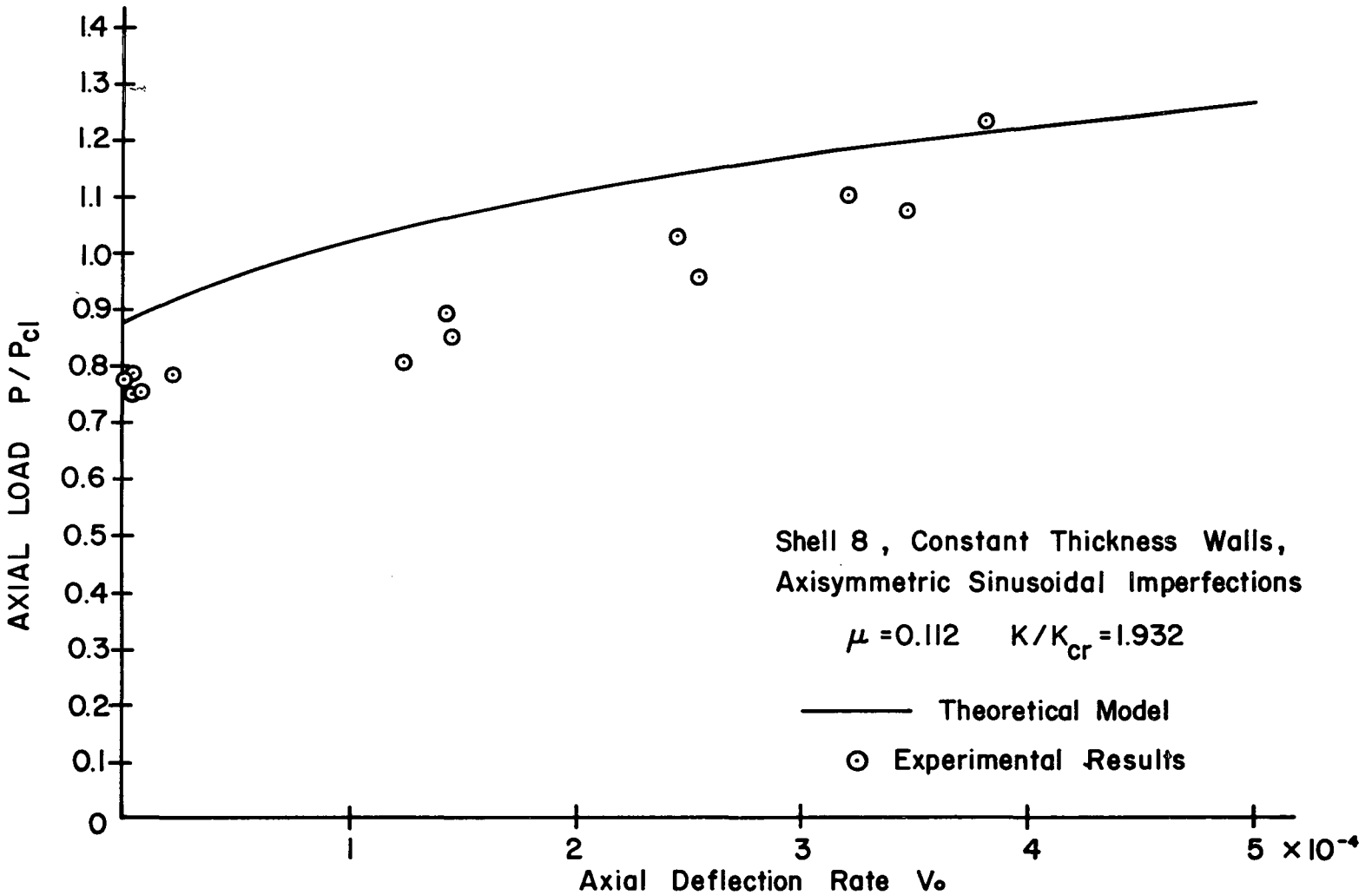

FIG. 25 DYNAMIC BUCKLING LOADS VS AXIAL DEFLECTION RATE

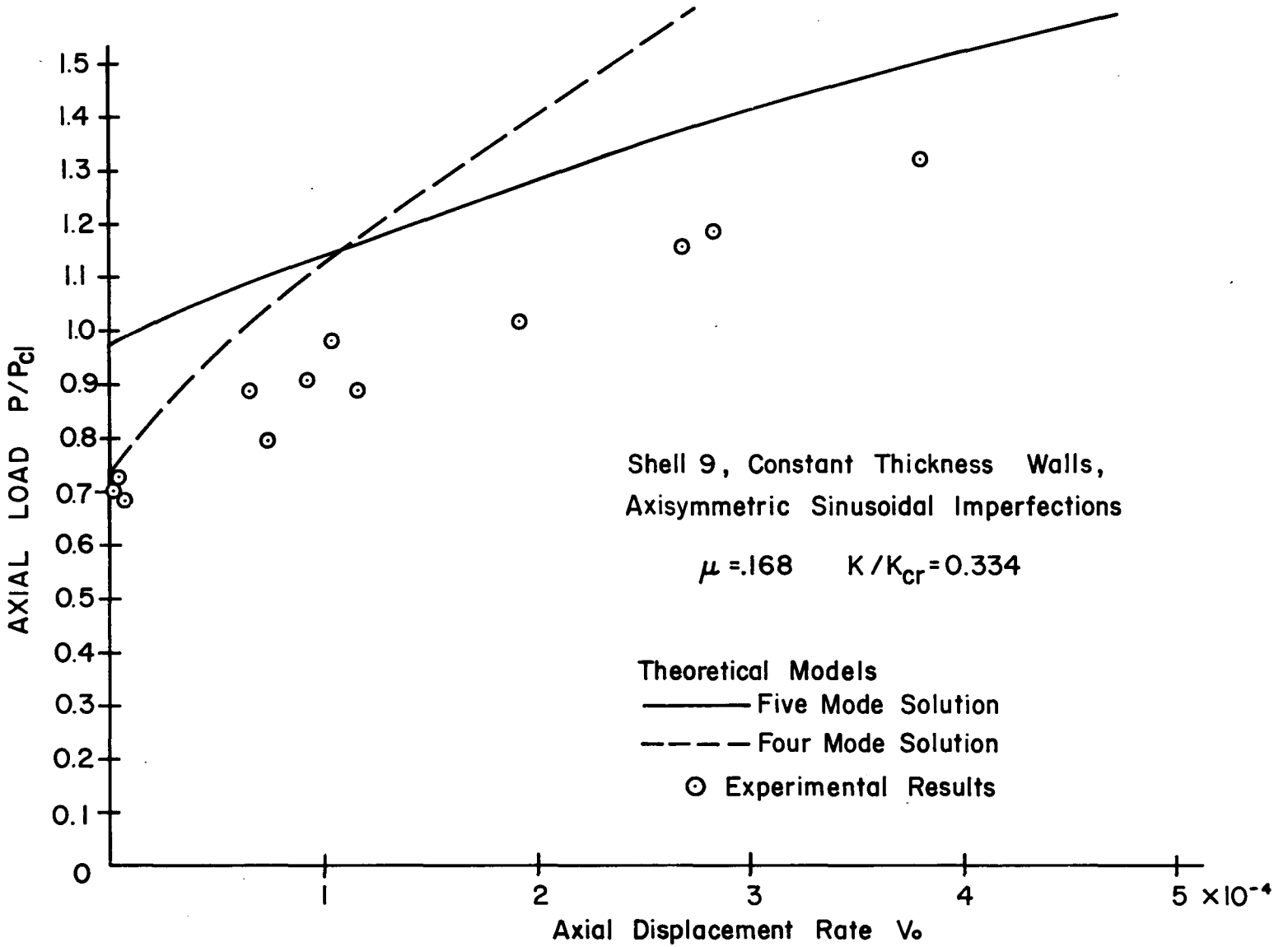

FIG. 26 DYNAMIC BUCKLING LOADS VS AXIAL DEFLECTION RATE

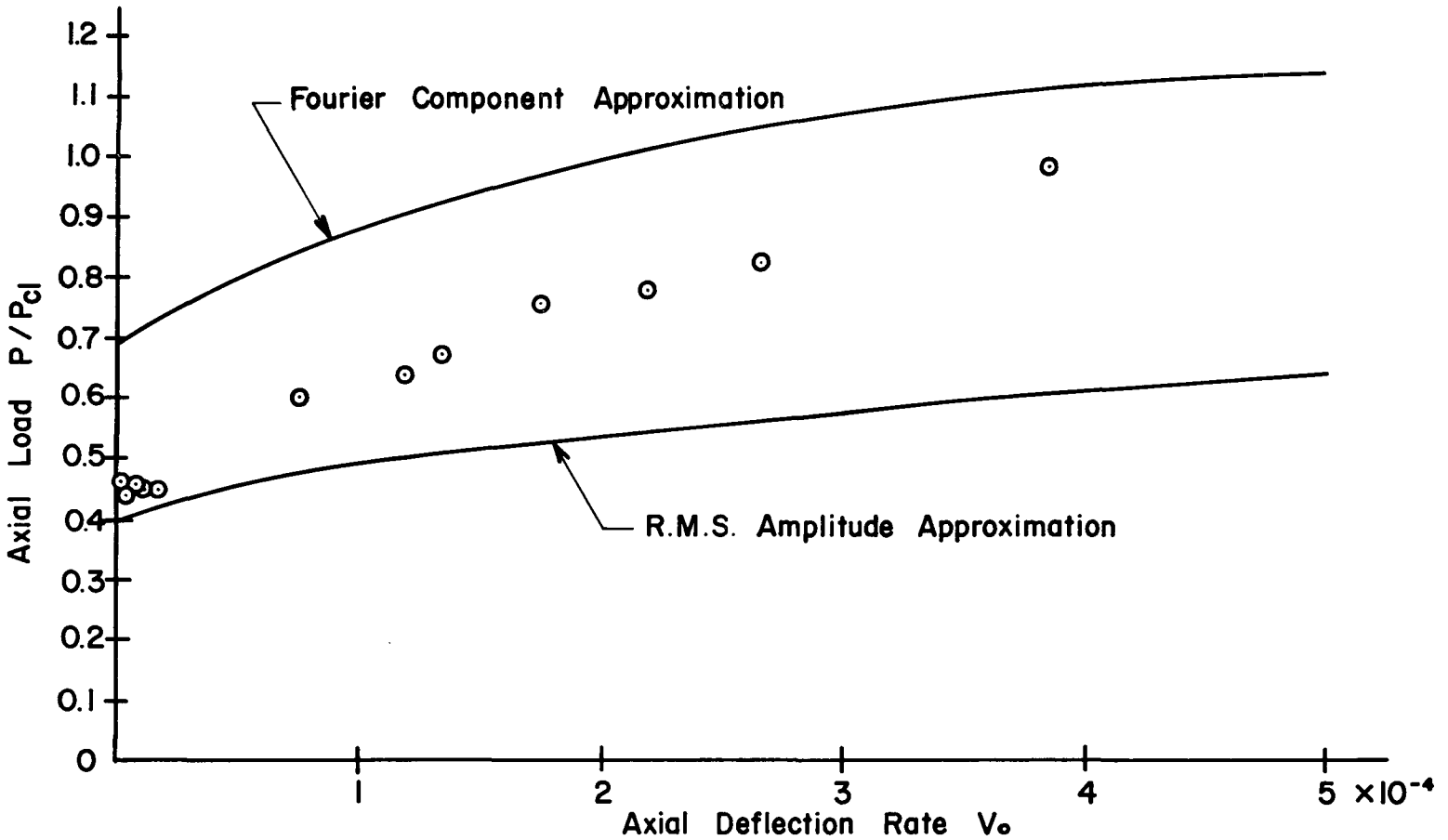

FIG. 27 DYNAMIC BUCKLING LOAD VS AXIAL DEFLECTION RATE
SHELL 10, QUASI-RANDOM IMPERFECTION

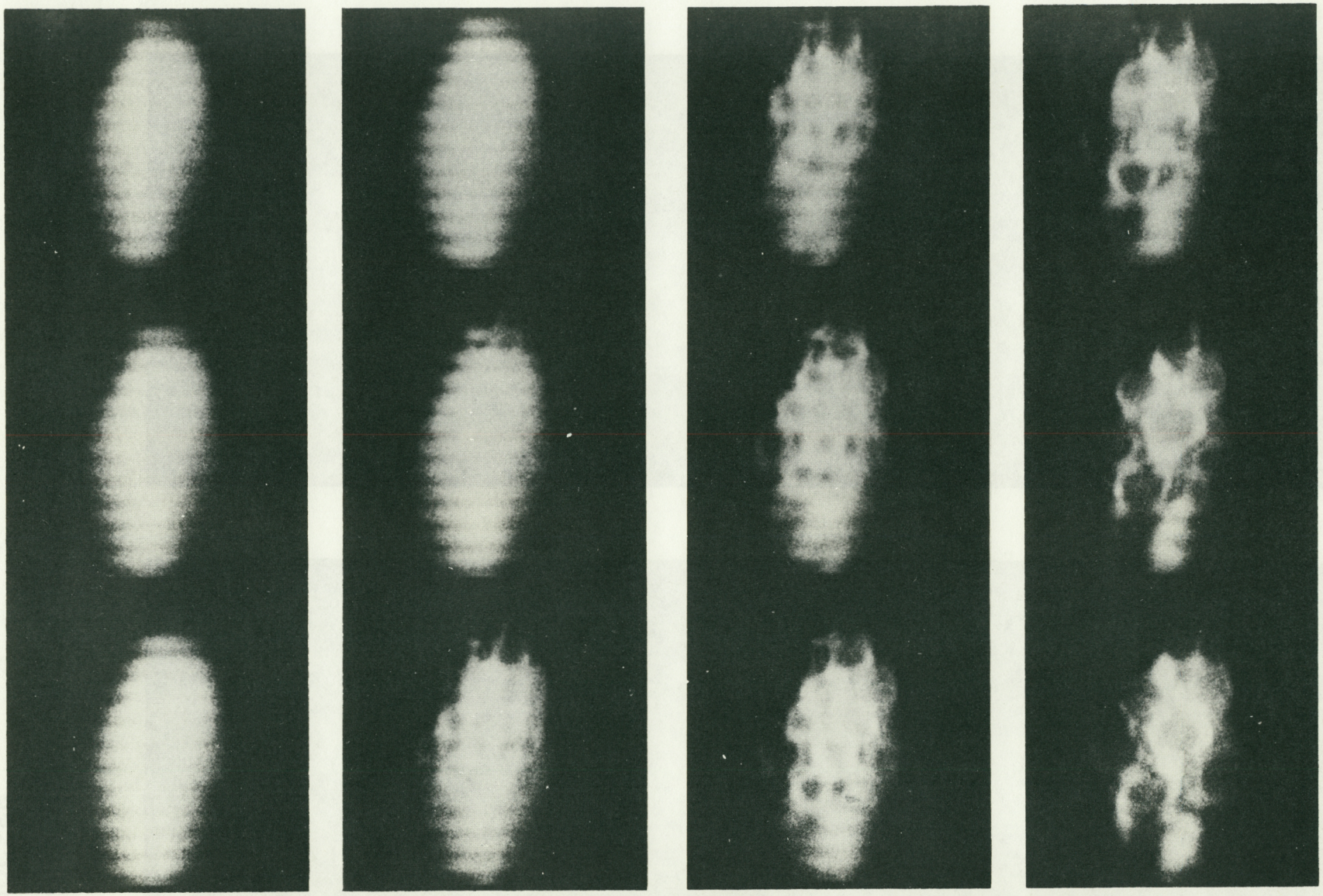

FIG. 28 HIGH-SPEED PHOTOGRAPHS OF DYNAMIC BUCKLING PROCESS

Shell 5 $V_o = 2.5 \times 10^{-4}$ 3600 Frames/Sec.

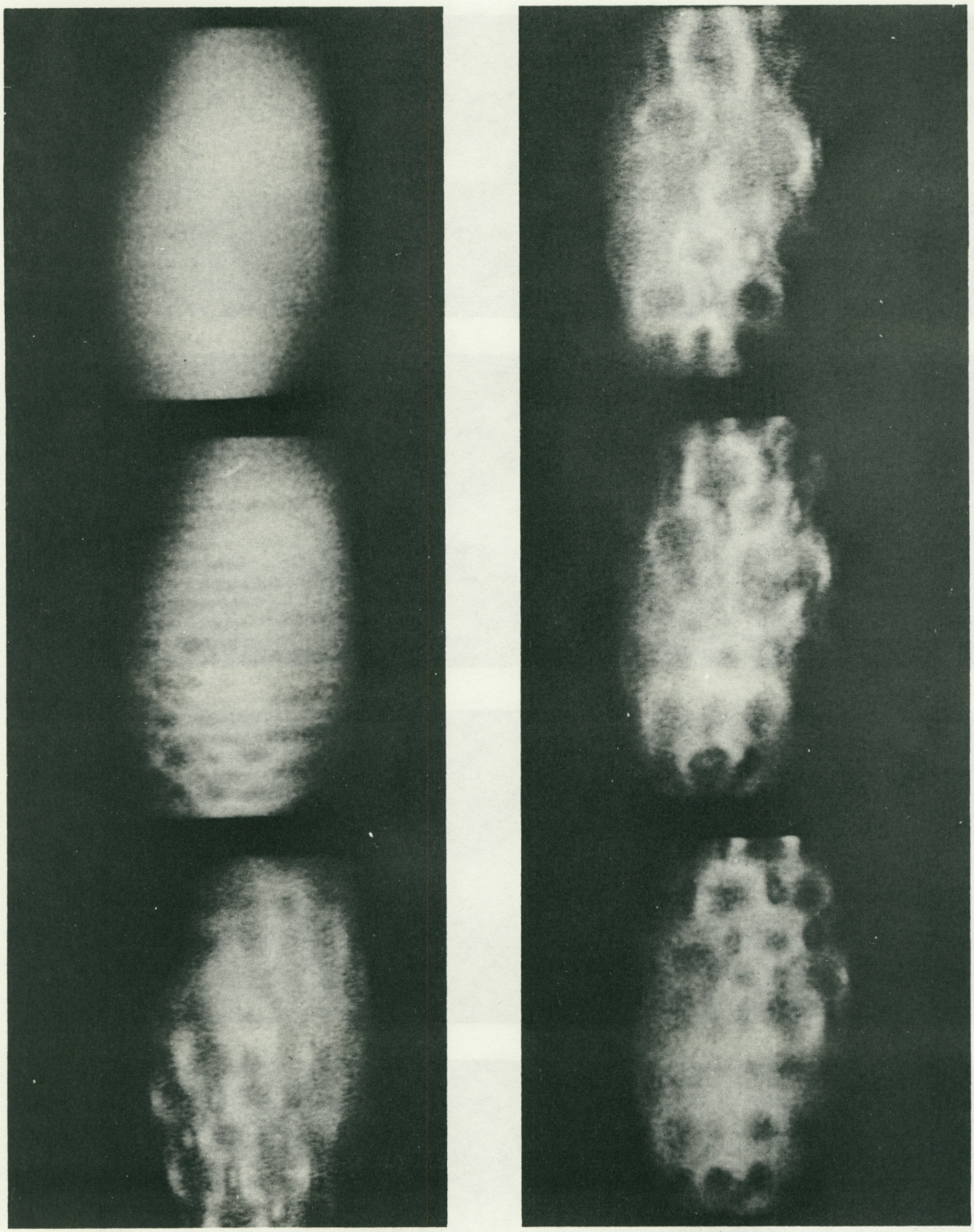

FIG. 29 HIGH-SPEED PHOTOGRAPHS OF DYNAMIC BUCKLING PROCESS

Shell 9 $V_o = 2 \times 10^{-4}$, 2500 Frames/Sec.

FIG. 30 SPLIT HOPKINSON BAR APPARATUS

BAR APPARATUS SCHEMATIC

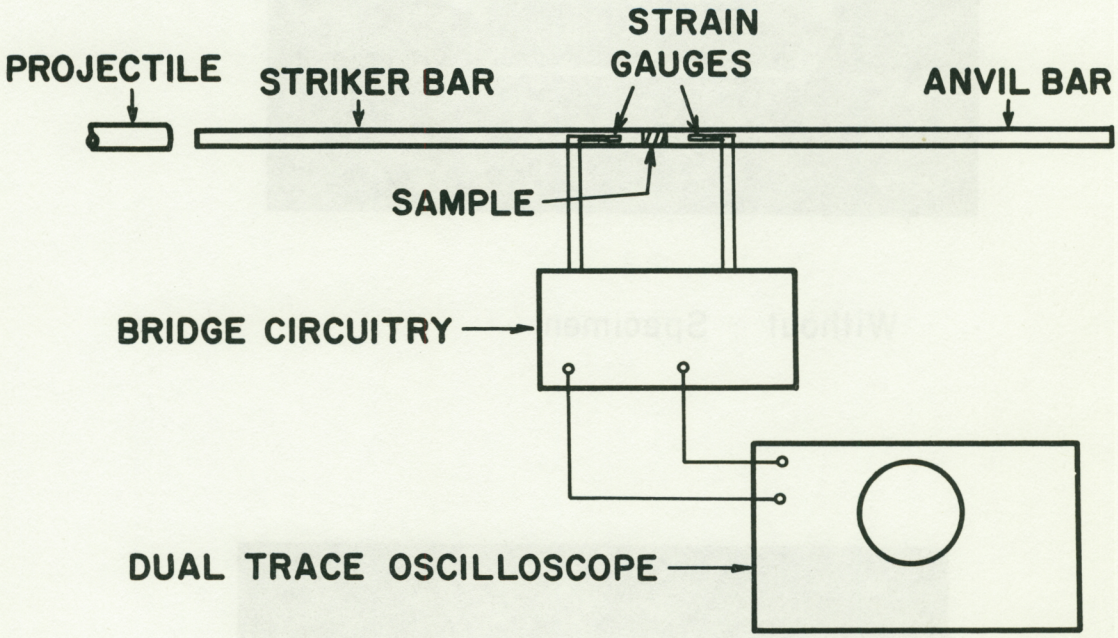

GUN AND BAR APPARATUS

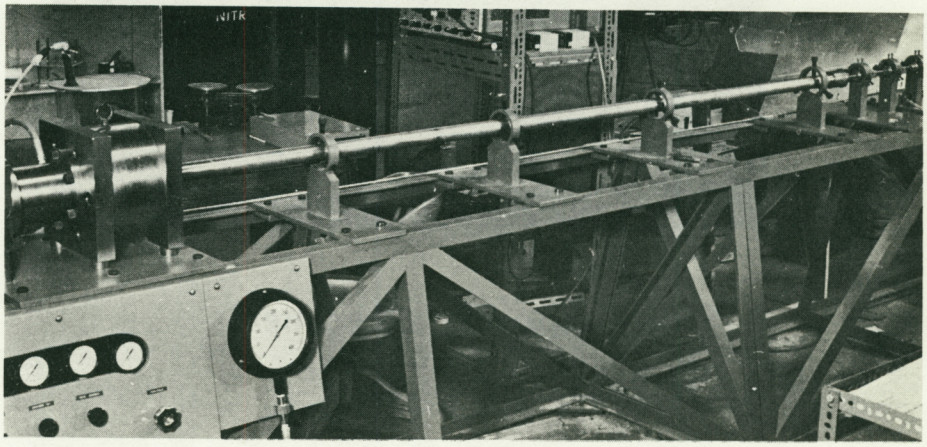

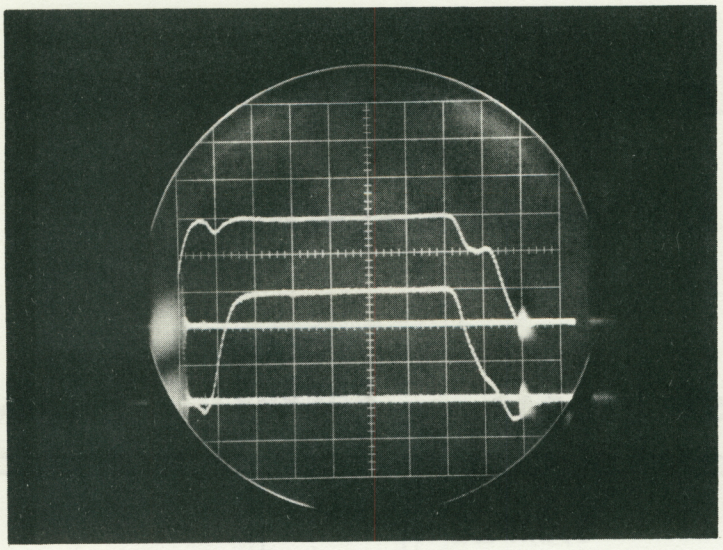

Without Specimen

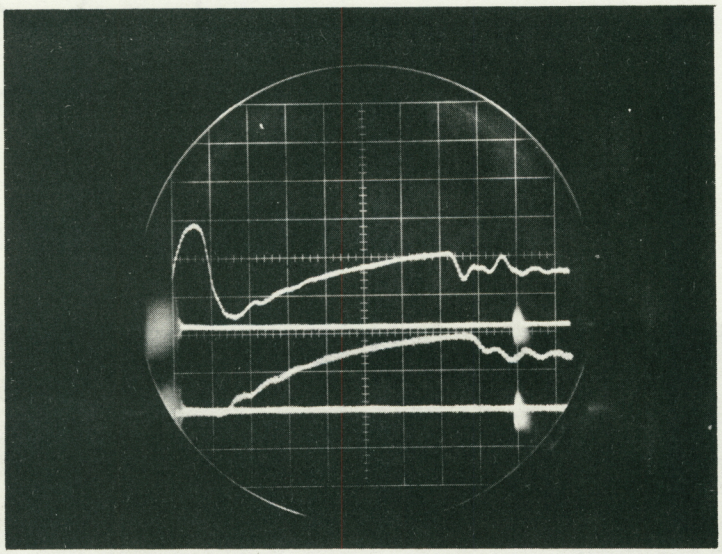

With Epoxy Specimen

FIG. 31 TYPICAL STRAIN GAUGE TRACES FROM SPLIT HOPKINSON BAR

FIG.32 STRESS-STRAIN RELATIONSHIP
(LOADING IN COMPRESSION)

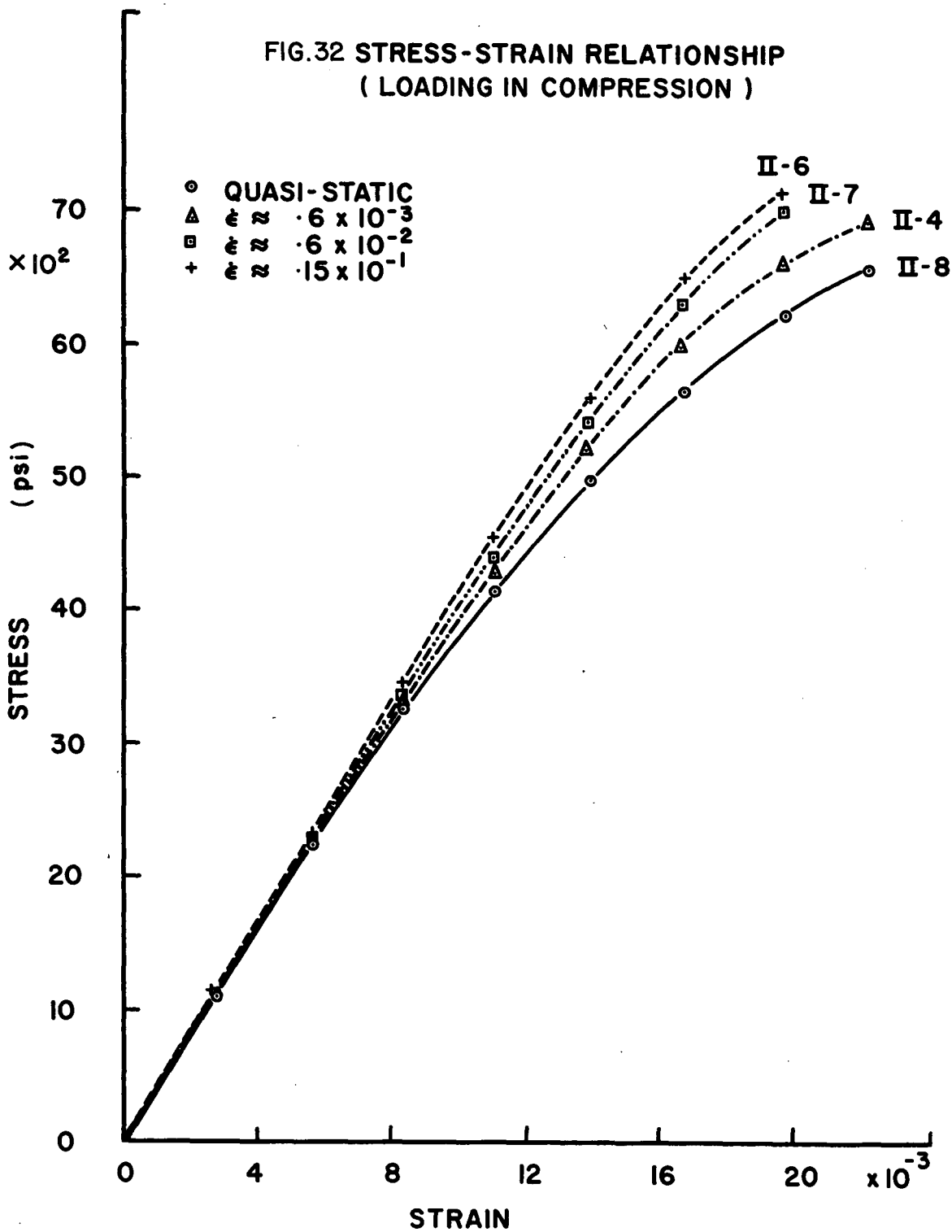

FIG. 33 STRESS-STRAIN CURVES FOR EPOXY PLASTIC AT HIGH STRAIN RATES